COMPARISON OF CRITICAL SUBMERGENCE EQUATIONS PROPOSED FOR HORIZONTAL INTAKE STRUCTURES

DALAL ABDULKAREEM HUSSEIN AL-OBAIDI

AUGUST 2025

ÇANKAYA UNIVERSITY

GRADUATE SCHOOL

CIVIL ENGINEERING DEPARTMENT

CIVIL ENGINEERING MASTER'S THESIS

COMPARISON OF CRITICAL SUBMERGENCE EQUATIONS PROPOSED FOR HORIZONTAL INTAKE STRUCTURES

DALAL ABDULKAREEM HUSSEIN AL-OBAIDI

AUGUST 2025

ABSTRACT

COMPARISON OF CRITICAL SUBMERGENCE EQUATIONS PROPOSED FOR HORIZONTAL INTAKE STRUCTURES

AL-OBAIDI, Dalal ABDULKAREEM HUSSEIN
CIVIL ENGINEERING MASTER'S THESIS

Supervisor: Prof. Dr. Mustafa GÖĞÜŞ
Co-Supervisor: Dr. Serkan GÖKMENER
August 2025, 99 pages

Air-entraining vortices at intake structures pose significant challenges to the operation of water intake systems, leading to efficiency losses and potential damage to hydraulic equipment. This study focuses on predicting critical submergence depth, S_c, the vertical distance required to prevent air-entrainment vortices, for horizontal intakes under symmetrical and asymmetrical approach flow conditions. Dimensional analysis is employed, analyzing the effect of intake geometry, Approach Froude number, Intake Froude number, Reynolds number, and Weber number. Experimental data from 409 and 225 observations for symmetrical and asymmetrical approach flow conditions, respectively, were reanalyzed from different studies to derive more general and accurate empirical equations predicting the dimensionless critical submergence, S_c/D_i. The analysis revealed that the intake Froude number and the geometric parameters are the dominant factors influencing S_c/D_i. Moreover, empirical equations derived exhibit strong statistical performance, with R^2 values up to 0.988 and 0.949 for symmetrical and asymmetrical conditions, respectively. The most accurate empirical equations are obtained while considering all the flow and geometric parameters to predict S_c/D_i. On the contrary, the accuracy of the empirical equations considering only $(Fr)_i$ gives moderate results in predicting S_c/D_i. These equations were compared with similar ones available in literature, and it was shown that the proposed

equations represent a balanced interpolation between small- and large-scale empirical equations and may offer improved generalizability across a wide range of hydraulic conditions.

Keywords: Horizontal intakes, Critical submergence, Air-entraining vortices, Approach Froude number, Intake Froude number.

ÖZET

YATAY SU ALMA YAPILARI IÇIN ÖNERILEN KRITIK BATIKLIK DENKLEMLERININ KARŞILAŞTIRILMASI

AL-OBAIDI, Dalal ABDULKAREEM HUSSEIN
İNŞAAT MÜHENDİSLİĞİ YÜKSEK LİSANS TEZİ

Danışman: Prof. Dr. Mustafa GÖĞÜŞ
Ortak Danışman: Dr. Serkan GÖKMENER
Ağustos 2025, 99 sayfa

Su alma yapılarında oluşan hava-sürükleyen girdaplar, su alma yapılarının işletilmesinde birtakım güçlüklere sebep olmakta, verim kayıplarına ve hidrolik ekipmanlarda olası hasarlara yol açabilmektedir. Bu çalışma, simetrik ve asimetrik yaklaşım akım koşulları altındaki yatay su alma yapıları için hava sürüklenmesini önlemek amacıyla gerekli düşey mesafe olan kritik batıklığın, S_c, tahminine odaklanmaktadır. Boyut analizi kullanılarak, giriş geometrisi, yaklaşım Froude sayısı, su alma yapısı Froude sayısı, Reynolds sayısı ve Weber sayısının kritik batıklığa olan etkileri analiz edilmiştir. Simetrik ve asimetrik yaklaşım akış koşulları için sırasıyla, farklı çalışmalardan alınmış, 409 ve 225 adet deney verisi, daha genel ve doğru ampirik denklemler türetmek amacıyla analiz edilmiştir. Analizler, su alma yapisi Froude sayısı ve geometrik parametrelerin boyutsuz kritik batıklık (S_c/D_i) üzerinde baskın etkiler gösterdiğini ortaya koymuştur. Ayrıca, türetilen ampirik denklemler istatistiksel olarak yüksek doğruluk sergilemiş ve R^2 değerleri sırasıyla simetrik koşullar için 0.988, asimetrik koşullar için ise 0.949 mertebelerinde elde edilmiştir. Tüm akış ve geometrik parametreleri dikkate alınarak oluşturulan ampirik denklemler, en tutarlı sonuçları göstermiştir. Buna karşılık, yalnızca $(Fr)_i$ dikkate alınarak türetilen denklemler, S_c/D_i'nin tahmininde orta düzeyde doğruluk sağlamıştır. Bu denklemler literatürdeki benzer denklemlerle karşılaştırılmış ve önerilen denklemlerin küçük ve büyük ölçekli modellere ait ampirik denklemler arasında dengeli bir korelasyon sunduğu, ayrıca daha geniş bir hidrolik koşul aralığında daha iyi genellenebilirlik sağlayabileceği gösterilmiştir.

Anahtar Kelimeler: Yatay su alma yapıları, Kritik batıklık, Hava-sürükleyici girdaplar, Yaklaşım Froude sayısı, Su Alma Yapisi Froude sayısı.

ACKNOWLEDGEMENT

I am grateful to my supervisor Prof. Dr. Mustafa Göğüş, and my co-supervisor Dr. Serkan Gökmener. I sincerely appreciate their invaluable advice and thoughtful feedback during this research. Their academic expertise, encouragement, and patience were instrumental in the successful completion of this thesis. I also extend my gratitude to the faculty members and administrative staff of the Department of Civil Engineering of Çankaya University for providing a supportive academic environment and the necessary resources to carry out this work. I am grateful to my colleagues and fellow researchers for their collaboration, insightful discussions, and moral support during this journey. Finally, I extend my deepest appreciation to my family for their steadfast support, patience, and unwavering encouragement. Their enduring presence has been a profound source of strength and inspiration throughout my academic journey.

TABLE OF CONTENTS

LIST OF TABLES

LIST OF FIGURES

LIST OF SYMBOLS AND ABBREVIATIONS

SYMBOLS

a	Intake gate height
b	Horizontal distance from the center of the intake to a side wall of the reservoir
b1	Horizontal distance from the center of the intake to the right-side plexiglass wall
b2	Horizontal distance from the center of the intake to the left-side plexiglass wall
c	Vertical distance between the lowest point of the intake pipe and reservoir bottom
c1	Regression variable
c2	Regression variable
c3	Regression variable
c4	Regression variable
g	Gravity acceleration
h	The depth of water above centerline of the intake
H	Submergence for vertical intakes
Ko	Intake Kolf number
Γ	Average circulation imposed to flow
R^2	Coefficient of correlation
R	Correlation coefficient
ν	Kinematic viscosity of water
ρ	Density of the fluid
μ	Dynamic viscosity of the fluid
βs	Scale effect correction coefficent for symmetrical approach flow conditions

βa	Scale effect correction coefficent for asymmetrical approach flow conditions
σ	Surface tension of the fluid
ψ	Representation of geometrical parameter for asymmetrical approach flow conditions

ABBREVIATIONS

D_i	Intake diameter
$(Fr)_{app}$	Approach Froude number
$(Fr)_i$	Intake Froude number
Ko	Intake Kolf number
Qi	Intake discharge
Re	Intake Reynolds number
Re_R	Radial Reynolds number
Sc	Critical submergence measured from the summit point of horizontal intakes
Sc*	Critical submergence measured from the center of horizontal intakes
V_i	Average velocity of the flow at the intake pipe
We	Intake Weber number

CHAPTER I
INTRODUCTION

1.1 THE INFLUENCE OF VORTEX ON THE EFFICIENCY OF INTAKE STRUCTURES

Dams and reservoirs are constructed to meet essential human needs, including providing drinking water, supporting agriculture, generating electricity, and mitigating floods. Water is usually taken from seas, lakes, rivers, or reservoirs through intake systems. These structures are important for ensuring a steady supply of water and controlling floods. Additionally, the hydropower generated from the water stored in dams is a clean, renewable, and sustainable way to produce energy. Therefore, dams are not only important for managing water but also play a key role in creating sustainable energy for the future.

The design of intake structures is important in the design process of dams. The application of the intake structures is fundamental for reducing the expenses and costs required for the construction to the minimum amount and to avoid any potential operational problems. One of the common problems that are seen at intakes is air-entraining vortices, induced by swirling flow at intake structures, which represent a prevalent challenge in the functioning of water intake structures. This can lead to significant economic and operational issues, including pipeline vibration and cavitation problems, decreased intake efficiency, the diminished performance of hydraulic machinery, increased hydraulic head loss and reduced discharge capacity at intake structures [1]. Consequently, the proper layout and functioning are crucial to avoid the occurrence of vortices. Ensuring adequate water level over the intake structure is essential for preventing vortex formation that decreases intake efficiency.

1.2 OVERVIEW OF CRITICAL SUBMERGENCE

The vertical distance from the free surface to the intake is known as submergence. In the literature, this distance has been presented from either the center of the intake or from its summit point as shown in Figure 1.1. The critical submergence is when the water levels are reduced to a point that causes vortices to form at the water surface [2]. For operating an intake structure effectively, the submergence must be high to avoid these vortices from reaching the intake entrance, while water use must be maximized. The formation of vortices leads to significant issues in hydraulic systems, including heightened hydraulic losses, reduced efficiency, decreasing outflow in the water intake, operational issues, vibration and cavitation issues in hydraulic machines [1,3].

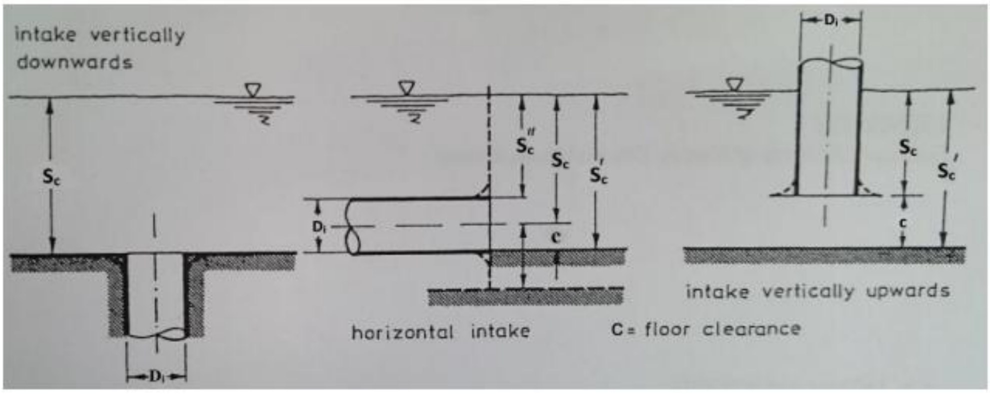

Figure 1.1: Critical submergences in different intake structures [4]

1.3 SOURCES OF VORTICES

In previous research, the causes of vortex generation were identified. Through extensive experimentation, Durgin and Hecker determined three primary reasons for vortex formation, as shown in Figure 1.2 [5]. These factors are:

a) Eccentric orientation of the symmetrical flow intake.

b) Shear layers caused by high velocity gradients.

c) Rotational wakes caused by obstructions.

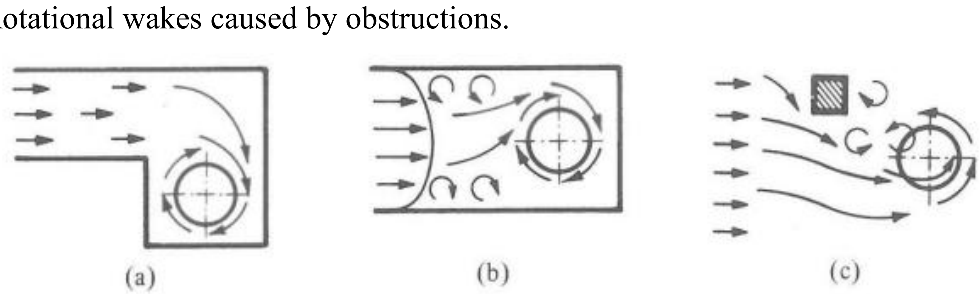

Figure 1.2: Sources of vortices [5]

1.4 INTAKES STRUCTURE TYPES

The classification of intakes is important to understand the critical submergence and air-entraining vortices. Intakes are classified based on their position and design as illustrated in Figure 1.3 [4].

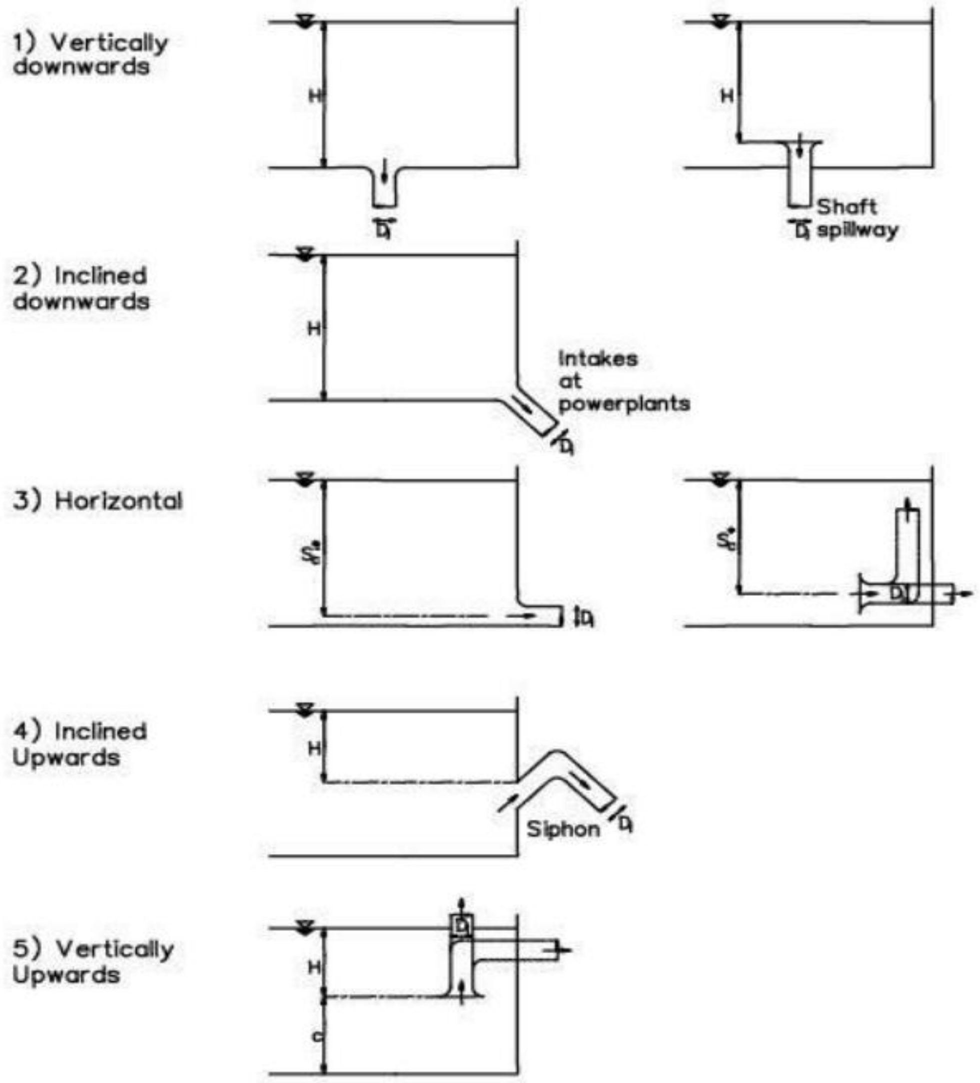

Figure 1.3: Intake types based on Knauss [4]

1.5 VORTEX TYPES

Vortices are generally classified based on different factors, one of which is their location, where the vortices are formed. Surface vortices can occur as a result of the swirl motion on the water surface that subsequently turns into a cone with an air core tail toward the intake. Subsurface vortices begin from the reservoir's bottom or walls and result in a swirling flow directed toward the intake [3]. Due to the fact that this classification is not thorough enough to encompass all the characteristics of the vortex, classifying the vortices according to their strength can be more effective. In a study conducted at the Alden Research Laboratory (ARL) by (Knauss, 1987) [4], where he used visual measuring techniques which is considered to be an efficient method to observe vortices, the formation stages of vortices could be described using the terms "swirl," "eddy," "dimple," and "vortex tail". The formation of the vortex starts with a small swirl motion before the transformation into a dimple. In the final phase, a vortex tail that reaches the intake will be formed as shown in Figure 1.4 [6].

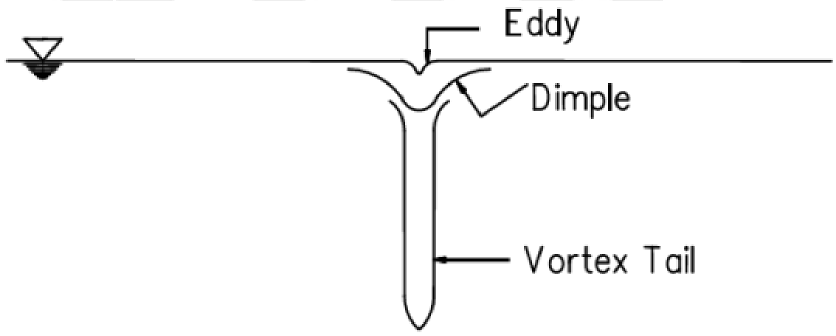

Figure 1.4: General form of an eddy, a dimple, and a vortex tail [4]. (Cited by Baykara 2013, [6])

Classification of vortex is divided into six types according to its appearance at ARL as shown in Figure 1.5 [4];

1. Observation of weak swirl motion without air core forms at the water surface.
2. The swirling motion begins to transition into a dimple.
3. The tail can be formed as a result of the development of the dimple, which can be detected with the use of dye. This type is called “the dye core to intake”.
4. The vortex grows stronger and begins to draw in floating objects, like debris, toward the intakes with their tails, though no air is sucked in.
5. The vortex in this type (5) has more strength than type (4), it conveys air to the intakes as bubbles by extracting it from the free surface.

6. The most powerful vortex type, drawing air from the surface toward the intake entrance. The body is conical in shape, with an air core tail stretching to the intake like a rope [7].

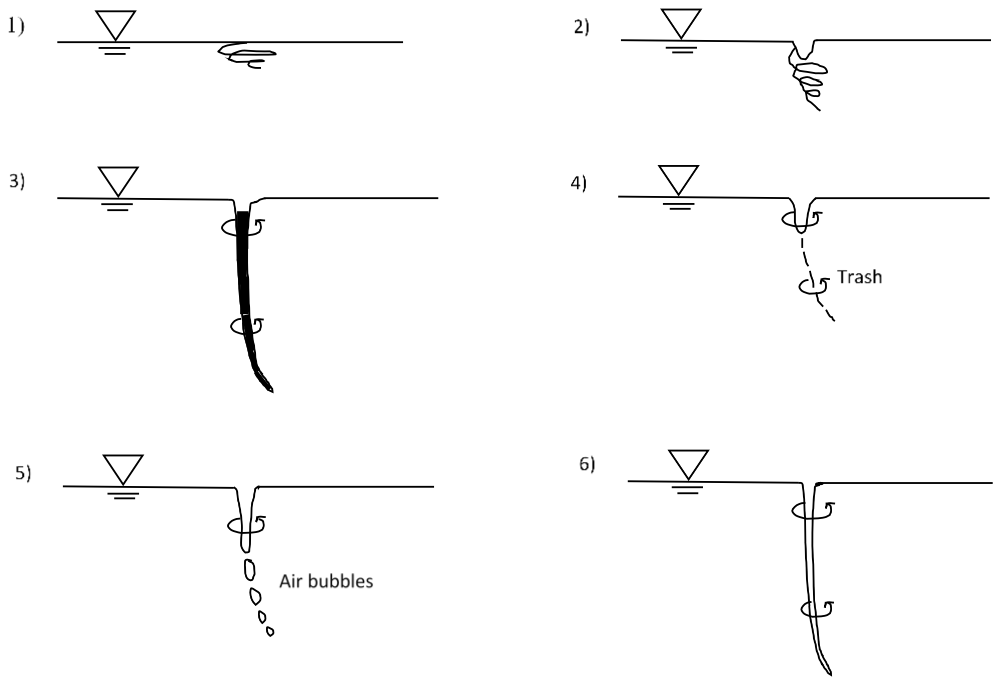

Figure 1.5: Classification of vortex types [4]. (Cited by Gogus and Gokmener, [1])

1.6 SCOPE OF THE PRESENT STUDY

In the literature, there are several empirical equations proposed by researchers to predict the critical submergence for horizontal intake structures. Analytical approaches were used to predict critical submergence at intakes and used experimental data to validate their findings [2, 8-14]. In addition, because of its turbulence nature, other researchers experimentally explained the occurrence of air-entraining vortex as a function of the intake Froude number [15-19]. Notably, they proposed empirical equations and charts to predict dimensionless critical submergence depending on the intake Froude number. In addition, the sole of the studies investigated the effect of approach Froude number and the intake geometry on the occurrence of air-entraining vortices considered the effect of intake orientation as a geometry parameter on predicting critical submergence along with intake Froude number [20-21]. Some researchers considered the effect of sidewall clearances as a geometry parameter on predicting dimensionless critical submergence along with intake Froude, Reynolds, and Weber numbers for horizontal intakes under symmetrical and asymmetrical approach flow conditions [3,6,7].

Besides that, recent studies presented dimensionless critical submergence as a function of intake Froude number along with approach Froude number at lateral intake structures [22,23]. They also investigated the impact of intake geometry on the formation of air-entraining vortices. Despite these extensive studies providing strong knowledge on proper intake design against the formation of the vortices, to the best of the authors' knowledge, the impact of the approach Froude number in vortex formation at horizontal intake structures has not been studied.

Furthermore, the studies of Gökmener, Baykara and Haspolat were the first to consider a geometry parameter based on the sidewall clearances and the intake size as a function of dimensionless critical submergence. However, they did not consider the effect of approach Froude number, and their studies contained limitations related to the flow conditions and geometrical properties. Gökmener has used a large-scale intake structure in his study, with a constant pipe diameter and small ranges of Froude, Reynolds and Weber numbers, while Haspolat and Baykara experimented small-scale intake structures with different intake pipe diameters and a wide range of Froude, Reynolds and Weber numbers [3,6,7].

Consequently, as the main aim of this study, the data of Gökmener, Baykara and Haspolat are combined and reanalyzed to eliminate the limitations of these studies and to propose new and more general dimensionless equations to predict the critical submergence under symmetrical approach flow as a function of flow and geometrical parameters. Furthermore, the impact of the approach Froude number on the effect of vortices is discussed for the first time at horizontal intakes.

The remainder of this study is structured as follows: Chapter 2 provides an extensive review of the relevant literature. Chapter 3 presents the theoretical background and methodology adopted in this research. The previous experimental studies, which are considered in this study, are mentioned in Chapter 4. The findings and their discussion are outlined in Chapter 5. Finally, Chapter 6 concludes the thesis by summarizing the key results and implications of the study.

CHAPTER II
LITERATURE REVIEW

Anwar focused on the prevention of vortices at intakes by conducting experiments inside a closed circular tank with a closed top. Based on experimental findings, the usage of floating rafts was presented as an effective way to prevent vortices at intakes [24].

Another study conducted by Anwar on the formation of vortex at low head intakes [25]. Studies were done, both theoretically and experimentally, on various flow types and how to stop swirl and vortex formation. It was suggested that intake placement is an important criterion in preventing vortex development. Furthermore, the study conducted by Anwar in 1968 was asserted that once the radial Reynolds number Re^r surpassed a value of 10^3, the occurrence of weak vortices and deep surface depressions became decoupled from variations in Re^r [25]. He further emphasized that enhancing the surface roughness of the solid boundary to elevate, Re^r could inhibit the initiation of vortex structures at intake points.

Gordon investigated 29 existing hydroelectric intake structures to formulate a design aimed at mitigating vortex formation in low-head intake systems [15]. The study identified that vortex inception is strongly affected by parameters including the configuration of the approach flow, intake velocity, dimensional characteristics of the intake, and the degree of submergence. Utilizing the empirical data collected, a set of predictive equations was developed to estimate the non-dimensional critical submergence for symmetrical and asymmetrical approach flow conditions respectively:

$$\frac{\mathrm{Sc}}{\mathrm{Di}} = 1.70(\mathrm{Fr})_{\mathrm{i}} \tag{2.1}$$

$$\frac{\mathrm{Sc}}{\mathrm{Di}} = 2.27(\mathrm{Fr})_{\mathrm{i}} \tag{2.2}$$

Reddy and Pickford conducted an analysis of vortex development at horizontal intakes within standard pump sump configurations. Their findings highlighted that the geometry of the approach channel plays a dominant role in governing vortex behavior. Moreover, they observed that the Reynolds number, defined as $Re = V_iD_i/\nu$, exerts minimal influence on critical submergence owing to the open channel characteristics inherent to vortex formation. As a result, the Reynolds number was omitted from the formulation of dimensionless critical submergence. Instead, a correlation was established between critical submergence and the intake Froude number with and without vortex prevention devices, respectively [16]:

$$\frac{S_c}{D_i} = (Fr)_i \tag{2.3}$$

$$\frac{S_c}{D_i} = (Fr)_i + 1 \tag{2.4}$$

The initiation of air-entrainment vortices at horizontal structures was examined. The findings revealed that these vortices are unaffected by surface tension, viscosity, radial Reynolds numbers above $3x10^4$, or Weber numbers over 10^4 [26]. Furthermore, the research indicated that entrance type does not affect critical submergence, although flush-mounted intakes were found to be more effective than bell-mouth intakes because of the reduced circulation observed at the intake [3].

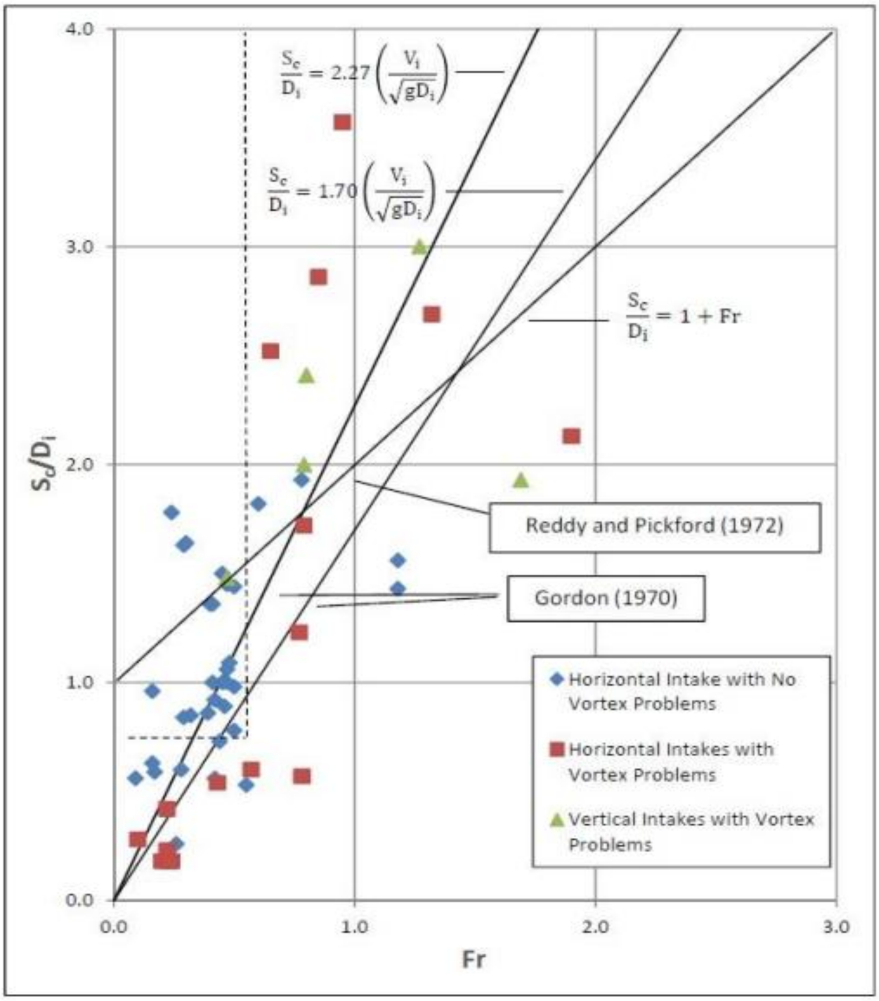

Figure 2.1: A graphical representation of combined findings from previous research on available intake systems [17]

Knauss evaluated the minimum design submergence levels of efficiently performing prototype systems and depicted the resulting curves in Figure 2.2 [4]. For large-scale intake systems used in power plants, particularly in pumped storage systems where $(Fr)_i \leq 1/3$, a submergence depth of 1 to 1.5 times the intake height (or diameter) was recommended [6]. For medium and small installations where $(Fr)_i \geq 1/3$, especially in pump sumps, submergence requirements can be calculated using the formula provided in Figure 2.2. These recommendations apply to intakes with optimal approach flow conditions. "h" in the figure, denotes the vertical distance from the free water surface to the center of the intake [27].

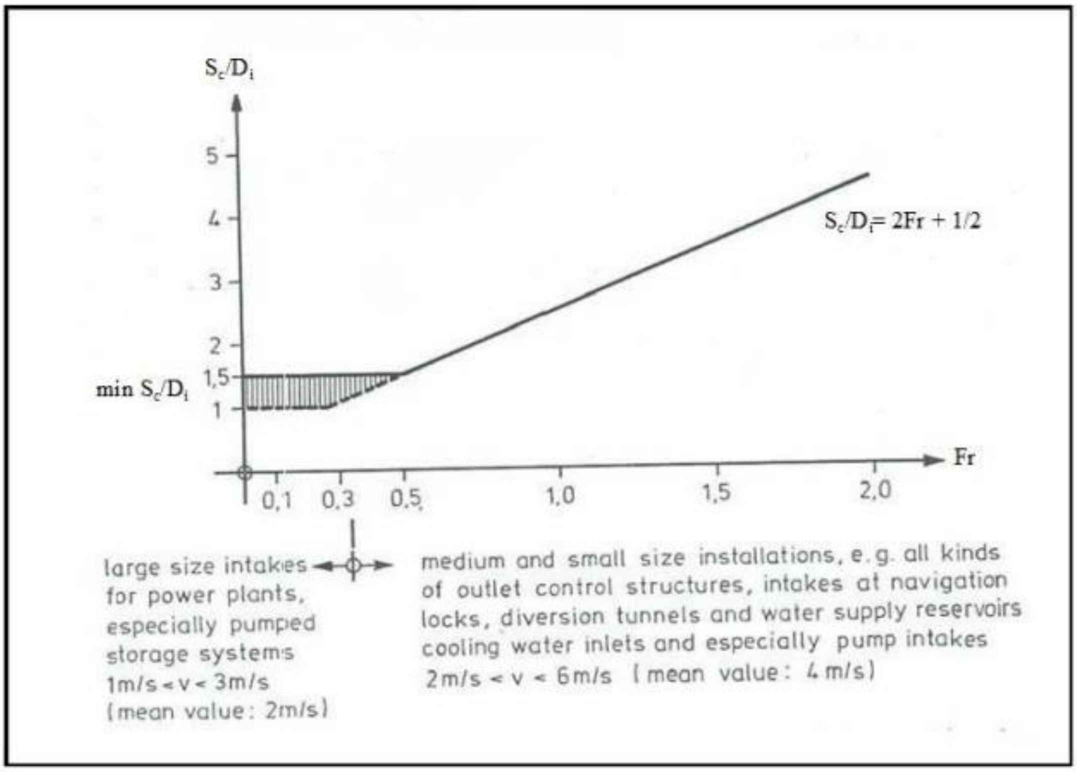

Figure 2.2: Optimal submergence criteria for intake structures with favorable approach flow conditions [4], [27]

Yıldırım and Kocabaş conducted both experimental and theoretical research to investigate the conditions under which air-entraining vortices form at intake structures within uniform canal flows [28]. Their analysis combined the point sink model with a uniform flow field commonly referred to as Rankine's half-body potential flow to address vortex behavior [27]. According to their theoretical framework, the onset of critical submergence corresponds to the radius of a notional spherical sink surface, also described as the critical spherical sink surface. From this, they derived the following dimensionless expression for critical submergence [6]:

$$\frac{S_c}{D_i} = \frac{1}{2\sqrt{2}}\left(C_d\ \frac{V_i}{U_\infty}\right)^{1/2} \tag{2.5}$$

In the intake pipe, Vi represents the velocity, while Cd denotes the discharge coefficient for a uniform canal flow intake, and U∞ represents the upstream canal flow velocity [28, 29].

Yıldırım investigated the impact of flow boundaries on the critical submergence of intake pipes to improve predictions of critical submergence [29]. Research was conducted on a horizontal intake pipe located in a dead-end canal [30].

They noticed that the divergence between theoretical predictions and experimental findings grew larger when the gap between the intake pipe and the dead-end wall became smaller than S_c. Despite this, the potential flow model continued to provide reasonably accurate results for distances below S_c, it tended to overestimate critical submergence by approximately 80% when the distance between the intake pipe and the dead-end was significantly decreases below S_c [30].

Jiming investigated large-scale models of Pressure intakes with dual inlets to find the dimensionless critical submergence [18]. The two empirical formulas that were generated as a result of the study to determine the critical submergence for symmetrical and asymmetrical approach flow conditions respectively [7]:

$$\frac{S_c}{D_i} = 2.39(\mathrm{Fr})_\mathrm{i} - 0.001 \tag{2.6}$$

$$\frac{\mathrm{S_c}}{\mathrm{D_i}} = 3.17(\mathrm{Fr})_\mathrm{i} - 0.001 \tag{2.7}$$

Gürbüzdal has carried out several experiments on horizontal structures to examine the potential scale effects on the development of air-entraining vortex [30]. His studies focused on key parameters influencing vortex formation, including the intake Froude number, Reynolds number, and side wall clearance. Based on the experimental findings, an empirical formula was derived:

$$\frac{\mathrm{S_c}}{\mathrm{D_i}} = (\mathrm{Fr})_\mathrm{i}{}^{0.865} \left(\frac{\mathrm{b}}{\mathrm{Di}}\right)^{-0.565} \mathrm{Re}^{0.0424} \tag{2.8}$$

Sarkardeh explored the influence of headwall slope and the trash rack on vortex development in a horizontal intake [20]. To eliminate the impacts of viscosity and surface tension, the experiments were performed under flow conditions exceeding the threshold limits suggested by previous studies. The study examined four different headwall slopes, revealing that as the wall slope became steeper, vortex formation weakened and became more unstable, particularly at lower Froude numbers. This change led to a corresponding reduction in critical submergence. The tests were also repeated with a trash rack installed, and the results indicated that the trash rack significantly reduced vortex intensity, especially in the presence of strong vortices, as it disrupted both the flow pattern and the development of vortices. Based on their findings, the authors proposed empirical equations to predict the dimensionless critical submergence for vortex types 5 and 3, as defined by the ARL vortex classification system.

For the type 5 and 3 vortex formation respectively [6].

$$\left(\frac{Sc}{Di}\right)_5 = 2\left(\frac{1}{Z}\right)^{0,008} (Fr)_i^{0\cdot 334}\, T^{0\cdot 369} \tag{2.9}$$

$$\left(\frac{Sc}{Di}\right)_3 = 2.43\left(\frac{1}{Z}\right)^{0,008} (Fr)_i^{0\cdot 334}\, T^{0\cdot 369} \tag{2.10}$$

Z is the wall slope, T is the cross-sectional trash rack opening percentage (T=1 for no trash rack).

Baykara investigated the formation of vortex at symmetrical flows by creating a new formula based on key parameters [6]. The research encompassed six distinct pipe diameters 30, 25, 19.4, 14.4, 10, and 5 cm and tested various symmetrical side wall clearance combinations for each diameter at different flow rates. According to the experimental results, S_c/D_i can be classified to three distinct categories, maximum, intermediate and minimum. It was observed that in the intermediate S_c/D_i values for a specific D_i, if the $(Fr)_i$ and the dimensionless wall clearance ratio exceed the values indicated in the figure, S_c/D_i remains constant for greater $2b/D_i$ values beyond those represented values.

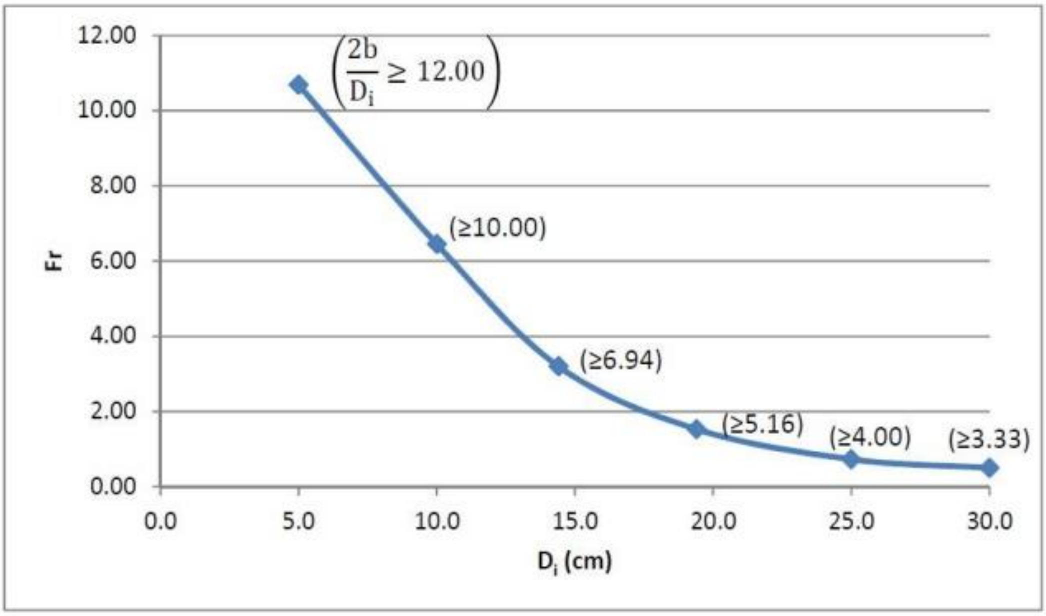

Figure 2.3: Limit values of $2b/D_i$ and $(Fr)_i$ for intake diameter D_i, over which S_c/D_i remains irrespective of $2b/D_i$ [6]

This study formulated simpler equations by removing Re, We, and $(2b/D_i)$ to evaluate their influence on the variance of S_c/D_i. The elimination of these values did not substantially influence the dimensionless critical submergence. In evaluating larger diameter intakes as prototypes and smaller as models, the values were established using the similarity of Froude, then, associated S_c/D_i values were compared. Disregarding the influences of Reynolds number and Weber number led to impacts on the S_c/D_i. Consequently, empirical formulas were derived as follows:

$$\frac{S_c}{D_i} = (Fr)_i^{0.336} Re^{-0.229} We^{0.401} \left(\frac{2b}{Di}\right)^{-0.261} \tag{2.11}$$

The aforementioned equation is simplified after eliminating the Re, We, and $2b/D_i$.

$$\frac{S_c}{D_i} = (Fr)_i^{0.639} \tag{2.12}$$

$$\frac{S_c}{D_i} = (Fr)_i^{0.324} Re^{-0.176} We^{0.282} \tag{2.13}$$

$$\frac{S_c}{D_i} = 1.278\ (Fr)_i^{\,0.558} \tag{2.14}$$

Haspolat carried out experimental studies to investigate the formation of air-entrained vortices and estimate critical submergence in horizontal intake structures under both symmetrical and asymmetrical approach flow conditions [7]. Experiments were conducted using a model composed of a reservoir and a horizontal intake, incorporating adjustable side walls with varying sizes. The results indicated that the S_c/D_i increases with higher values of the intake Froude, Reynolds, and Weber numbers. Empirical dimensionless equations to predict the dimensionless critical submergence based on flow parameters and geometric factors for the tested ranges in the study. The dimensionless empirical equations presented for symmetrical approach flow conditions are presented below:

$$\frac{S_c}{D_i} = (Fr)_i^{\,0.193}\ Re^{\,-0.331}\ We^{0.544} \left(\frac{2b}{Di}\right)^{-0.241} \tag{2.15}$$

$$\frac{S_c}{D_i} = (Fr)_i^{\,0.066}\ Re^{\,-0.503}\ We^{0.747} \tag{2.16}$$

$$\frac{S_c}{D_i} = (Fr)_i^{\,0.580}\ Re^{\,0.00795} \tag{2.17}$$

And

$$\frac{S_c}{D_i} = (Fr)_i^{\,0.609} \tag{2.18}$$

For asymmetrical approach flow conditions, where $\psi = \frac{(b_1+b_2)}{D_i}\left(\frac{b_1}{b_2}\right)$.

$$\frac{S_c}{D_i} = (Fr)_i^{\,0.154}\ Re^{\,-0.315}\ We^{\,0.462}\ \Psi^{0.071} \tag{2.19}$$

$$\frac{S_c}{D_i} = (Fr)_i^{\,0.209}\ Re^{\,-0.281}\ We^{0.421} \tag{2.20}$$

$$\frac{S_c}{D_i} = (Fr)_i^{0.555}\ Re^{\ 0.0025} \tag{2.21}$$

And

$$\frac{S_c}{D_i} = (Fr)_i^{0.564} \tag{2.22}$$

The experimental findings by Haspolat demonstrated that S_c under symmetrical flow was increased when intake Fr, Re, and We numbers increased [7]. Once the threshold values are surpassed, critical submergence will become irrespective to geometric variables. Likewise, critical submergence escalates with increasing the independent parameters under asymmetrical flow conditions, although there is no definitive limiting value that influences its reliance on geometric factors.

Gökmener examined the variation of critical submergence by using three pipes of the same diameters of 0.265 m that were evaluated under diverse discharge conditions and changing side wall clearances [3]. Through dimensional analysis, empirical dimensionless equations were formulated to predict dimensionless critical submergence based on essential flow and geometric characteristics. The findings demonstrated lower critical submergence values in single intakes as compared to multiple intakes. The dimensionless empirical equations for symmetrical approach flow conditions are as follows:

$$\frac{S_c}{D_i} = (Fr)_i^{-0.126}\ Re^{\ -0.423}\ We^{0.692} \left(\frac{2b}{Di}\right)^{0.084} \tag{2.23}$$

$$\frac{S_c}{D_i} = (Fr)_i^{-0.065}\ Re^{\ -0.414}\ We^{0.632} \tag{2.24}$$

$$\frac{S_c}{D_i} = (Fr)_i^{0.753}\ Re^{\ 0.032} \tag{2.25}$$

And

$$\frac{S_c}{D_i} = 1.520\ (Fr)_i^{0.785} \tag{2.26}$$

For asymmetrical approach flow conditions:

$$\frac{S_c}{D_i} = (Fr)_i^{4.046}\, Re^{1.741}\, We^{-2.446}\, \Psi^{0.145} \tag{2.27}$$

$$\frac{S_c}{D_i} = (Fr)_i^{-0.017}\, Re^{-0.417}\, We^{0.631} \tag{2.28}$$

$$\frac{S_c}{D_i} = (Fr)_i^{0.799}\, Re^{0.028} \tag{2.29}$$

And

$$\frac{S_c}{D_i} = 1.441\, (Fr)_i^{0.827} \tag{2.30}$$

Sönmez studied the development of air-entraining vortex at horizontal single structures in symmetric flow conditions, focusing on the impact of different approach channel sidewall angles [27]. A series of tests was conducted across a range of discharges and three different approach channel configurations to determine the critical submergence required for vortex formation. Based on experimental findings, it was stated that critical submergence increases with increasing Froude, Reynolds and Weber numbers independent of the approach channel shape. Furthermore, the critical submergence can be decreased with increasing sidewall clearances and approach flow sidewall angle. Dimensionless empirical equations to predict critical submergence, incorporating hydraulic and geometrical parameters, were derived using dimensional analysis.

Hashid conducted both analytical and experimental studies on horizontal side circular intakes in open channel flow, with and without bellmouth intakes [14]. A series of experiments was carried out by two intake configurations: a standard circular intake without entry transitions, designed to minimize entry losses, and an intake with a bellmouth transition. The study revealed that S_c/D_i increases with parameters such as the intake Froude number, the ratio of discharge coefficients and the Reynolds number, while it decreases with an increase in the approach Froude number. Analytical models were developed to estimate the critical submergence for different bottom clearances, with an error margin of less than ±15%. The results indicate that incorporating a bellmouth transition significantly reduces the critical submergence, improving intake efficiency by minimizing air-entrainment vortices. However, it was stated that the presence of flow boundaries in horizontal side intakes may negatively impact critical submergence.

Hashid investigated the critical submergence of lateral dual square structure caused by the pipe blockage in the intake subjected to a uniform perpendicular approach flow [22]. This research aimed to assess how varying intake protrusions influence critical submergence while maintaining one intake flush. This study involved systematically altering the protrusion of upstream and downstream intakes to analyze their effects. It was observed that increasing the protrusion of the downstream intake significantly reduced critical submergence, whereas increasing the protrusion of the upstream resulted in greater critical submergence. At greater protrusions (double the intake size), there was minimal mutual impact of the intakes, leading to multiple vortices development around each intake. An empirical equation was developed to estimate critical submergence for lateral dual protruded intakes, and it showed strong agreement with experimental results. The findings suggest that intake protrusion could be strategically utilized to decrease critical submergence. Additionally, an increase in the approach flow Froude number was found to decrease the dimensionless critical submergence, highlighting the vortex formation due to flow inertia. The study also identifies the limiting values of differential protrusions for optimal dual intake design.

Das carried out an experimental study to focus on the critical submergence of a laterally placed single rectangular intake under uniform approach flow in an open channel [23]. Their findings indicate that critical submergence is influenced by several factors, including intake size, aspect ratio, and flow characteristics such as the approach Froude number, intake Froude number, intake Reynolds number, and Weber number. Among these, the intake Froude number and aspect ratio were identified as the most significant parameters affecting critical submergence. The study revealed that a greater approach Froude number reduces critical submergence by increasing flow inertia, which suppresses air-entraining vortices, while a lower approach Froude number facilitates early air entrainment. In contrast, an increase in intake Froude number, Reynolds number, and Weber number led to increased critical submergence values.

CHAPTER III
THEORETICAL ANALYSIS

3.1 INTRODUCTION

In hydraulics, determining the critical submergence is a fundamental aspect in the design and operation of intake structures. Critical submergence refers to the minimum water depth over the intake necessary to avoid the formation of vortices, which can significantly affect system performance and lead to operational issues. Due to the range of problems that can arise in intake structures, such as cavitation, reduced efficiency, and mechanical vibrations, it is crucial to apply theoretical equations to optimize intake designs and avoid these issues. Implementing well-defined equations helps minimize potential problems and reduces the financial burden associated with repairs and maintenance.

The most common and challenging issue in intake structures is the formation of vortices, which can disrupt the flow and introduce air into hydraulic systems. Over the years, many researchers have proposed various equations to predict critical submergence and design intake systems effectively. However, each of these equations is typically suited to a specific intake configuration or set of conditions, making their general application limited. Given the diversity of intake designs and operational environments, it would be highly beneficial to systematically compare the existing equations and develop a more universal formula. Such a general equation would enhance the design process, providing engineers with a tool that can be applied across different scenarios, ensuring efficient, cost-effective, and problem-free intake structures in hydraulic systems.

3.2 DIMENSIONAL ANALYSIS

The key parameters relating to critical submergence must be systematically identified and thoroughly analyzed. Based on their specific properties, Gökmener divided them as follows: fluid Properties, flow Properties, and geometric Properties. Figure (3.1) [3]:

1- Fluid Properties: Fluid density (ρ), dynamic viscosity of the fluid (μ) and surface tension of the fluid (σ) [7].

2- Flow Properties: Average velocity of flow in the intake pipe (V_i), average approach flow velocity in the reservoir in front of the intake entrance (V_{app}), average circulation exposed to flow (Γ) and gravity acceleration (g) [7].

3- Geometric Properties of the Intake and Reservoir: Intake pipe diameter (D_i), right and left approach channel side wall distances (with respect to flow direction) of the intake structure to the intake center axis b_1 and b_2, respectively, and the vertical distance between the bottom point of the intake and the base of the reservoir (c) [7].

As shown in Figure 3.1, S_c is the critical submergence considered as a function of the independent variables;

$$S_c = f_1(\rho, \mu, \sigma, g, V_i, Vapp, \Gamma, D_i, c, b_1, b_2) \tag{3.1}$$

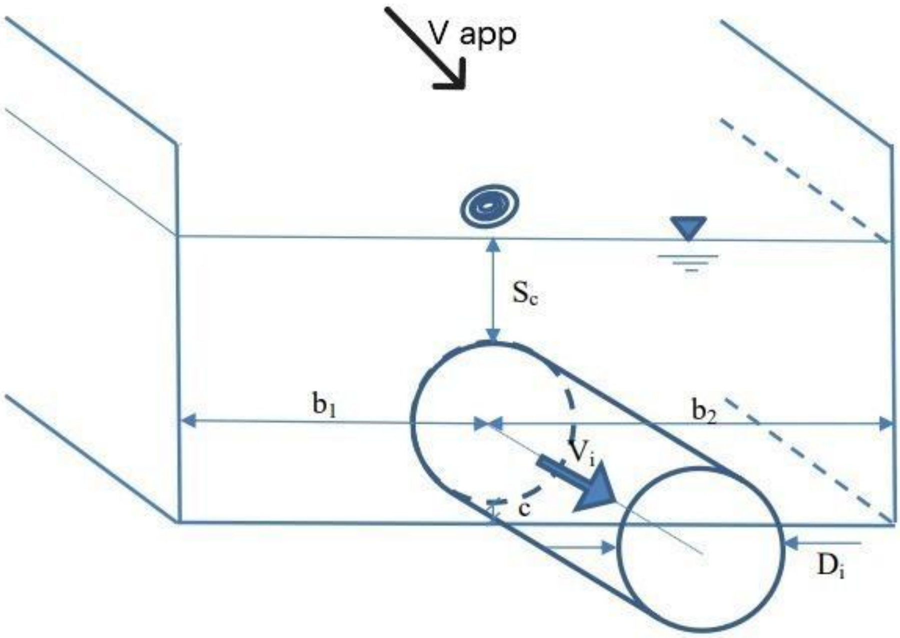

Figure 3.1: Horizontal intake structure

Using Buckingham's π theorem on the variables defined in equation above results in the dimensionless critical submergence below;

$$\frac{S_c}{D_i} = f_2\left(\frac{b_1}{D_i}, \frac{b_2}{D_i}, \frac{c}{D_i}, (Fr)_i, Re, We, K_o\right) \tag{3.2}$$

where:

$\frac{b_1}{D_i}$ = Aspect ratio of right side wall clearance to intake diameter

$\frac{b_2}{D_i}$ = Aspect ratio of left side wall clearance to intake diameter

$\frac{c}{D_i}$ = Aspect ratio of bottom clearance to intake diameter

Re = Intake Reynolds number = $\frac{V_i\, D_i\, \rho}{\mu}$

$(Fr)_i$ = Intake Froude number = $\frac{V_i}{\sqrt{g\, D_i}}$

We = Intake Weber number = $\frac{\rho\, {V_i}^2 D_i}{\sigma}$

K_o = Intake Kolf number = $\frac{\Gamma}{V_i\, D_i}$

Experimental studies that are analyzed in this study did not have any bottom clearance, c, is the distance from the intake pipe to the reservoir base. Therefore, In Equation 3.2 $\frac{c}{D_i}$ parameter can be removed. Thus, Equation 3.3 can be used for both symmetrical and asymmetrical approach flow conditions.

$$\frac{S_c}{D_i} = f_2 \left[\frac{(b_1 + b_2)}{D_i}.\ \left(\frac{b_1}{b_2}\right), (Fr)_i, Re, We, K_o\right] \tag{3.3}$$

For symmetrical approach flow conditions, the term of $\frac{(b_1+b_2)}{D_i}\left(\frac{b_1}{b_2}\right)$ is converted to $\frac{2b}{D_i}$ because b_1=b_2=b as shown in Equation 3.4:

$$\frac{S_c}{D_i} = f_2 \left(\frac{2b}{D_i}, (Fr)_i, Re, We, K_o\right) \tag{3.4}$$

If not, $\frac{(b_1+b_2)}{D_i}\left(\frac{b_1}{b_2}\right)$ becomes the dimensionless term of the asymmetry of the approach flow and Equation 3.5 can be written for asymmetrical approach flow conditions as:

$$\frac{S_c}{D_i} = f_2 \left[\frac{(b_1+b_2)}{D_i}\left(\frac{b_1}{b_2}\right), (Fr)_i, Re, We, K_o\right] \tag{3.5}$$

In the analysis below, b_1 and b_2 will be considered as small and large wall clearances, respectively, so that b_1/b_2 becomes less than unity all the time. Moreover, the approach flow velocity, $V_{app} = \frac{Q}{[(b_1+b_2)(S_c+D_i)]}$ was not directly considered as one of the variables involved in the equation of S_c/D_i. To see the direct effect of approach flow velocity on the value of critical submergence, the approach flow Froude number $(Fr)_{app}$ can be included to the equation.

$$(Fr)_{app} = \frac{Vapp}{\sqrt{g(Di + Sc)}} \tag{3.6}$$

In this case, Equations (3.4) and (3.5) can be written for symmetrical and asymmetrical approach flow conditions, respectively, in the following forms,

$$\frac{S_c}{D_i} = f_2\left(\frac{2b}{Di}, (Fr)_{app}, (Fr)_i, Re, We, K_o\right) \tag{3.7}$$

and

$$\frac{S_c}{D_i} = f_2\left[\frac{(b_1+b_2)}{D_i}\left(\frac{b_1}{b_2}\right), (Fr)_{app}, (Fr)_i, Re, We, K_o\right] \tag{3.8}$$

When constructing a model of a prototype, achieving complete similarity between the model and the prototype is essential. However, to achieve full similarity, dimensionless parameters for (S_c/D_i) must be identical for both the model and the prototype, as stated in Equations 3.4 and 3.5. This condition leads to a model length ratio of ($L_r = 1$), which cannot be practically achieved. Therefore, parameters of lesser significance for vortex formation should be neglected from the equation, and one of the remaining parameters should be chosen as the primary factor for proper modeling. This study disregards the equivalence of Re and We numbers, opting to focus on the Fr number as the primary parameter, as vortices generation is influenced by gravity [3].

3.3 EFFECT OF FROUDE NUMBER

Prior research on vortex formation has identified the Froude number as the paramount dimensionless parameter influencing vortex development. For example, Gordon, considered Fr as the primary parameter affecting Sc. As a result, the Froude similitude law is commonly applied for modeling, however, it results in non-resemblance between the prototype and model, causing scale effects [15].

3.4 EFFECT OF REYNOLDS NUMBER

The Reynolds number represents a fundamental dimensionless parameter in hydraulic engineering, especially in the analysis of flow within pipes. that indicates the influence of viscosity on the flow. Previous research has indicated that the Reynolds number has no impact on vortex generation after a certain limit value. Anwar suggested that when ($Re> 3x\ 10^4$), it is possible to discard the Reynolds number for the formation of vortices [26]. Similarly, Jain defined this limit at ($Re > 2.5 \times 10^3$) [7,31].

3.5 EFFECT OF WEBER NUMBER

It is a dimensionless parameter that indicates the influence of (σ) forces in the fluid. The identicality of We is essential to avoid scale effects on the similarity of the dynamic models, although this similarity cannot be applied to small-scale models that are developed using the Froude similitude law. Many researchers have investigated the scale effect issues that arise from disregarding the Weber number. They have suggested certain threshold values for the Weber numbers as (1.2×10^2) and 600 [31,32]. Anwar indicated that vortex development at large Weber numbers is not influenced by surface tension (σ), thus, it can be ignored [3,26].

3.6 EFFECT OF KOLF NUMBER

It is a dimensionless parameter which indicates the influence of flow dynamics circulation. The primary characteristics for circulation are approach flow conditions, and the geometry of water intake and release. All these parameters are defined in Equations 3.7 and 3.8. This study does not generate unnatural circulation through external forces, therefore, related dimensionless parameter, Kolf number can be neglected from these formulas [27]. The formulas can be presented as follows:

For symmetrical approach flow:

$$\frac{S_c}{D_i} = f_2\left(\frac{2b}{Di}, (Fr)_{app}, (Fr)_i, Re, We\right) \tag{3.9}$$

For asymmetrical approach flow;

$$\frac{S_c}{D_i} = f_2\left[\frac{(b_1 + b_2)}{D_i}\left(\frac{b_1}{b_2}\right), (Fr)_{app}, (Fr)_i, Re, We\right] \tag{3.10}$$

CHAPTER IV

EXPERIMENTAL SETUPS USED IN THE PREVIOUS STUDIES

4.1 THE EXPERIMENTAL SETUP USED BY GÖKMENER

A physical model was developed by Gökmener [3]. The setup featured a sizable reservoir incorporating three identical horizontal intakes. Figures (4.1–4.2) display the system from multiple viewpoints, offering visual context for the experimental arrangement. Complementary schematic representations, including the general layout, longitudinal profile, are provided in Figures (4.3–4.4). The reservoir itself had dimensions of 6.35 m, 6.7 m, and 2.05 m, in width, length, and in height, respectively.

To regulate the kinetic energy of inflowing water, an energy dissipation device was installed at the reservoir's upstream section. The experimental configuration included three operational intake structures; each connected to pipes with a uniform internal diameter of D_i=26.5 cm that conveyed flow toward the downstream discharge channel. Additionally, a fourth intake, originally integrated into the setup with a smaller diameter of D_i=10.9 cm, remained inactive during testing and was kept closed, as indicated in the corresponding figure. Discharge through each active intake pipe was monitored using electromagnetic flow meters installed at each connection point [3].

Figure 4.1: Downstream of the experiment [3]

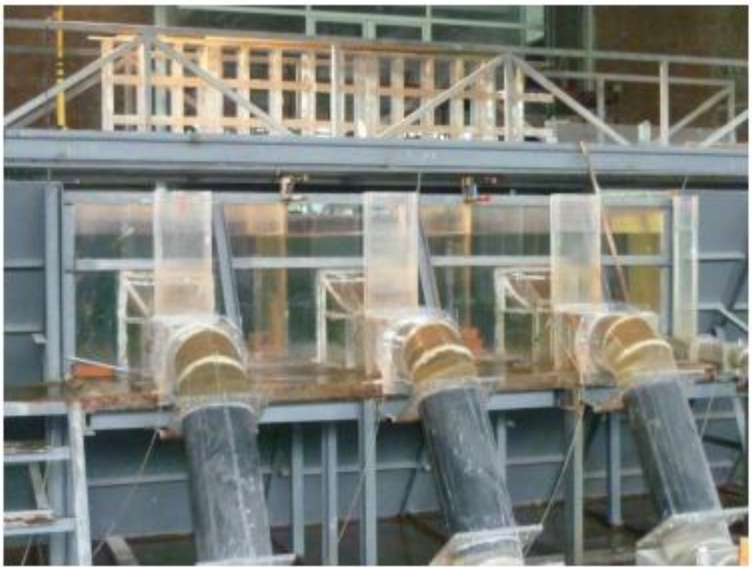

Figure 4.2: Close-up downstream demonstration of the three water intakes [3]

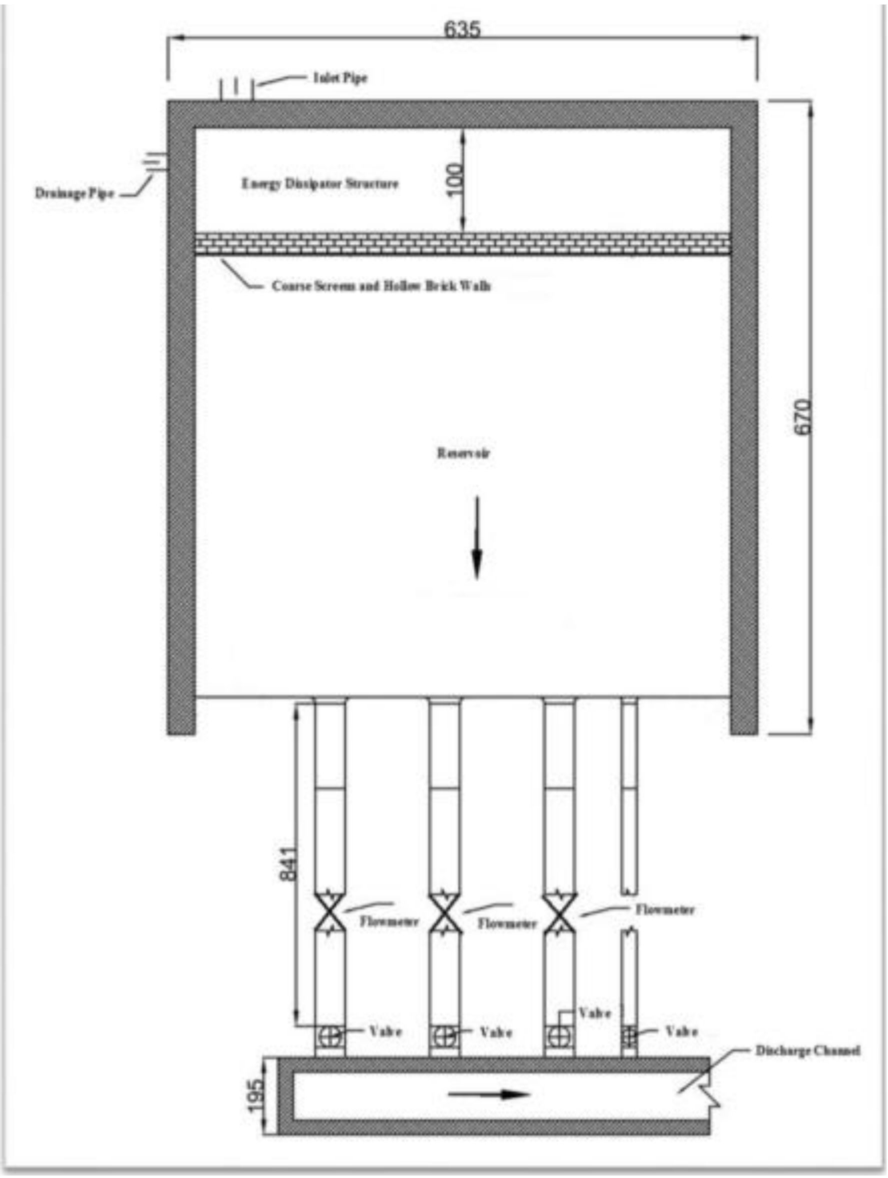

Figure 4.3: General Layout of the triple intakes structure [3]

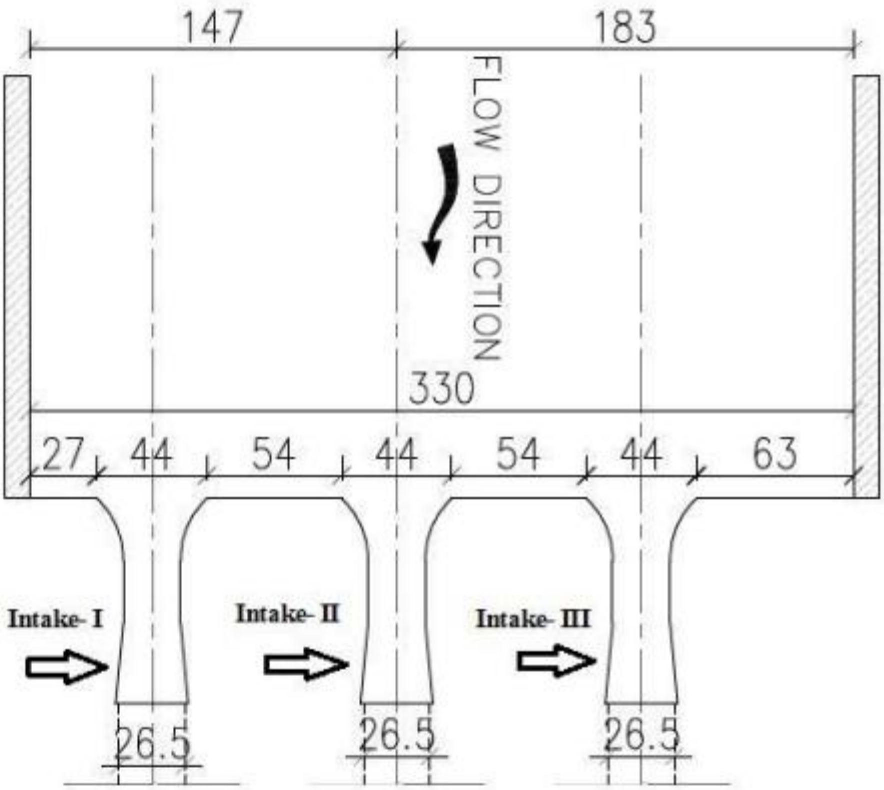

Figure 4.4: Comprehensive demonstration indicating the numbers and their relative placements [3]

4.2 THE EXPERIMENTAL SETUP USED BY BAYKARA AND HASPOLAT

Baykara and Haspolat carried out experiments using a common setup constructed at the METU Hydromechanics Laboratory [6,7]. The experimental setup consists of three primary components: the reservoir, the horizontal intake pipe, and the rectangular open channel. Water was supplied from a sump located beneath the laboratory and pumped into the upper reservoir. Once the reservoir was filled, a drainage pipe system regulated the water level and prevented overtopping. The reservoir included plexiglass front walls installed above a diaphragm slab to allow visual observation of vortex formation. Two pipes were serving as the inflow and drainage lines fixed to the reservoir. The reservoir dimensions were nearly identical in both studies: Baykara's setup had a reservoir measuring 3.10 m in both length and width, and 2.20 m in depth, while Haspolat setup measured 3.10 m in length and 2.20 m in both width and depth, as shown in Figures 4.5–4.8 [6,7]. A diaphragm slab divided the reservoir horizontally into a dead volume and an active reservoir section, ensuring that the incoming flow was calmed before entering the active zone.

Additionally, screens were installed at the transition to further stabilize the flow and eliminate circulation. Adjustable side walls of plexiglass were installed orthogonally between the screens and the dead-end. The position was varied to study the influence of the clearance of the side wall on vortex development. During experiments, the dead volume was filled first, followed by the active section as water levels rose. This arrangement helped minimize turbulence in the active zone. The plexiglass intake pipe discharged water into a small collection pool, which connected to a rectangular open channel. This channel ended in a sharp-crested weir, 17 cm and 1 m in height and width respectively. The weir was calibrated before each experiment using an acoustic flowmeter. In Haspolat's experiments, four intake diameters were tested: 30 cm, 25 cm, 10 cm, and 5 cm. Additional pumping was required to supply sufficient discharge for the smaller diameters (10 cm and 5 cm) [7]. In contrast, Baykara's study employed six pipe sizes: 30.0 cm, 25.0 cm, 19.4 cm, 14.4 cm, 10.0 cm, and 5.0 cm, for different test conditions [6].

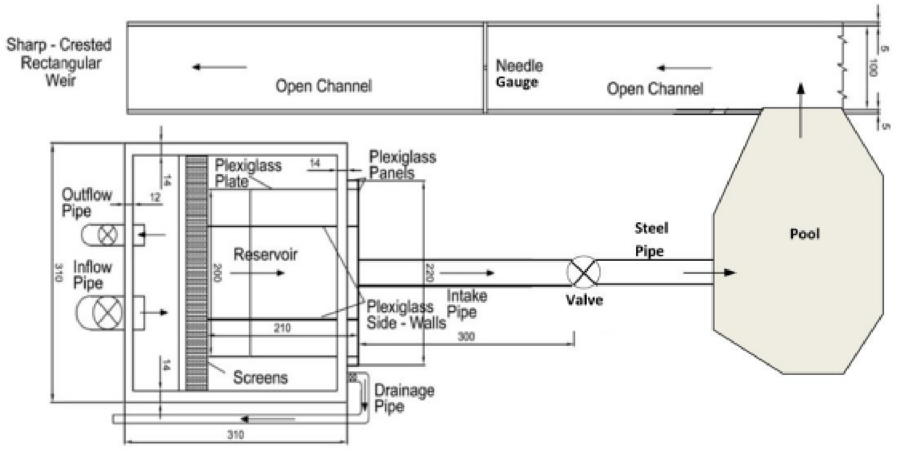

Figure 4.5: The model plan without pump [33]

Figure 4.6: General view of the experiment without pump [7]

a) Plan view

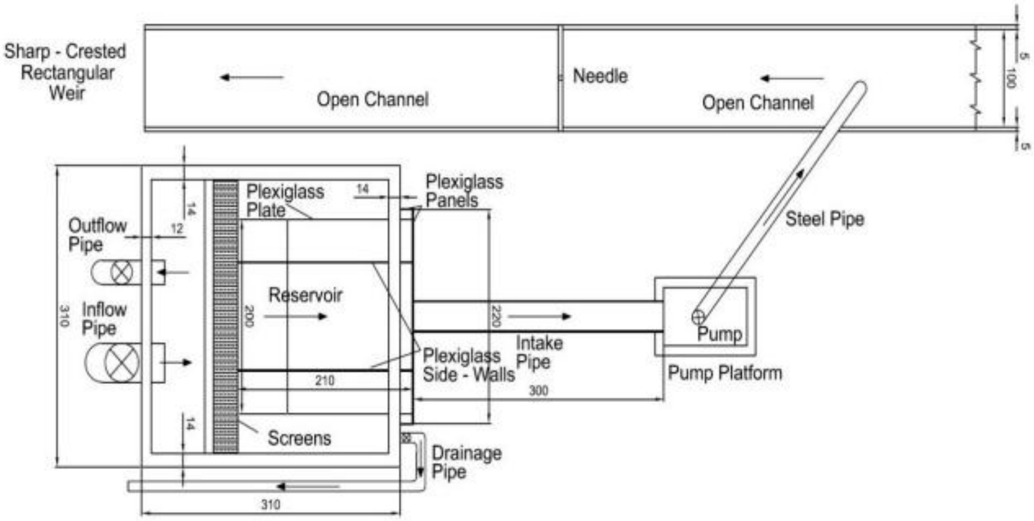

b) Side view

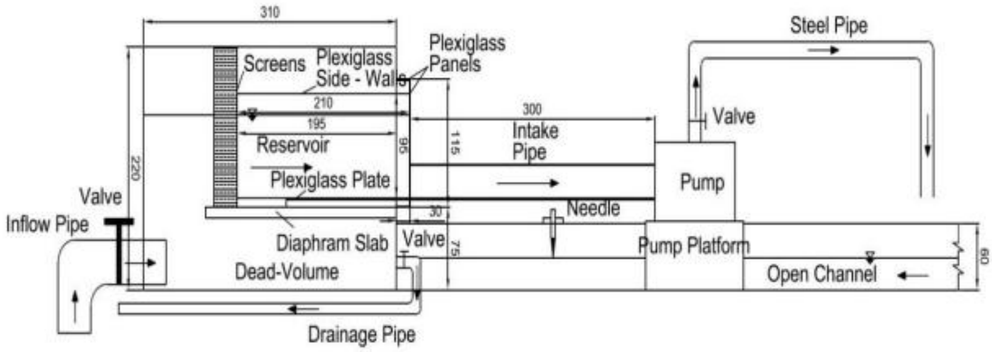

Figure 4.7: Plan of side and top view of the experimental setup [6]

Figure 4.8: General view of the physical model [6]

4.3 METHODOLOGY OF THE EXPERIMENTS CONDUCTED BY BAYKARA, HASPOLAT AND GÖKMENER

In the previous research, the procedures implemented are as follows: To begin the experiment, the reservoir was filled above the critical submergence level. A constant water surface level was obtained in the system by adjusting the inflow and the outflow rates. Observation of the flow conditions for 10 to 20 minutes is essential to ensure that no formation of vortices occurs at this stage. Then the level was decreased gradually, slowly and carefully, by opening a drainage pipe valve until an air-entraining vortex on the free surface is observed. After the formation of the vortex, the water level, location of the vortex and discharge values were measured and recorded. Depending on the experiment, this procedure took 30 minutes to 7 hours.

Repeatability tests were carried out to enhance the critical submergence measurements accuracy. The water level in the reservoir was adjusted and measured on two further occasions to reproduce the conditions at which vortex formation occurred, after recording the initial critical submergence. The average of these three measurements was then taken to represent the final critical submergence value, lower than 5% variation of the critical submergence from the mean for a certain intake discharge was found in this study [34].

4.4 STATISTICAL PERFORMANCE INDICATORS

In order to assess the accuracy and reliability of empirical equations, several statistical performance indicators were employed. These indicators provide a comprehensive assessment of the equation's predictive performance [35].

4.4.1 Coefficient of Determination (correlation) (R^2)

The coefficient of determination (R^2) measures the proportion of the variance in the observed data that is explained by the model. An R^2 value closer to 1 indicates a better fit between the observed and predicted values [36].

$$\mathbf{R^2 = 1 - \frac{\sum_{i=1}^{n}\left(\left(\frac{S_c}{D_i}\right)_{obs,i} - \left(\frac{S_c}{D_i}\right)_{pred,i}\right)^2}{\sum_{i=1}^{n}\left(\left(\frac{S_c}{D_i}\right)_{obs,i} - \overline{\left(\frac{S_c}{D_i}\right)_{obs}}\right)^2}} \tag{4.1}$$

where:

$\left(\frac{S_c}{D_i}\right)_{obs,i}$ = observed (measured) value

$\left(\frac{S_c}{D_i}\right)_{pred,i}$ = predicted (calculated) value

$\overline{\left(\frac{S_c}{D_i}\right)_{obs}}$ = average of observed values

n = the number of data points (observations)

4.4.2 Standard Error of Regression (SER)

The standard error of regression (SER) represents the standard deviation of the residuals (errors) and indicates the typical size of prediction errors made by the model. Lower SER values reflect better model performance.

$$\text{SER} = \sqrt{\frac{\sum_{i=1}^{n}\left(\left(\frac{S_c}{D_i}\right)_{obs,i} - \left(\frac{S_c}{D_i}\right)_{pred,i}\right)^2}{n-2}} \tag{4.2}$$

4.4.3 Mean Absolute Percentage Error (MAPE)

The mean absolute percentage error (MAPE) expresses the prediction error as a percentage and provides a normalized measure of prediction accuracy. A lower MAPE value indicates higher prediction accuracy.

$$\text{MAPE} = \frac{100}{n}\sum_{i=1}^{n}\left|\frac{\left(\frac{S_c}{D_i}\right)_{obs,i} - \left(\frac{S_c}{D_i}\right)_{pred,i}}{\left(\frac{S_c}{D_i}\right)_{obs,i}}\right| \tag{4.3}$$

4.4.4 Average Absolute Deviation (AAD)

The average absolute deviation (AAD) measures the average magnitude of errors in a set of predictions, without considering their direction. Smaller AAD values imply that the model predictions are close to the observed data.

$$\text{AAD}=\frac{1}{n}\sum_{i=1}^{n}\left|\left(\frac{S_c}{D_i}\right)_{obs,i}-\left(\frac{S_c}{D_i}\right)_{pred,i}\right| \tag{4.4}$$

4.4.5 Root Mean Square Error (RMSE)

The root mean square error (RMSE) is another measure of the differences between observed and predicted values. It penalizes larger errors more severely than AAD. A lower RMSE indicates a better predictive capability of the model.

$$\text{RMSE}=\sqrt{\frac{1}{n}\sum_{i=1}^{n}\left(\left(\frac{S_c}{D_i}\right)_{obs,i}-\left(\frac{S_c}{D_i}\right)_{pred,i}\right)^2} \tag{4.5}$$

CHAPTER V

ANALYSIS AND DISCUSSION OF RESULTS

5.1 INTRODUCTION

The study analyzed data from Baykara, Haspolat and Gökmener investigated the effect of flow and geometry properties on critical submergence at the single horizontal intake under symmetrical and asymmetrical approach flow conditions. Moreover, empirical equations varying with approach Froude number, intake Froude number, Reynold number, Weber number and geometrical parameter were derived to predict dimensionless critical submergence, S_C/D_i [3,6,7].

5.2 SYMMETRICAL APPROACH FLOW CONDITIONS

409 experimental data were considered under symmetrical approach flow conditions. The ranges of significant flow and geometric parameters are listed in Table 5.1.

Table 5.1: Ranges of significant hydraulic and geometric parameters analyzed in the study under symmetrical approach flow conditions

D_i (cm)	Range							
	Q_i (lt/s)	S_c/D_i	$(Fr)_{app}$	$(Fr)_i$	Re	We	$2b/D_i$	No. Of Observations
30	64.34 ~ 29.19	1.91 ~ 0.28	0.112 ~ 0.029	0.53 ~ 0.24	273053 ~ 123883	3408 ~ 701	4.67 ~ 1.33	63
26.5	126.83 ~ 77.53	2.08 ~ 1.37	0.067 ~ 0.018	1.43 ~ 0.87	609393 ~ 372496	19215 ~ 7179	10.57 ~ 3.02	21
25	62.55 ~ 24.35	2.43 ~ 0.44	0.111 ~ 0.031	0.81 ~ 0.32	317168 ~ 123419	5561 ~ 842	5.60 ~ 1.60	90
19.4	62.55 ~ 21.69	3.33 ~ 0.64	0.114 ~ 0.034	1.53 ~ 0.53	408721 ~ 141729	11902 ~ 1431	7.22 ~ 2.01	73
14.4	62.55 ~ 21.69	5.24 ~ 1.07	0.133 ~ 0.038	3.23 ~ 1.12	550638 ~ 190941	29102 ~ 3499	9.72 ~ 2.78	67
10	51.65 ~ 17.84	6.65 ~ 1.88	0.123 ~ 0.038	6.64 ~ 2.29	654745 ~ 227213	59251 ~ 7079	12.00 ~ 4.00	67
5	14.69 ~ 5.20	4.42 ~ 1.04	0.115 ~ 0.038	10.68 ~ 3.78	372438 ~ 132522	38343 ~ 4816	20.00 ~ 8.00	28

5.2.1 Variation of S_c/D_i with dimensionless flow and geometric parameters

Variation of dimensionless critical submergence, S_c/D_i, with approach Froude number, $(Fr)_{app}$, intake Froude number, $(Fr)_i$, Reynolds number, Re, and Weber number, We are illustrated in Figures 5.1-5.4, respectively. From Figure 5.1, clear comments cannot be made on the relationship between S_c/D_i and, $(Fr)_{app}$, since the trend of the data is irregular. Consequently, S_c/D_i could be independent of the $(Fr)_{app}$ at single horizontal intakes. Nevertheless, higher peak values of S_c/D_i when the $(Fr)_{app}$ is within the ranges of 0.04 and 0.1 might be attributed to a transitional flow regime.

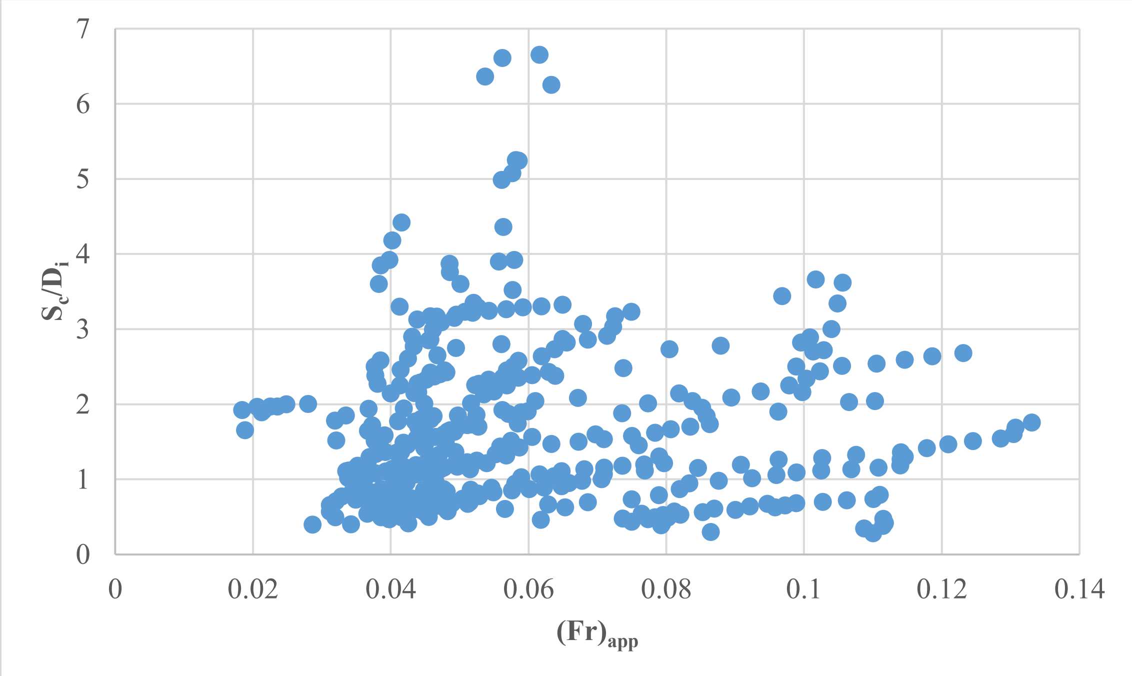

Figure 5.1: Variation of dimensionless critical submergence, S_c/D_i vs. $(Fr)_{app}$ under symmetrical approach flow conditions

According to Figures 5.2-5.4, S_c/D_i elevates constantly with $(Fr)_i$, Re and We increments. However, the increment rate of S_c/D_i slows down with increasing flow parameters and forms a plateau, which reflects a reduction in the impact of energy levels on the system's behavior as inertia becomes dominant.

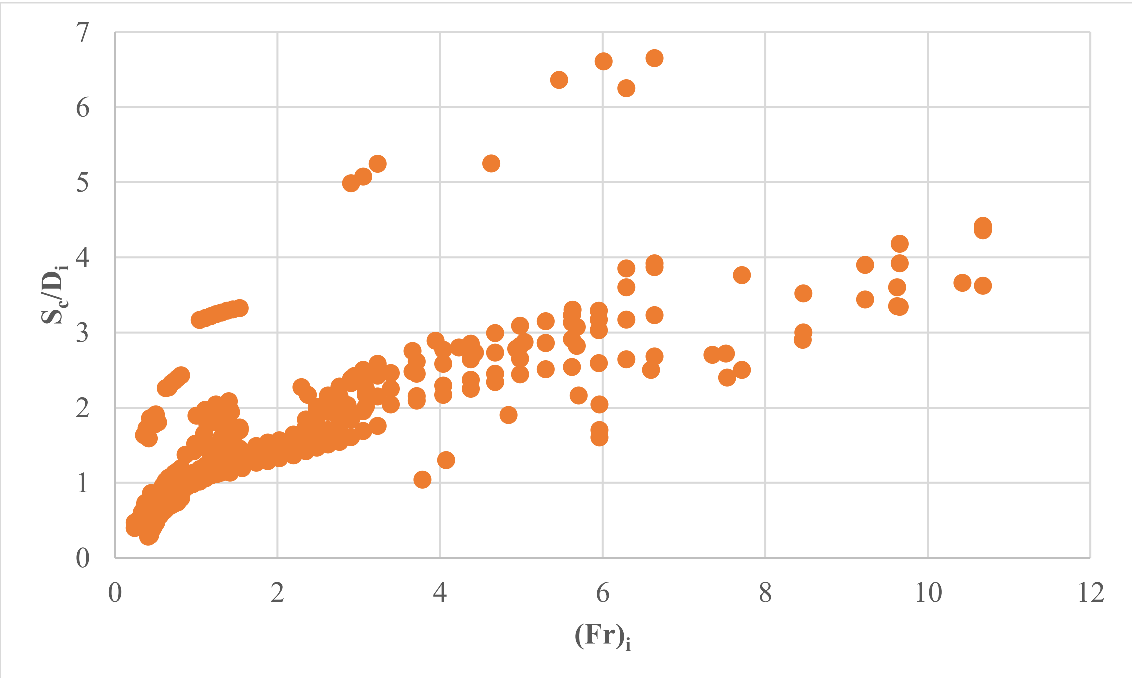

Figure 5.2: Variation of dimensionless critical submergence, S_c/D_i vs. $(Fr)_i$ under symmetrical approach flow conditions

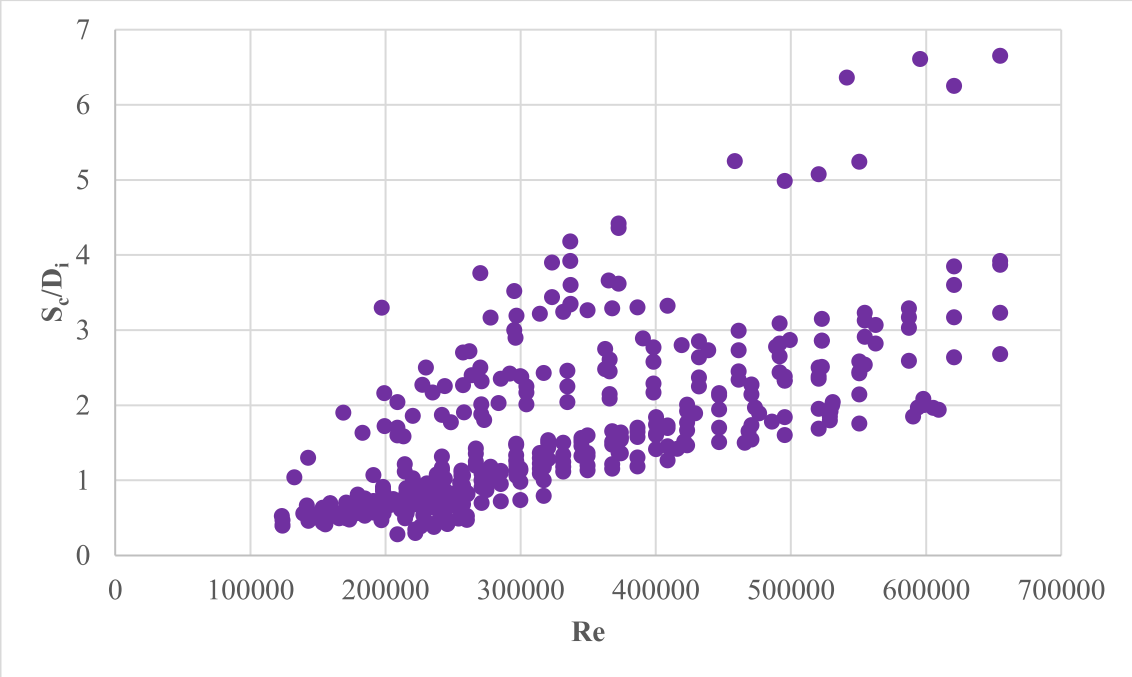

Figure 5.3: Variation of dimensionless critical submergence, S_c/D_i vs. Re under symmetrical approach flow conditions

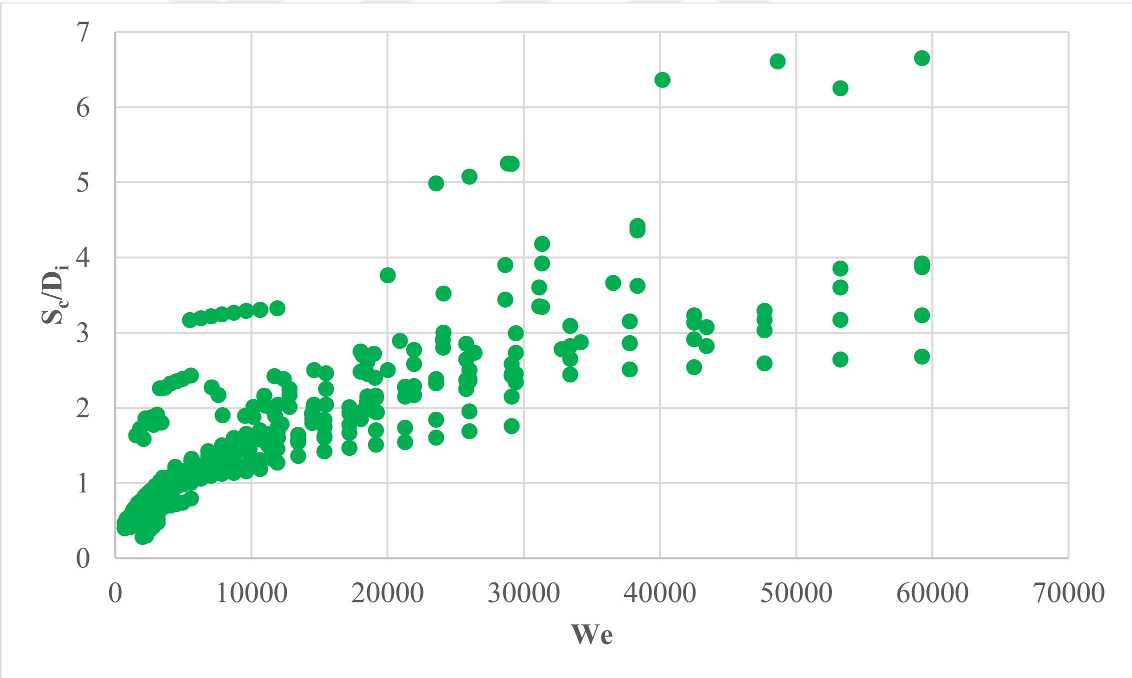

Figure 5.4: Variation of dimensionless critical submergence, S_c/D_i vs. We under symmetrical approach flow conditions

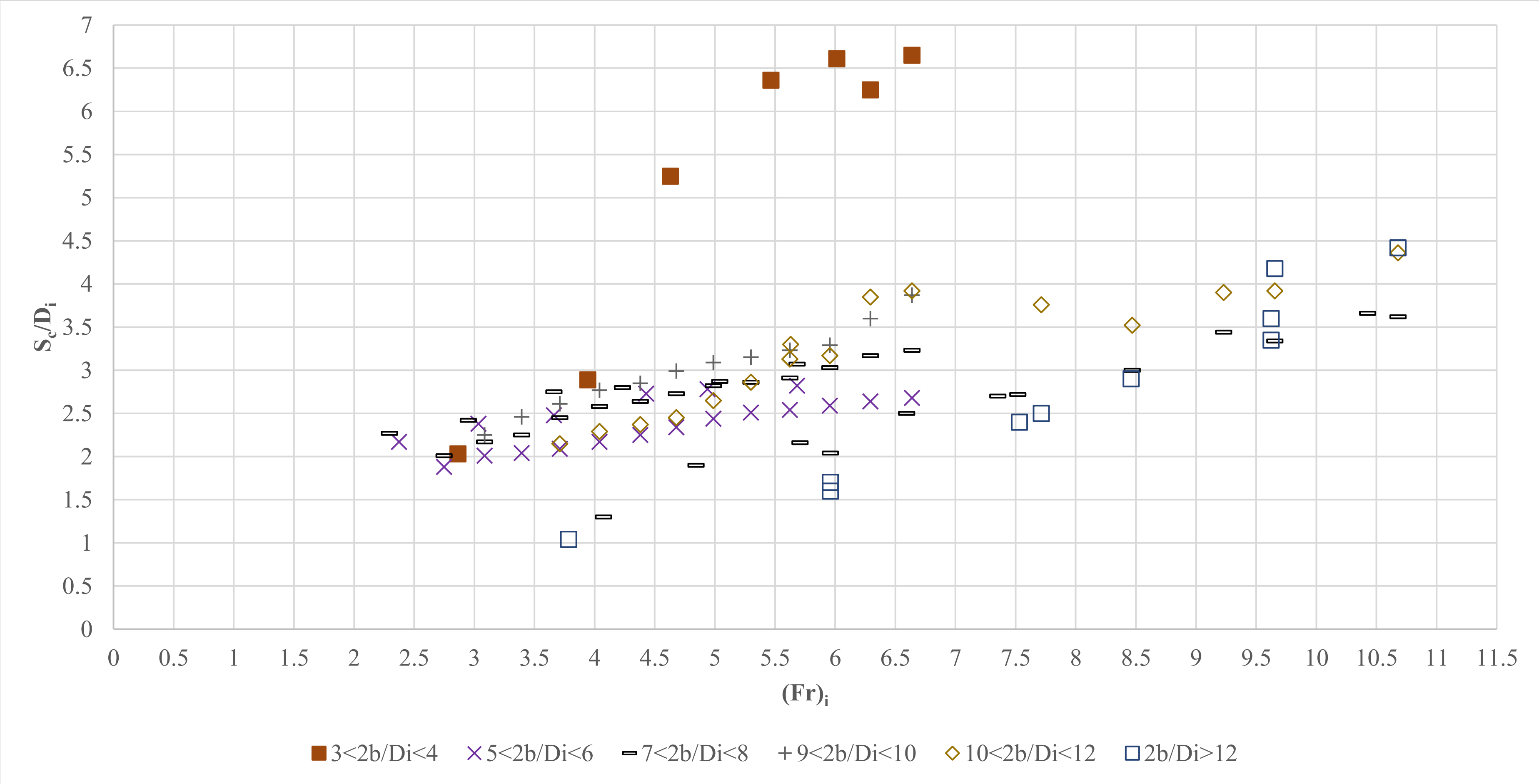

Figure 5.5: Variation of S_c/D_i with $(Fr)_i$ for varying $2b/D_i$ while $D_i \leq$ 10 cm under symmetrical approach flow conditions

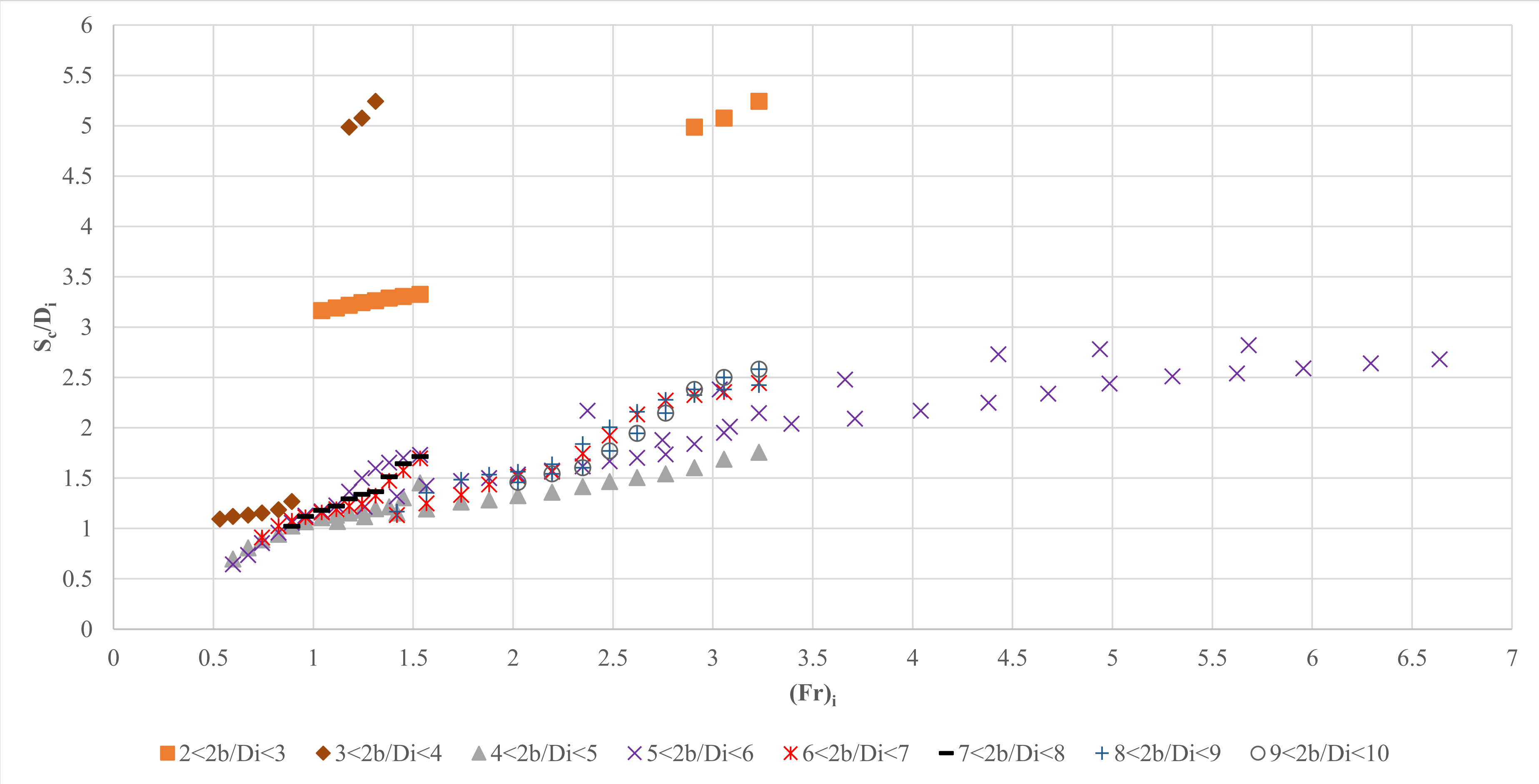

Figure 5.6: Variation of S_c/D_i with $(Fr)_i$ for varying $2b/D_i$ while $10<D_i \leq 20$ cm under symmetrical approach flow conditions

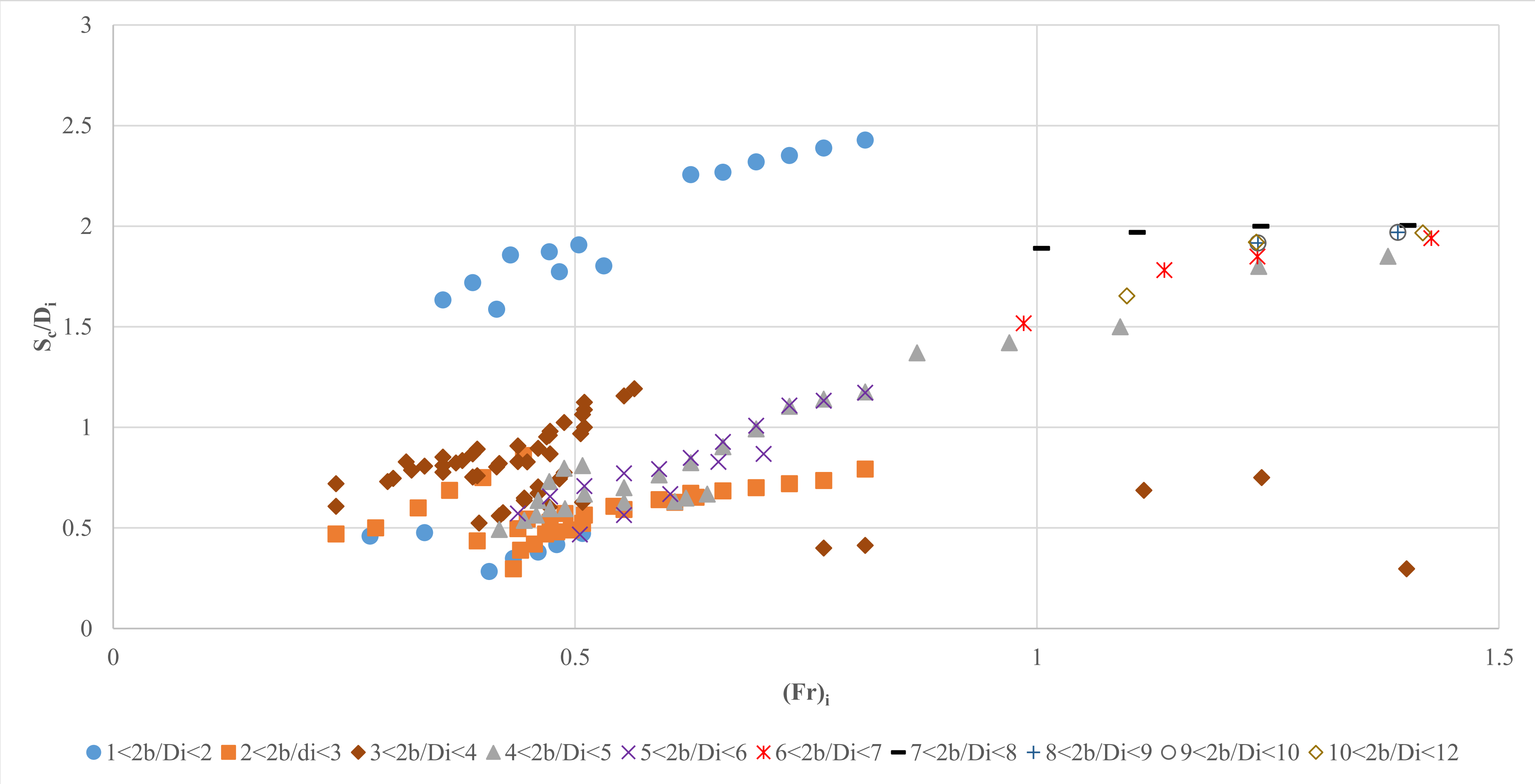

Figure 5.7: Variation of S_c/D_i with $(Fr)_i$ for varying $2b/D_i$ while $D_i \geq 20$ cm under symmetrical approach flow conditions

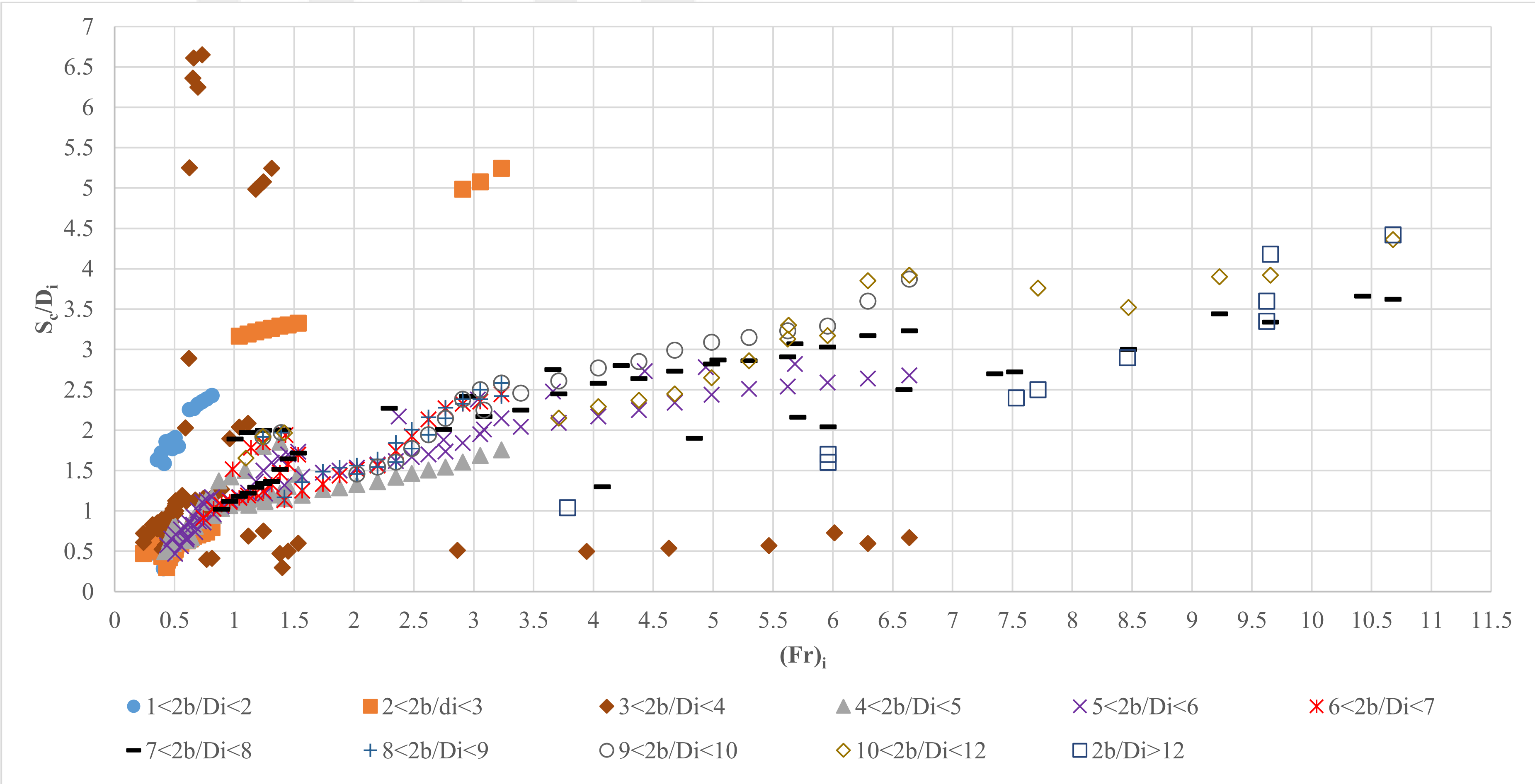

Figure 5.8: Variation of S_c/D_i with $(Fr)_i$ for varying $2b/D_i$ under symmetrical approach flow conditions

5.2.2 Derivation of Empirical Formulas to Predict Dimensionless Critical Submergence, S_c/D_i

In order to predict S_c/D_i for single horizontal intake structures under symmetrical approach flow conditions, 10 empirical equations are derived as a function of $(Fr)_{app}$, $(Fr)_i$, Re, We and $2b/D_i$ with varying combinations. These equations are tabulated in Table 5.2 with their performance indicators as R^2, SER, MAPE, AAD, and RMSE.

Table 5.2: Derived empirical equations with their performance indicators

No	Equation	R^2	SER	MAPE	AAD	RMSE
5.1	$\frac{S_C}{D_i} = (Fr_{app})^{-0.910} (Fr)_i^{0.808} (Re)^{-0.226} (We)^{0.198} \left(\frac{2b}{D_i}\right)^{-0.895}$	0.988	0.118	9.61%	0.089	0.117
5.2	$\frac{S_C}{D_i} = (Fr_{app})^{-0.931} (Fr)_i^{0.982} (Re)^{-0.089} \left(\frac{2b}{D_i}\right)^{-0.937}$	0.984	0.137	11.79%	0.116	0.136
5.3	$\frac{S_C}{D_i} = (Fr_{app})^{-0.522} (Fr)_i^{0.877} \left(\frac{2b}{D_i}\right)^{-0.862}$	0.937	0.272	19.50%	0.219	0.272
5.4	$\frac{S_C}{D_i} = (Fr_{app})^{-0.088} (Fr)_i^{0.502}$	0.675	0.618	26.97%	0.367	0.617
5.5	$\frac{S_C}{D_i} = (Fr_{app})^{-0.162}$	-0.025	1.096	73.66%	0.841	1.095
5.6	$\frac{S_C}{D_i} = (Fr)_i^{0.333} (Re)^{-0.218} (We)^{0.412} \left(\frac{2b}{D_i}\right)^{-0.417}$	0.780	0.510	23.02%	0.343	0.507
5.7	$\frac{S_C}{D_i} = (Fr)_i^{0.687} (Re)^{0.076} \left(\frac{2b}{D_i}\right)^{-0.502}$	0.762	0.530	27.07%	0.385	0.528
5.8	$\frac{S_C}{D_i} = (Fr)_i^{0.560} \left(\frac{2b}{D_i}\right)^{0.056}$	0.621	0.668	19.23%	0.348	0.666
5.9	$\frac{S_C}{D_i} = (Fr)_i^{0.629}$	0.616	0.671	19.44%	0.361	0.671
5.10	$\frac{S_C}{D_i} = 1.261(Fr)_i^{0.505}$	0.660	0.633	26.42%	0.376	0.631

Equation 5.1, which includes all the dependent parameters considered, demonstrates the highest performance with an R^2 value of 0.988, indicating a very strong fit to the data. Its error metrics, including SER (0.118), MAPE (9.61%), AAD (0.089), and RMSE (0.117), are exceptionally low, making it the most reliable and accurate model among the ten equations. Similarly, Equations 5.2 and 5.3, which are derived by excluding We and both Re and We from equation 1, respectively, perform very well with R^2 of 0.984 and 0.937. Since the occurrence of air-entraining vortices is related to open channel flow and highly depends on the turbulence, the effect of Re and We can also be considered as insignificant while predicting critical submergence.

However, equations 5.2 and 5.3 have slightly higher error metrics compared to Equation 5.1, making these equations the second-best choice. Consequently, equations 5.1-5.3 are highly recommended for predicting S_c/D_i as they exhibit strong statistical reliability. Moreover, Equation 5.4, which is derived by excluding the geometry parameter, $2b/D_i$, from Equation 5.3 shows moderate performance in predicting S_c/D_i with R^2 of 0.675 when compared to Equations 5.1- 5.3. This situation is directly proportional by ignoring the geometry of the intake structure when predicting S_c/D_i and it is the evident strong influence of intake geometry on critical submergence.

Moreover, notably, Equation 5.5, which predicts S_c/D_i by only considering the $(Fr)_{app}$ is entirely invalid, with a negative R^2 value of -0.025, indicating it fails to explain the data and cannot be used for predictions. These performance indicators can be explained by the incompatible relationship between S_c/D_i and $(Fr)_{app}$ that is plotted in Figure 5.1 above. Therefore, for single horizontal intakes under symmetrical approach flow conditions, it is obvious that the effect of $(Fr)_{app}$ does not show meaningful insights. By considering the low correlation of $(Fr)_{app}$ with S_c/D_i, Equations 5.1- 5.4 are reevaluated by excluding $(Fr)_{app}$ from these equations and Equations 5.6- 5.8 are derived. Equations 6-8 show moderate results in predicting S_c/D_i with R^2 values of 0.780, 0.762 and 0.621 when compared to Equations 5.1-5.3. Besides that, Equations 5.9 and 5.10 are derived only depending on the $(Fr)_i$, which is the most significant parameter affecting S_c/D_i and show moderate results on predicting critical submergence. Overall, the statistical analysis highlights that Equations 5.1 and 5.2 are the most robust and effective models for predicting dimensionless critical submergence, despite the effects of $(Fr)_i$, Re and We are being less important when compared to $(Fr)_i$ and $2b/D_i$. They should be prioritized in applications where accuracy and reliability are critical. Other equations may be suitable for specific scenarios but generally show weaker performance. The comparison of measured and predicted S_c/D_i values, along with error lines, is plotted in figures 5.9-5.18.

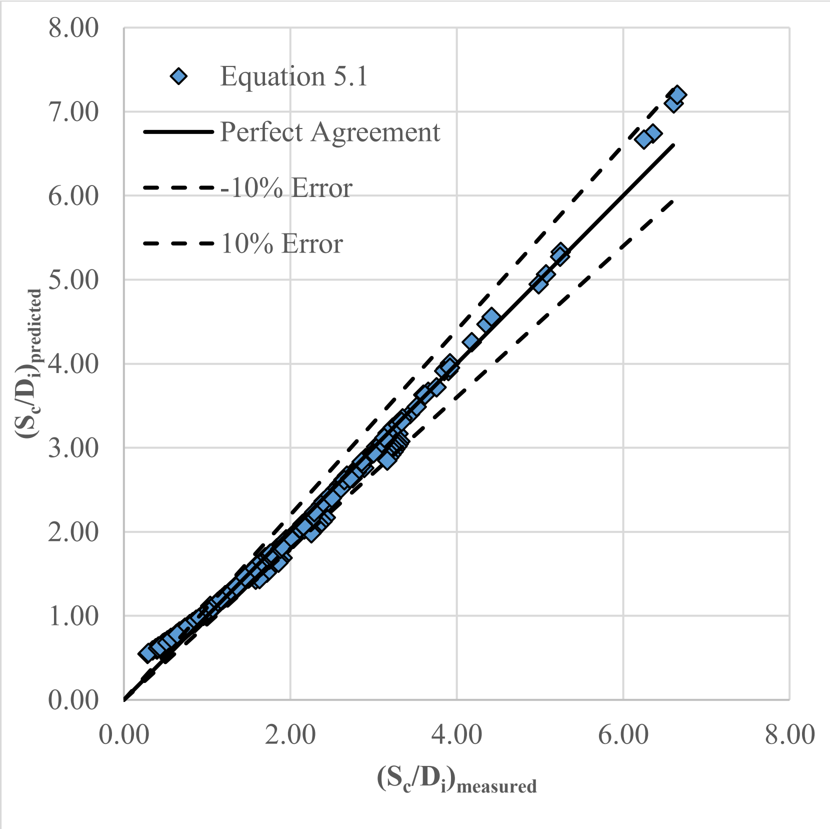

Figure 5.9: Comparison of $(S_c/D_i)_{measured}$ data with $(S_c/D_i)_{predicted}$ data obtained from Equation 5.1 under symmetrical approach flow conditions

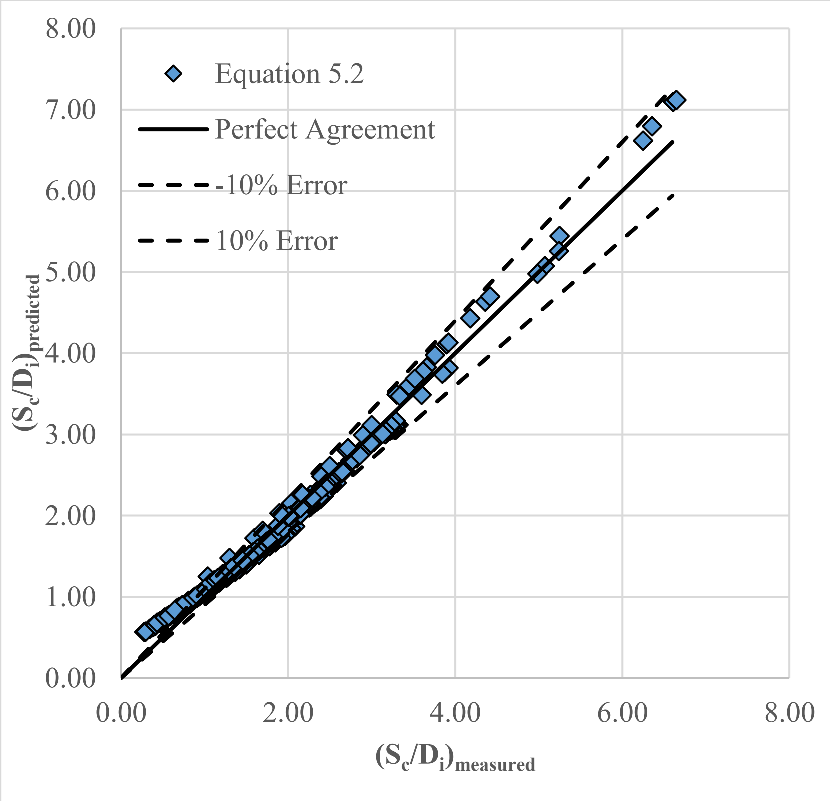

Figure 5.10: Comparison of $(S_c/D_i)_{measured}$ data with $(S_c/D_i)_{predicted}$ data obtained from Equation 5.2 under symmetrical approach flow conditions

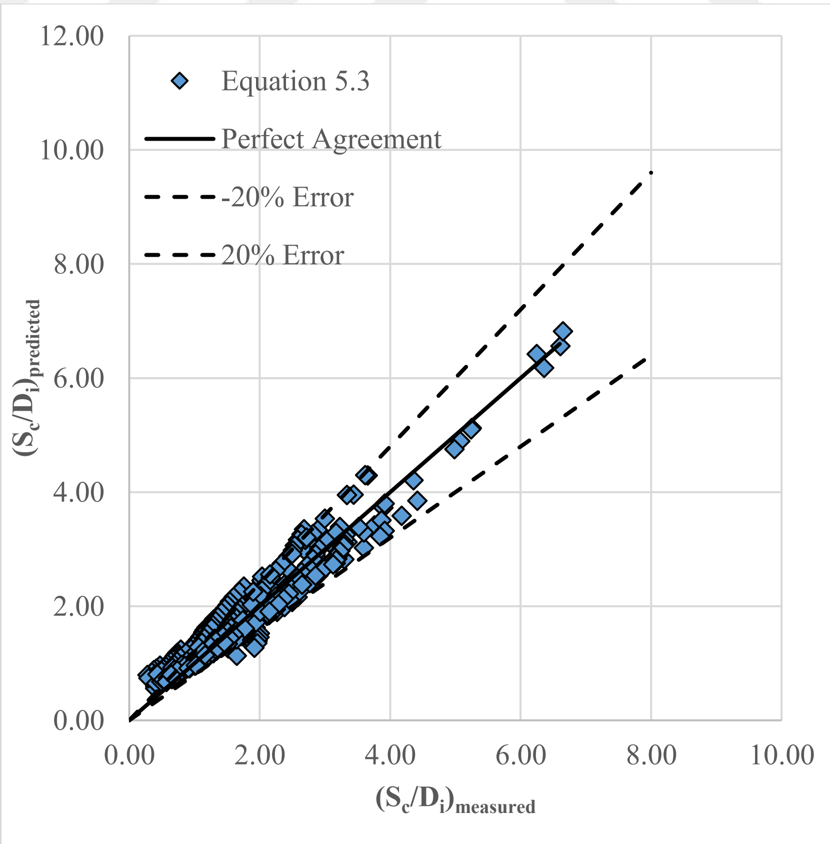

Figure 5.11: Comparison of $(S_c/D_i)_{measured}$ data with $(S_c/D_i)_{predicted}$ data obtained from Equation 5.3 under symmetrical approach flow conditions

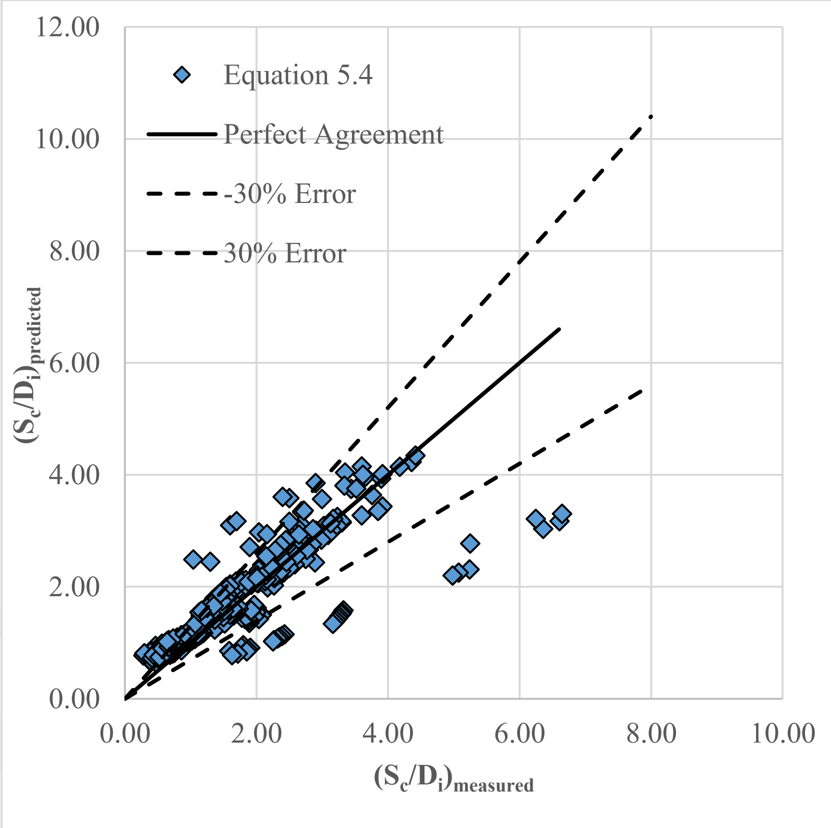

Figure 5.12: Comparison of $(S_c/D_i)_{measured}$ data with $(S_c/D_i)_{predicted}$ data obtained from Equation 5.4 under symmetrical approach flow conditions

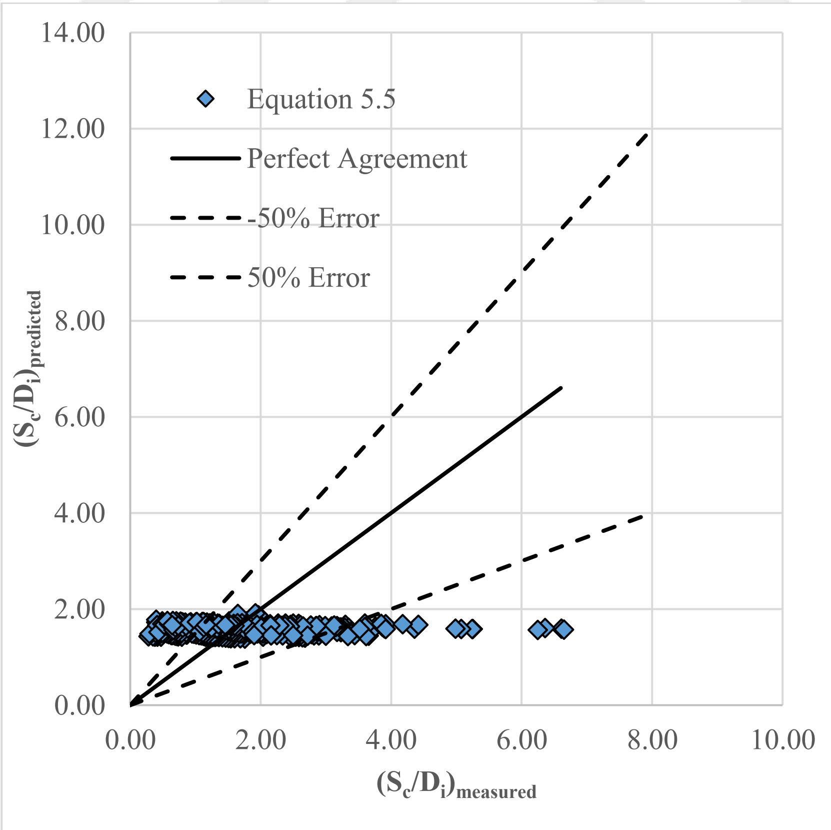

Figure 5.13: Comparison of $(S_c/D_i)_{measured}$ data with $(S_c/D_i)_{predicted}$ data obtained from Equation 5.5 under symmetrical approach flow conditions

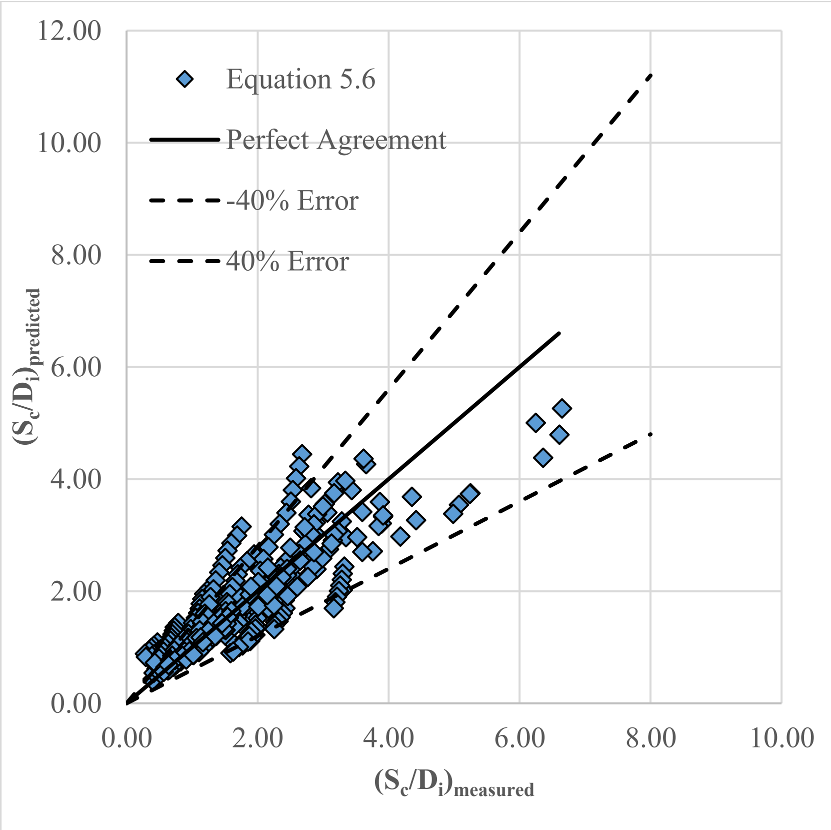

Figure 5.14: Comparison of $(S_c/D_i)_{measured}$ data with $(S_c/D_i)_{predicted}$ data obtained from Equation 5.6 under symmetrical approach flow conditions

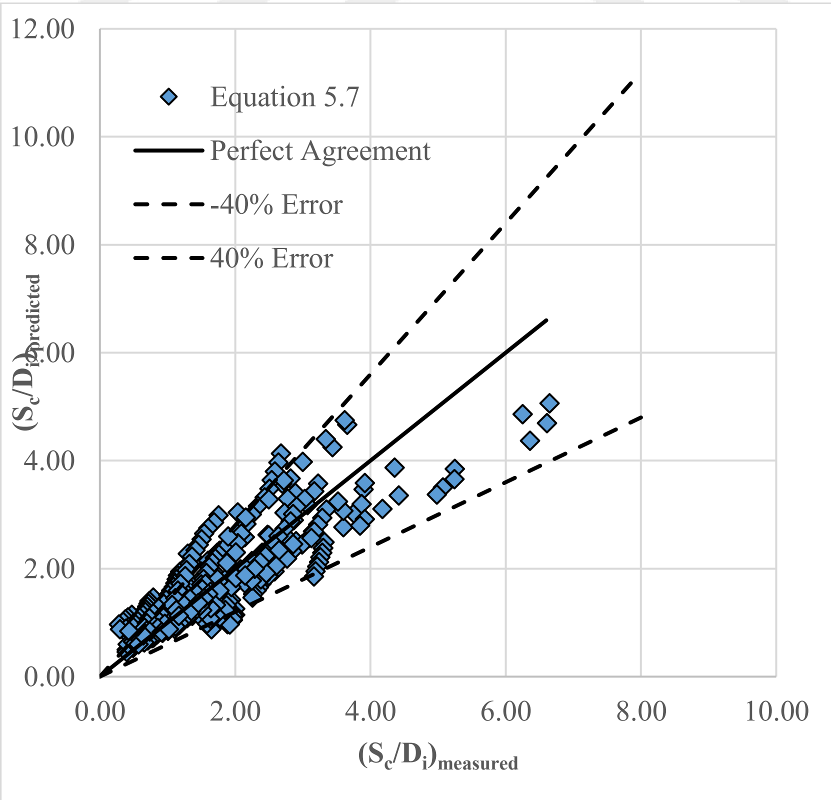

Figure 5.15: Comparison of $(S_c/D_i)_{measured}$ data with $(S_c/D_i)_{predicted}$ data obtained from Equation 5.7 under symmetrical approach flow conditions

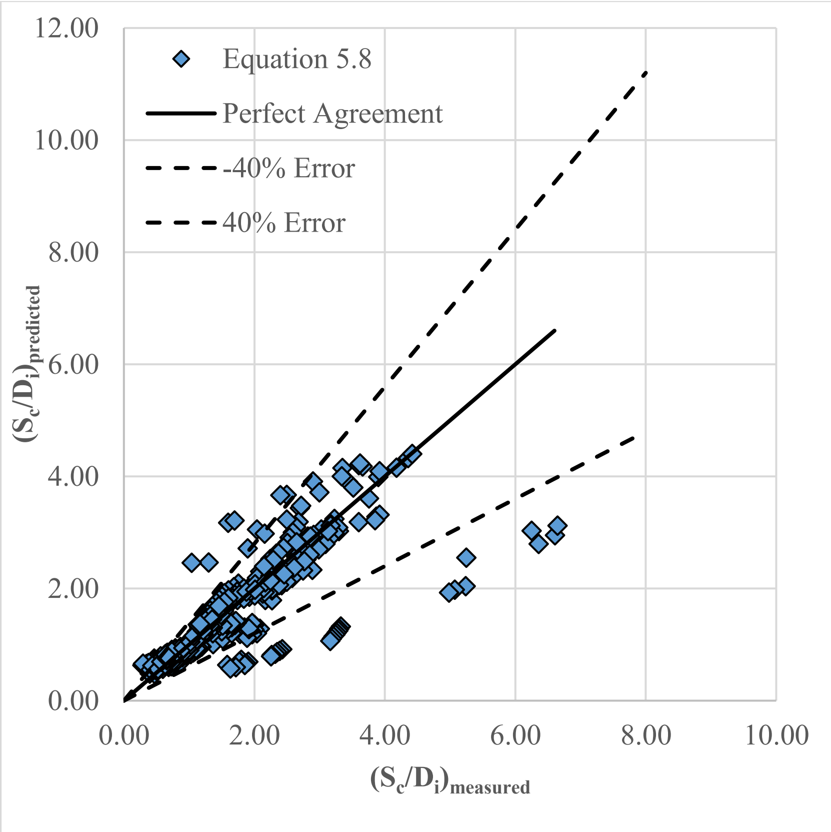

Figure 5.16: Comparison of $(S_c/D_i)_{measured}$ data with $(S_c/D_i)_{predicted}$ data obtained from Equation 5.8 under symmetrical approach flow conditions

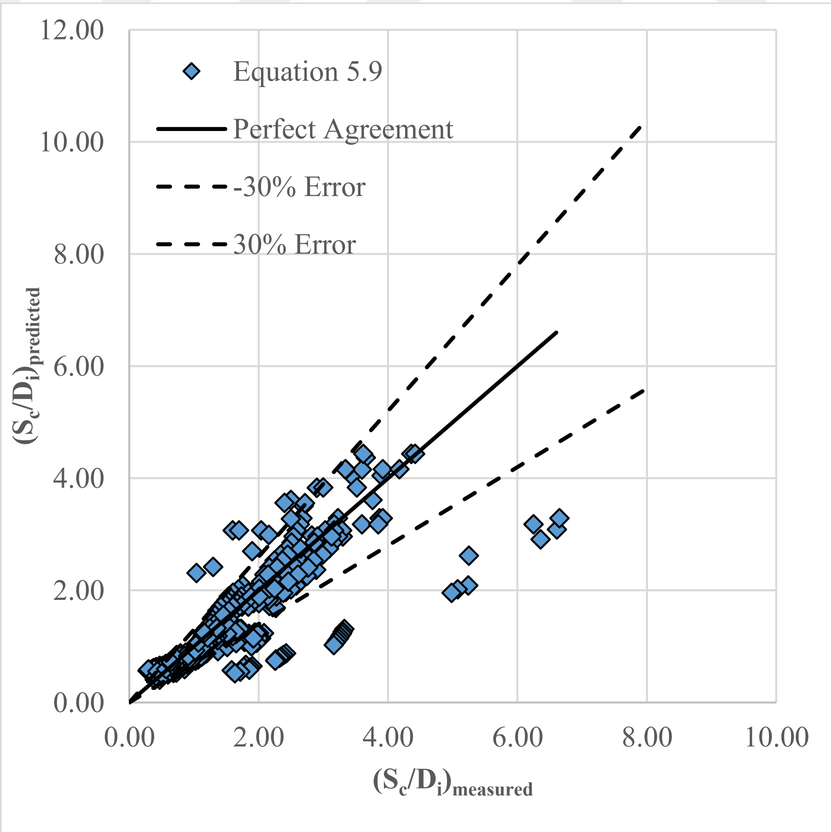

Figure 5.17: Comparison of $(S_c/D_i)_{measured}$ data with $(S_c/D_i)_{predicted}$ data obtained from Equation 5.9 under symmetrical approach flow conditions

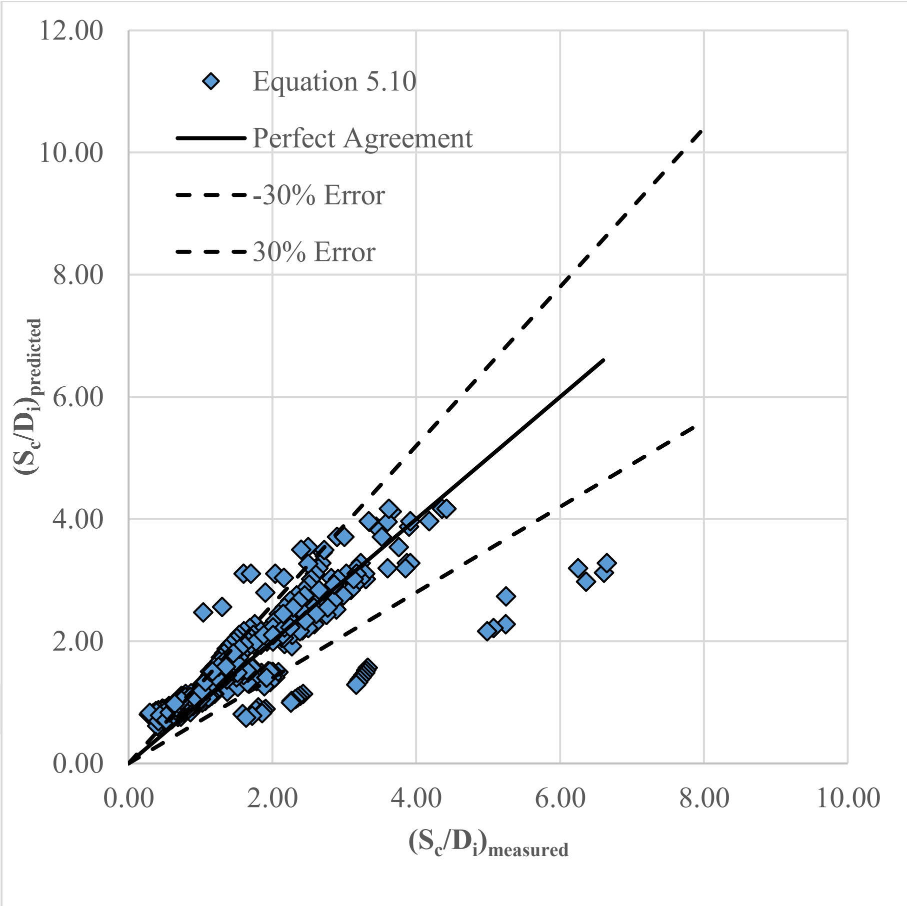

Figure 5.18: Comparison of $(S_c/D_i)_{measured}$ data with $(S_c/D_i)_{predicted}$ data obtained from Equation 5.10 under symmetrical approach flow conditions

5.3 ASYMMETRICAL APPROACH FLOW CONDITIONS

225 experimental data were considered under asymmetrical approach flow conditions. The ranges of significant flow and geometric parameters are listed in Table 5.3.

Table 5.3: Ranges of significant hydraulic and geometric parameters analyzed in the study under asymmetrical approach flow conditions

D_i (cm)	Range							
	Q_i (lt/s)	S_c/Di	$(Fr)_{app}$	$(Fr)_i$	Re	We	ψ	No. Of Observations
30	66.31 ~ 24.95	1.81 ~ 0.41	0.070 ~ 0.029	0.55 ~ 0.21	281439 ~ 105895	3620 ~ 513	3.06 ~ 1.50	32
26.5	126.81 ~ 68.67	2.47 ~ 1.08	0.052 ~ 0.016	1.43 ~ 0.77	609260 ~ 329921	19206 ~ 5632	7.92 ~ 2.01	34
25	52.98 ~ 24.27	1.08 ~ 0.35	0.114 ~ 0.031	0.69 ~ 0.32	268875 ~ 123169	3997 ~ 839	4.46 ~ 1.03	88
10	45.03 ~ 11.63	3.21 ~ 1.29	0.130 ~ 0.032	5.79 ~ 1.50	573617 ~ 148120	45116 ~ 3008	9.17 ~ 2.80	43
5	14.33 ~ 4.07	4.40 ~ 1.32	0.081 ~ 0.034	10.43 ~ 2.96	365146 ~ 103697	36564 ~ 2949	14.40 ~ 5.60	28

5.3.1 Variation of S_c/D_i with dimensionless flow and geometric parameters

Variations of dimensionless critical submergence, S_c/D_i, with approach Froude number, $(Fr)_{app}$, intake Froude number, $(Fr)_i$, Reynolds number, Re, and Weber number, We, are illustrated in Figures 5.19-5.22, respectively. Figure 5.19 presents the relationship between S_c/D_i and $(Fr)_{app}$. For S_c/D_i values lower than 1, S_c/D_i values are almost the same to each other regardless of an increment on the $(Fr)_{app}$. On the other hand, when S_c/D_i values are greater than 1, the relationship between S_c/D_i and $(Fr)_{app}$ becomes complex under asymmetrical approach flow conditions as well as symmetrical approach flow conditions. The data points display a relatively stable trend, with S_c/D_i values greater than 1 while $(Fr)_{app}<0.07$, where S_c/D_i values generally tend to increase with increasing $(Fr)_{app}$. However, when $(Fr)_{app}$ values are greater than 0.05, the variability in critical submergence becomes more pronounced, indicating a potential influence of additional governing parameters, such as intake geometry or asymmetric flow conditions. The absence of a clear monotonic trend suggests that the relationship between these parameters under asymmetrical approach flow conditions is non-trivial, likely governed by complex hydrodynamic interactions rather than a simple functional dependence similar to the symmetrical approach flow conditions.

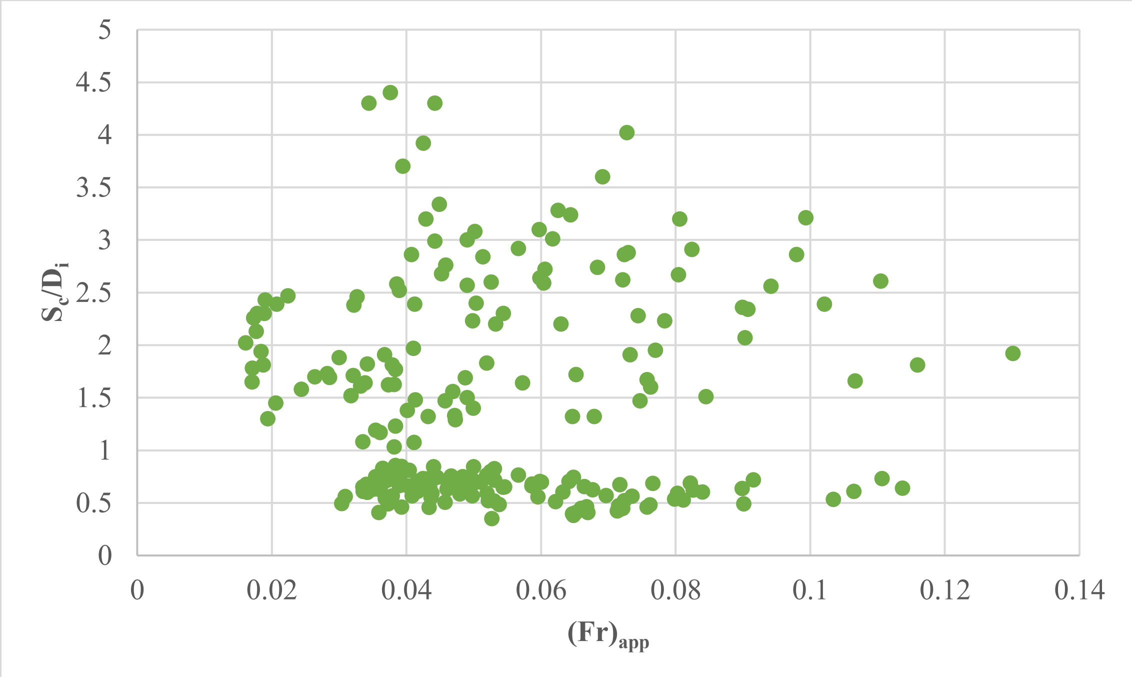

Figure 5.19: Variation of dimensionless critical submergence, S_c/D_i vs. $(Fr)_{app}$ under asymmetrical approach flow conditions

The correlations between S_c/D_i and intake Froude number, $(Fr)_i$, Reynolds number, Re, and Weber number, We, are illustrated in Figures 5.20-5.22, respectively. In Figures 5.20-5.21, S_c/D_i generally increases with $(Fr)_i$, showing a scattered but upward trend, particularly for $(Fr)_i$ values above 2. Conversely, it is possible to mention that S_c/D_i values generally increase with the increment of Re, especially when S_c/D_i values are lower than 1 or Re values are greater than 300000. However, for the Re values greater than 200000 and S_c/D_i values greater than 1, a transition zone is observed, and the spread of data shows an irregular distribution. Obtaining smaller S_c/D_i values where the Re values are smaller than 200000 can be explained by relatively low turbulence and high stability of the approach flow caused by larger sidewall clearances or large intake pipe diameters, where the intake velocity is small.

However, when Reynolds number exceeds 200000, the turbulence becomes more significant along with the geometrical considerations such as sidewall clearance, intake pipe diameter and asymmetry degree on critical submergence. Thus, strong increments are obtained for S_c/D_i values with increasing Reynolds numbers.

Finally, Figure 5.22, which presents the relationship between S_c/D_i and We demonstrates a similar trend to Figure 5.20, where higher We values correspond to greater S_c/D_i values. Across figures 5.20-5.22, a lower S_c/D_i value indicates small flow parameter values, suggesting a regime where submergence remains relatively low before increasing with flow intensity. The variability of S_c/D_i values for given $(Fr)_i$, Re and We, particularly at intermediate values, indicates the influence of additional governing factors such as turbulence, surface tension effects, or asymmetric intake conditions.

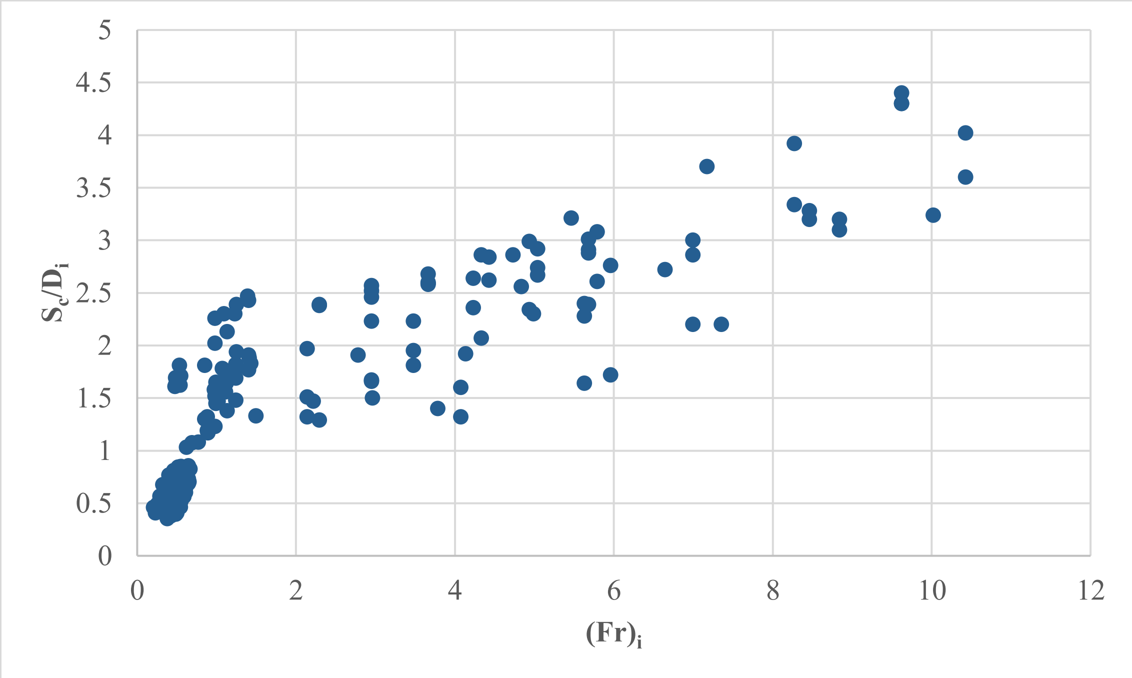

Figure 5.20: Variation of dimensionless critical submergence, S_c/D_i vs. $(Fr)_i$ under asymmetrical approach flow conditions

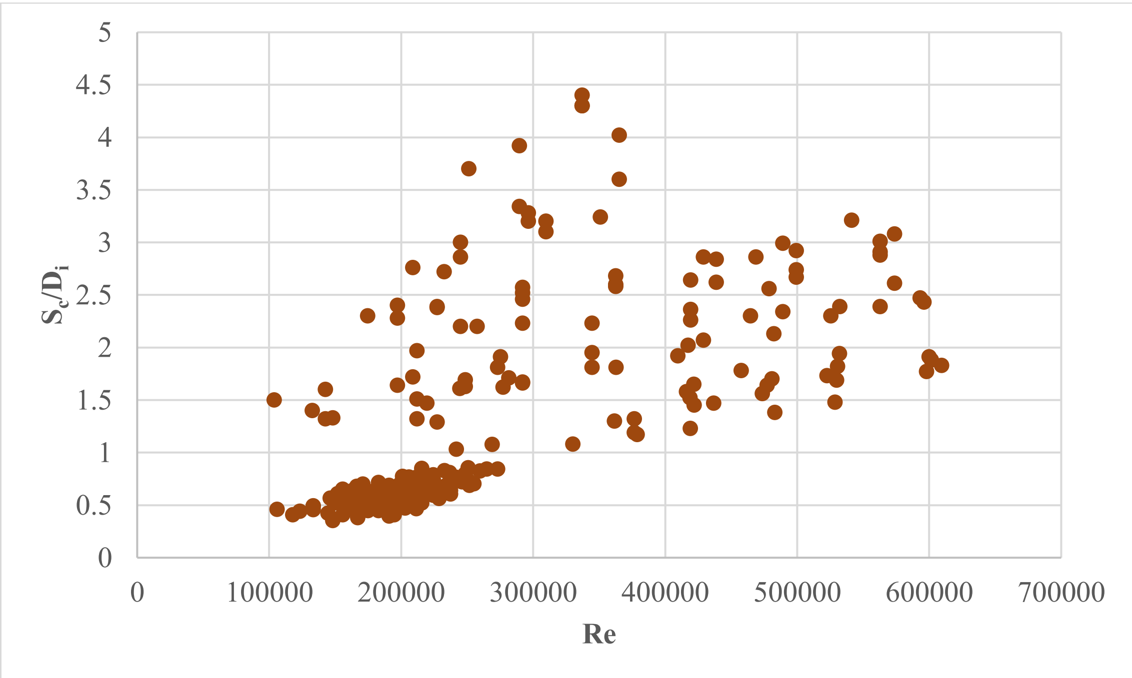

Figure 5.21: Variation of dimensionless critical submergence, S_c/D_i vs. Re under asymmetrical approach flow conditions

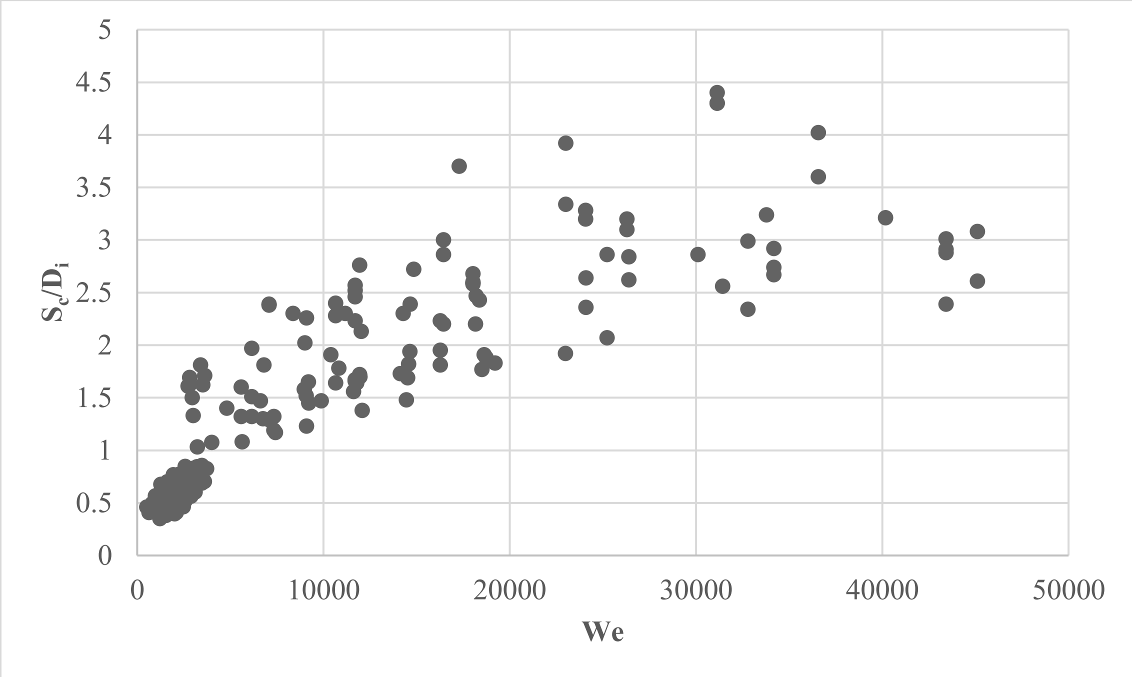

Figure 5.22: Variation of dimensionless critical submergence, S_c/D_i vs. We under asymmetrical approach flow conditions

Figure 5.23 illustrates the variation of S_C/D_i as a function of the $(Fr)_i$ for varying dimensionless geometric parameter, ψ, values while $D_i \leq 10$ cm. From the figure, it can be clearly seen that as the $(Fr)_i$ increases, S_C/D_i also increases under asymmetrical approach flow conditions as well as symmetrical approach flow conditions. This indicates that higher-energy flow conditions require greater submergence to avoid any air-entraining vortices from forming at the intake. In other words, greater $(Fr)_i$ values correspond to stronger inertial forces, increasing the tendency for vortex formation.

Consequently, a greater submergence depth is required to suppress vortex formation, thereby ensuring stable flow conditions at the intake. The geometric parameter ψ, defined as $\psi = (b_1 + b_2)(b_1/b_2)/D_i$, accounts for the sidewall clearance and the asymmetric degree of the intake structure. Greater ψ values indicate wider or lower asymmetric intake structures, influencing flow convergence and vortex development. A detailed analysis of the data reveals that for small ψ values ($2 < \psi < 5$), the corresponding S_C/D_i values are relatively low, and these points are predominantly observed at lower $(Fr)_i$ values than 6. This suggests that narrower intake structures require lower submergence in low-energy flow conditions. On the other hand, greater ψ values ($\psi > 5$) are observed within the range of all tested $(Fr)_i$ values ($1.5 < (Fr)_i < 10.5$) This scattered trend may be explained because of the reduced asymmetry, leading to relatively weaker vortices on the approach flow conditions, which leads formation of air-entraining vortices even at relatively lower $(Fr)_i$ values. While $(Fr)_i$ values are smaller than 6, S_C/D_i values generally increase with increasing ψ value within the range of $2 < \psi < 5$. However, for ψ values exceeding 5, S_C/D_i values are independent of intake geometry because of the aforementioned situation. On the contrary, for $(Fr)_i$ values greater than 6, the development of air-entraining vortices is observed for only ψ values greater than 5. In this range, the general trend shows that as ψ values are increased S_C/D_i values are increasing for a given $(Fr)_i$ value.

Variation of S_c/D_i with $(Fr)_i$ for varying ψ while $D_i > 10$ cm under asymmetrical approach flow conditions is demonstrated in Figure 5.24. While $(Fr)_i$ values are smaller than 0.8, the formation of air-entraining vortices is observed for the narrower sidewall clearances ($1 < \psi < 5$). On the other hand, for the ψ values greater than 5, air-entraining vortices occur for the $(Fr)_i$ values greater than 0.8. For the cases of $(Fr)_i < 0.5$ and $\psi < 5$, S_c/D_i values are close to each other for a given $(Fr)_i$. Therefore, this situation indicates that the effect of intake geometry is low compared to the intake Froude number for smaller $(Fr)_i$ values. However, when $(Fr)_i$ values exceed 0.8, S_c/D_i values increase with increasing ψ for a given $(Fr)_i$. As the only exception, the obtained S_c/D_i values for $\psi > 6$ fall at similar points with the obtained S_c/D_i values for $2 < \psi < 4$ and lower points with the S_c/D_i values for $4 < \psi < 6$ for a given $(Fr)_i$. This situation can be explained by the decreased effect of sidewall clearances as the sidewall clearance increases. As the distance between the intake and the sidewalls increases, the flow separations occurring along the sidewalls dissipate before reaching the intake entrance, thereby reducing the likelihood of vortex formation. Moreover, as the sidewall clearance increases, the approach flow area becomes wider, which weakens the rotational characteristics of the flow. Thus, the air-entraining vortices occur at lower submergence for wider sidewall clearances after a limit for a given $(Fr)_i$.

The relationship between S_c/D_i and $(Fr)_i$ for varying ψ values for all tested intake pipe diameters is demonstrated in Figure 5.25. The graph reveals a generally positive correlation between the S_c/D_i and $(Fr)_i$. As $(Fr)_i$ increases, so does S_c/D_i, indicating that higher flow energy necessitates greater submergence depths to avoid the formation of air-entraining vortices. This trend is physically consistent, as higher intake Froude numbers imply stronger inertial forces, which intensify surface disturbances and increase the potential for vortex formation. Consequently, higher submergence is required to maintain intake efficiency and suppress vortex development. The influence of geometry is clearly illustrated through the classification of data by the dimensionless geometric parameter ψ. At low ψ values (i.e., $1< \psi <2$), which correspond to narrower sidewall clearances, the data show relatively high S_c/D_i values even at low and $(Fr)_i$ values. This suggests that narrower geometries promote stronger vortex activity due to more pronounced sidewall effects, resulting in the earlier onset of air entrainment. Under such conditions, a higher submergence depth is necessary to mitigate vortex formation. In the intermediate range of ψ (approximately $2 < \psi < 6$), both hydraulic and geometric influences appear to interact more dynamically. Data in this range show greater dispersion, indicating that in addition to $(Fr)_i$ and ψ, other flow parameters such as the Reynolds and Weber numbers may also play a role in determining critical submergence. This variability suggests that moderate geometries are more sensitive to changes in secondary hydraulic factors. For greater values of ψ (i.e., $\psi > 8$), which represent wider sidewall clearances, the observed (S_c/D_i) values tend to be lower, even at greater $(Fr)_i$ values. This trend reflects improved flow stability associated with broader approach flow zones. In such configurations, the distance between the intake and the sidewalls reduces the impact of boundary layer separation near the walls. As a result, separation vortices dissipate before reaching the intake entrance, minimizing their contribution to vortex formation.

Additionally, greater sidewall spacing provides a wider approach flow area, which weakens the rotational component of the flow and suppresses vortex strength. Physically, narrow geometries cause the flow to closely interact with sidewalls, where boundary layer separation is more likely to generate coherent rotational structures near the intake. These vortices can evolve into air-entraining vortices if the submergence is insufficient. However, when the distance between the intake and the sidewalls increases, these flow separations dissipate before affecting the intake. Moreover, wider geometries allow the approach flow to develop more uniformly and symmetrically, thereby reducing the intensity and likelihood of vortex formation. Consequently, lower submergence depths are sufficient to maintain stable operation under these conditions. In summary, the graph provides a comprehensive depiction of how both hydraulic conditions and structural geometry influence critical submergence. These findings prove the importance of considering sidewall clearance in the design of horizontal intake structures. Wider geometries not only reduce the risk of vortex formation but also enable more efficient and stable hydraulic performance by lowering the submergence requirement under asymmetrical approach flow conditions.

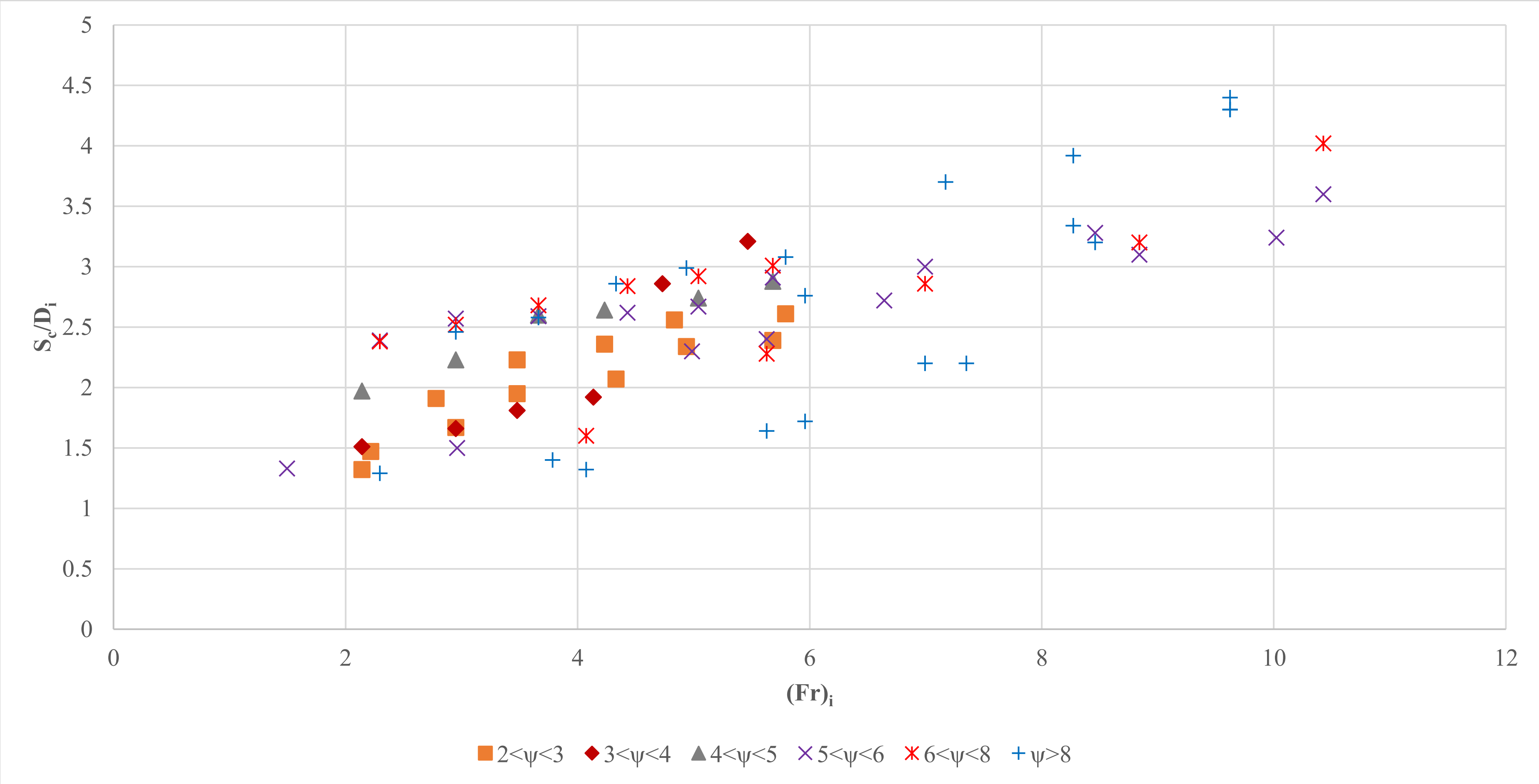

Figure 5.23: Variation of S_c/D_i with $(Fr)_i$ for varying ψ while $D_i \leq$ 10 cm under asymmetrical approach flow conditions

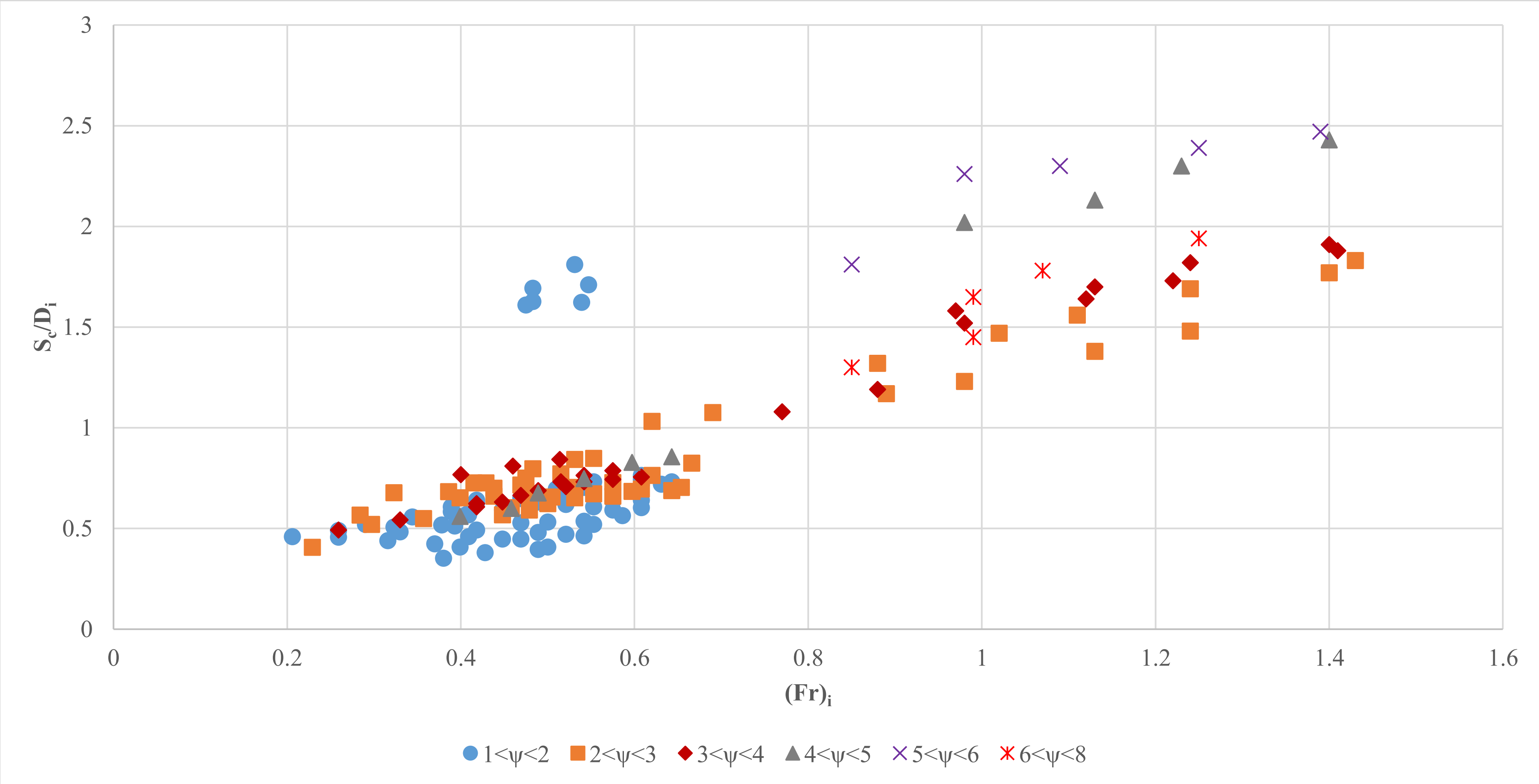

Figure 5.24: Variation of S_c/D_i with $(Fr)_i$ for varying ψ while D_i> 10 cm under asymmetrical approach flow conditions

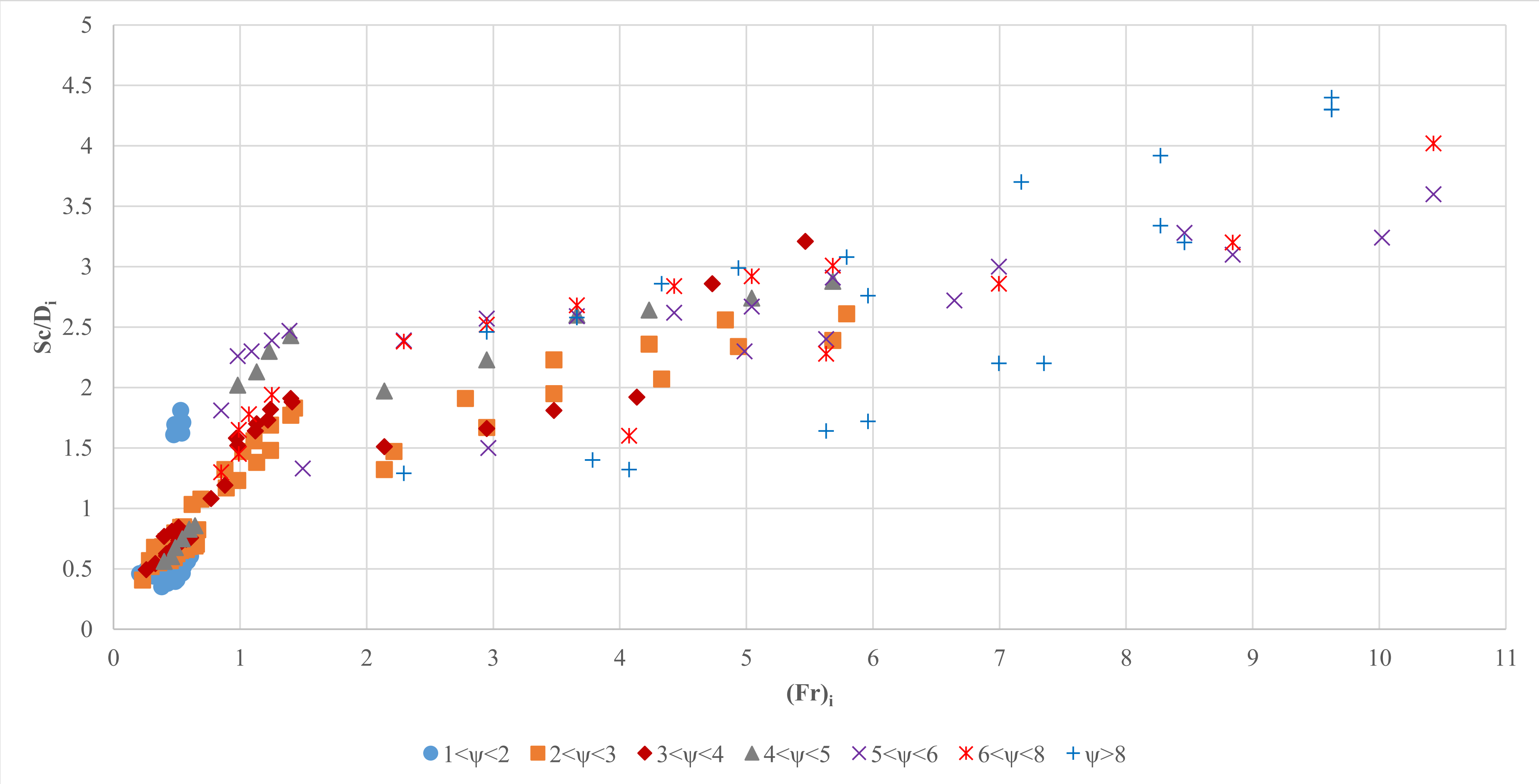

Figure 5.25: Variation of S_c/D_i with (Fr)i for varying ψ under asymmetrical approach flow conditions

5.3.2 Derivation of Empirical Formulas to Predict Dimensionless Critical Submergence, S_c/D_i

In order to predict S_c/D_i for single horizontal intake structures under asymmetrical approach flow conditions, 10 empirical equations are derived as a function of $(Fr)_{app}$, $(Fr)_i$, Re, We and ψ with varying combinations. These equations are tabulated in Table 5.4 with their performance indicators as R^2, SER, MAPE, AAD, and RMSE.

Table 5.4: Derived empirical equations with their performance indicators

No	Equation	R^2	SER	MAPE	AAD	RMSE
5.11	$\frac{S_C}{D_i} = \left(Fr_{app}\right)^{-0.488}(Fr)_i^{0.214}(Re)^{-0.488}(We)^{0.576}(\psi)^{-0.158}$	0.949	0.220	11.98%	0.149	0.218
5.12	$\frac{S_C}{D_i} = \left(Fr_{app}\right)^{-0.589}(Fr)_i^{0.696}(Re)^{-0.102}(\psi)^{-0.313}$	0.895	0.316	22.04%	0.243	0.314
5.13	$\frac{S_C}{D_i} = \left(Fr_{app}\right)^{-0.093}(Fr)_i^{0.508}(\psi)^{-0.061}$	0.847	0.381	29.74%	0.310	0.378
5.14	$\frac{S_C}{D_i} = \left(Fr_{app}\right)^{-0.067}(Fr)_i^{0.479}$	0.846	0.382	29.47%	0.308	0.380
5.15	$\frac{S_C}{D_i} = \left(Fr_{app}\right)^{-0.118}$	0.002	0.969	83.55%	0.820	0.967
5.16	$\frac{S_C}{D_i} = (Fr)_i^{-0.089}(Re)^{-0.459}(We)^{0.665}(\psi)^{0.201}$	0.904	0.303	16.28%	0.209	0.300
5.17	$\frac{S_C}{D_i} = (Fr)_i^{0.457}(Re)^{0.009}(\psi)^{0.062}$	0.833	0.398	27.85%	0.308	0.395
5.18	$\frac{S_C}{D_i} = (Fr)_i^{0.443}(\psi)^{0.133}$	0.829	0.402	25.00%	0.297	0.401
5.19	$\frac{S_C}{D_i} = (Fr)_i^{0.576}$	0.801	0.433	19.31%	0.291	0.432
5.20	$\frac{S_C}{D_i} = 1.182\ (Fr)_i^{0.493}$	0.827	0.405	27.53%	0.313	0.403

In Table 5.4, a comparative assessment of various empirical equations developed to predict the dimensionless critical submergence, S_c/D_i, for horizontal intake structures under asymmetrical approach flow conditions. Each equation incorporates different combinations of hydraulic and geometric parameters such as the $(Fr)_{app}$, $(Fr)_i$, Re, We and ψ. Their predictive performances are evaluated using several statistical indicators, including the correlation coefficient (R^2), standard error of regression (SER), mean absolute percentage error (MAPE), average absolute deviation (AAD), and root mean square error (RMSE). Among all equations, Equation 5.11 exhibits the highest predictive accuracy with an R^2 value of 0.949 and minimal error metrics (SER = 0.220, MAPE = 11.98%, RMSE = 0.218). This equation includes a comprehensive set of parameters: $(Fr)_{app}$, $(Fr)_i$, Re, We and ψ, indicating that a full representation of both flow dynamics and geometrical configuration enhances the equation's reliability. Similarly, Equation 5.16 also shows robust performance (R^2=0.904), and includes $(Fr)_i$, Re, We and ψ, making it a practical yet accurate alternative. These models reinforce the notion that the inclusion of multiple flow and geometry-related variables significantly improves the prediction of critical submergence. In contrast, equation 5.15, which relies solely on the approach Froude number, $(Fr)_{app}$, yields an extremely low R^2 value of 0.002, indicating that $(Fr)_{app}$ alone has negligible explanatory power for predicting S_c/D_i. Even Equation 5.14, which involves $(Fr)_{app}$ and $(Fr)_i$ achieves only moderate accuracy (R^2=0.846) and relatively high MAPE and RMSE values. These results suggest that while the approach Froude number may have a minor supplementary role, it is not sufficient on its own to model vortex-induced submergence behavior accurately.

Equations 5.19 and 5.20, which include only $(Fr)_i$, yield R^2 values of 0.801 and 0.827, respectively. These moderate but acceptable performance metrics suggest that the intake Froude number is the single most influential parameter when predicting critical submergence, likely due to its direct relationship with the inertial forces at the intake entrance. Nevertheless, these simpler models, while useful in practice, may not be adequate in scenarios involving complex flow or geometrical interactions. As a summary, the analysis clearly highlights that incorporating a comprehensive set of parameters, particularly $(Fr)_i$, Re, We and ψ, significantly enhances the accuracy of empirical formulations for predicting dimensionless critical submergence.

While simpler models may be easier to implement, their reduced predictive power limits their applicability in high-precision engineering contexts. Equation 11, by capturing the key physical mechanisms governing vortex formation, stands out as the most reliable and generalizable model for design and analysis purposes. The comparison of measured and predicted S_c/D_i values along with error lines are plotted in Figures 5.26-5.35.

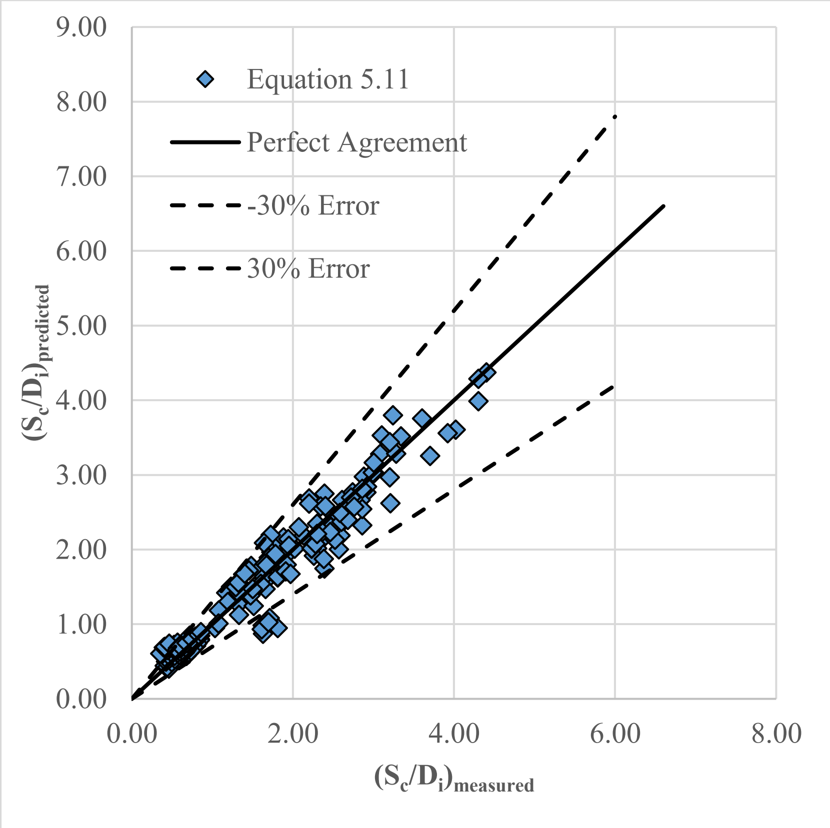

Figure 5.26: Comparison of $(S_c/D_i)_{measured}$ data with $(S_c/D_i)_{predicted}$ data obtained from Equation 5.11 under asymmetrical approach flow conditions

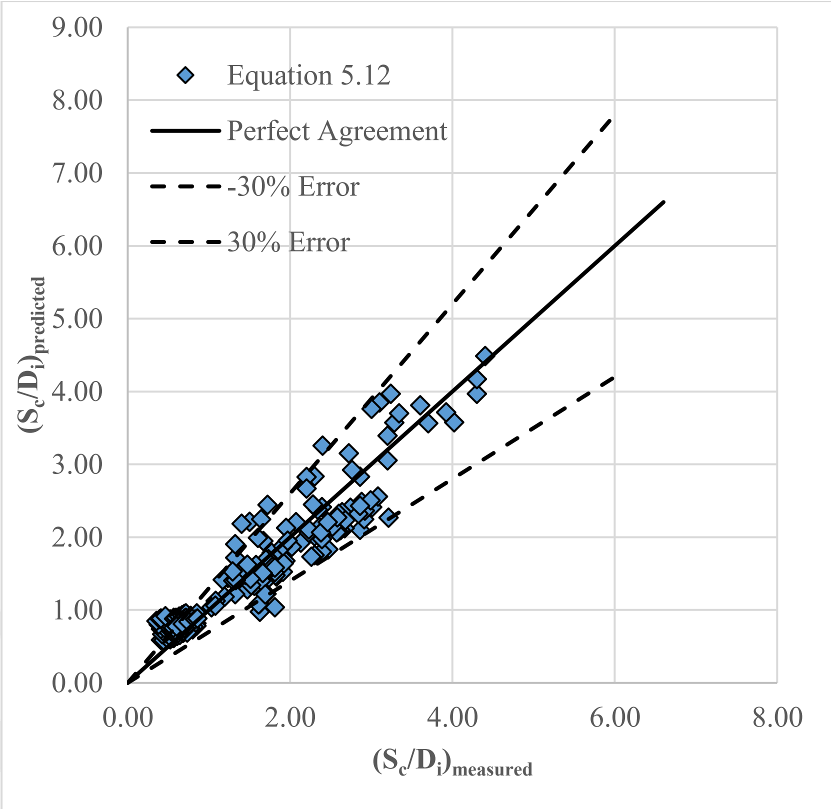

Figure 5.27: Comparison of $(S_c/D_i)_{measured}$ data with $(S_c/D_i)_{predicted}$ data obtained from Equation 5.12 under asymmetrical approach flow conditions

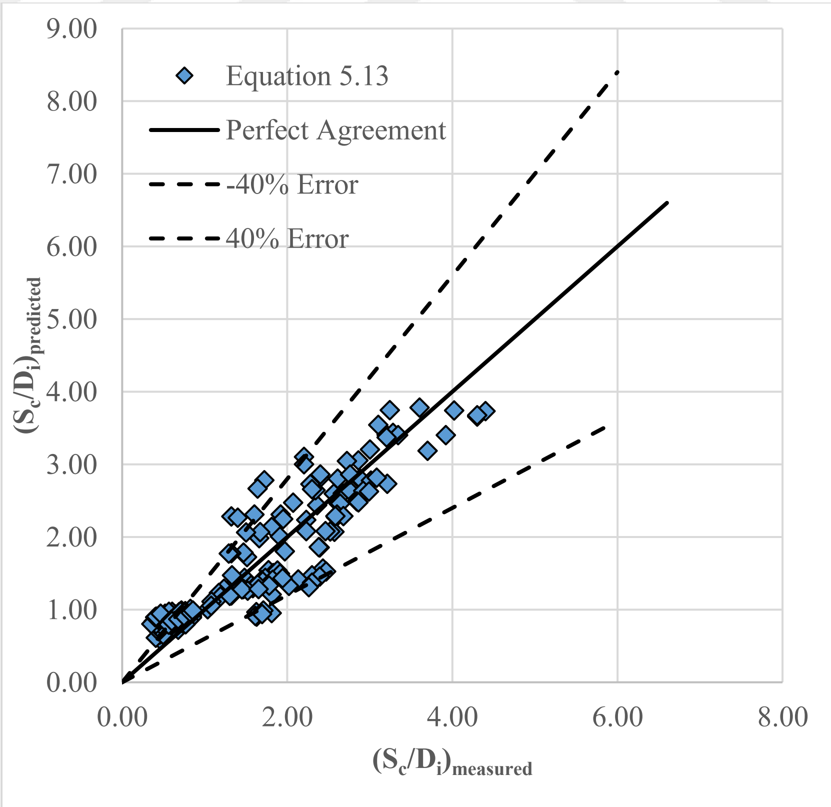

Figure 5.28: Comparison of $(S_c/D_i)_{measured}$ data with $(S_c/D_i)_{predicted}$ data obtained from Equation 5.13 under asymmetrical approach flow conditions

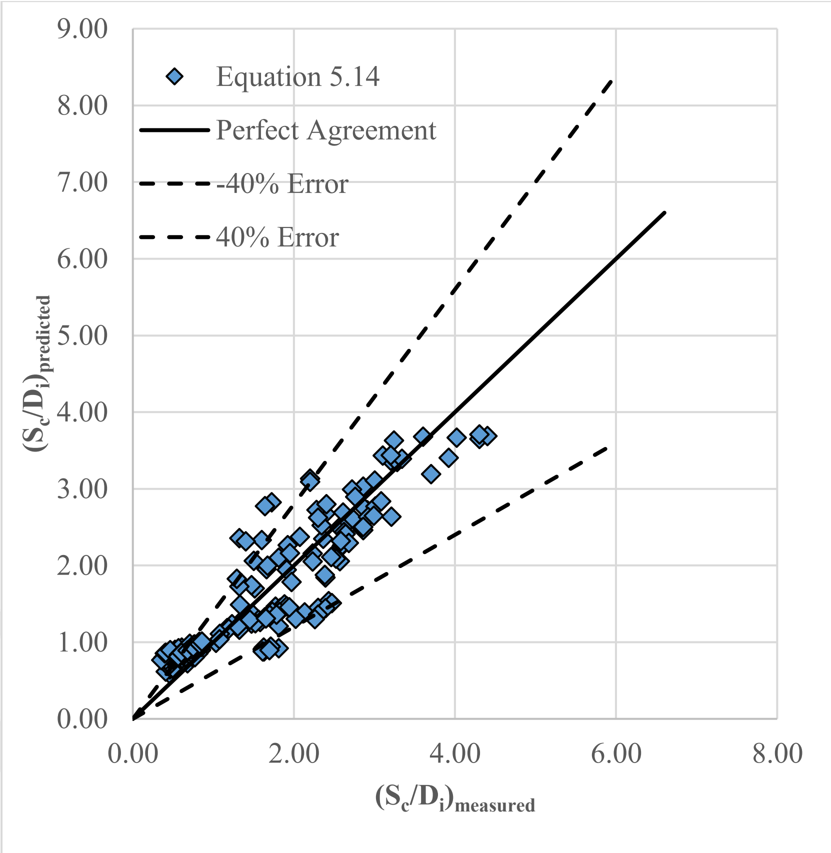

Figure 5.29: Comparison of $(S_c/D_i)_{measured}$ data with $(S_c/D_i)_{predicted}$ data obtained from Equation 5.14 under asymmetrical approach flow conditions

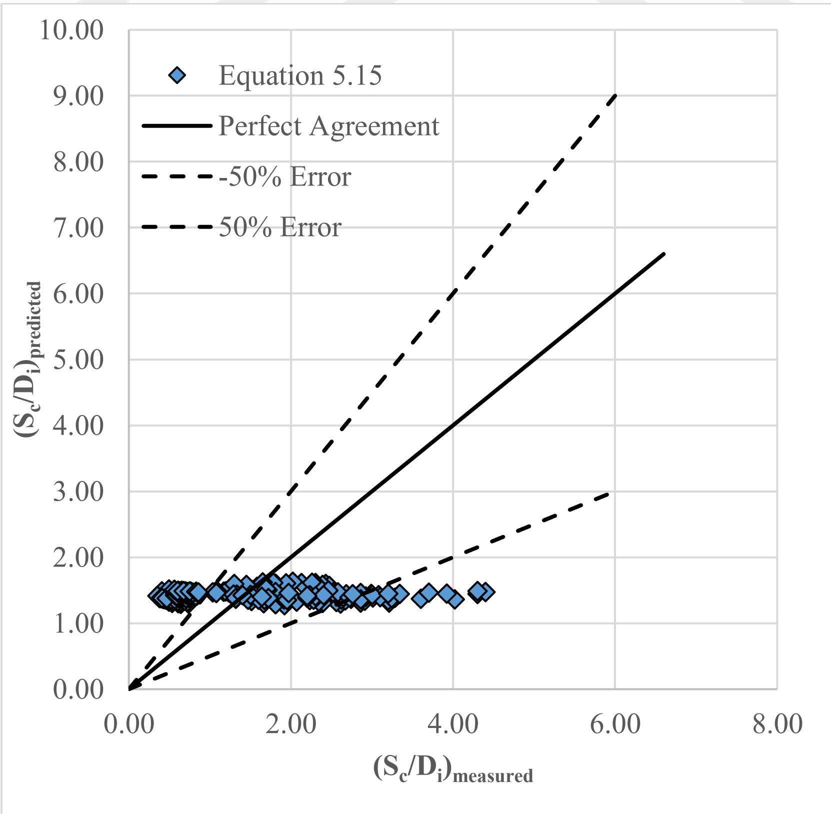

Figure 5.30: Comparison of $(S_c/D_i)_{measured}$ data with $(S_c/D_i)_{predicted}$ data obtained from Equation 5.15 under asymmetrical approach flow conditions

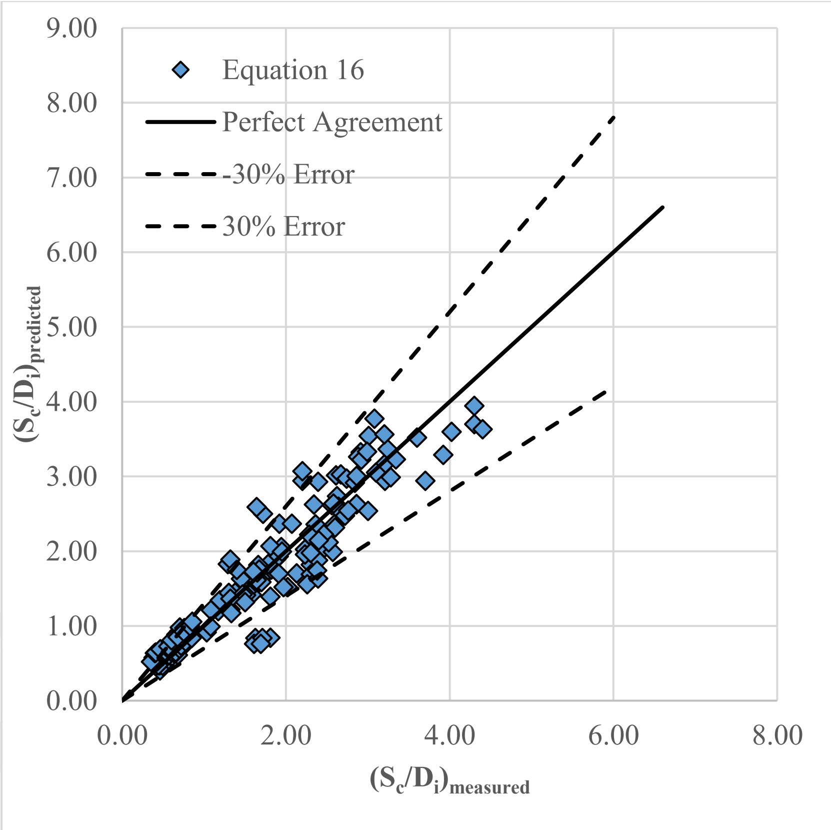

Figure 5.31: Comparison of $(S_c/D_i)_{measured}$ data with $(S_c/D_i)_{predicted}$ predicted data obtained from Equation 5.16 under asymmetrical approach flow conditions

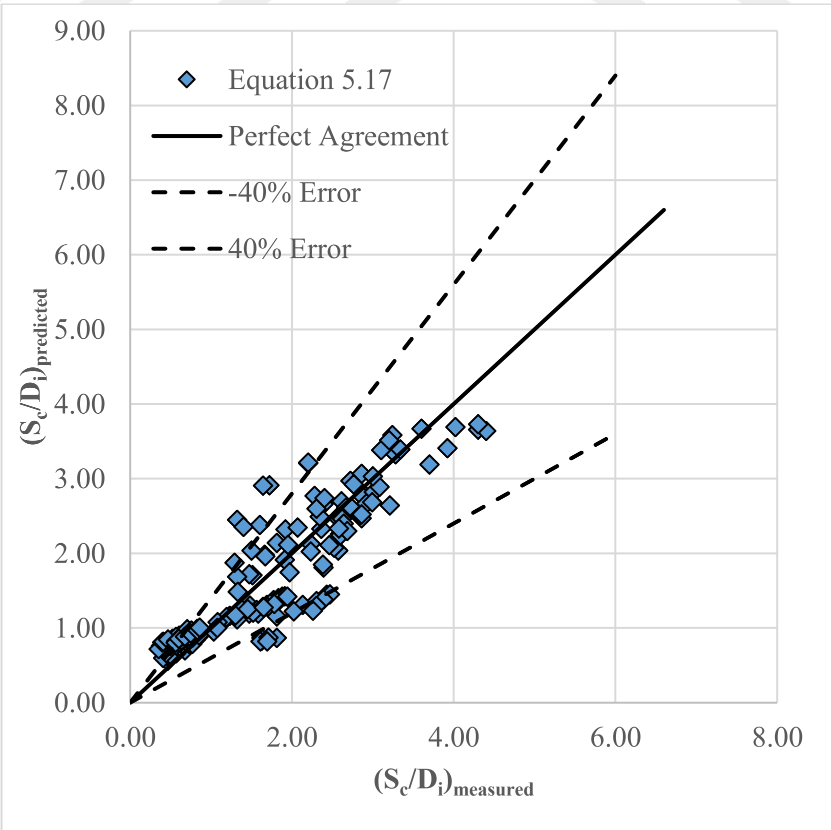

Figure 5.32: Comparison of $(S_c/D_i)_{measured}$ data with $(S_c/D_i)_{predicted}$ data obtained from Equation 5.17 under asymmetrical approach flow conditions

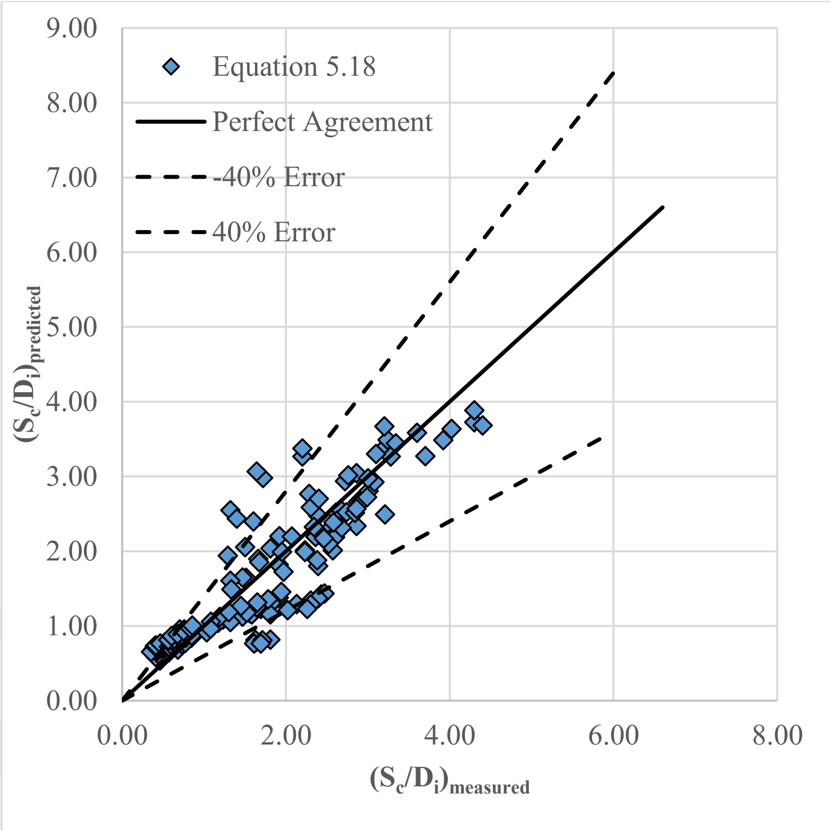

Figure 5.33: Comparison of $(S_c/D_i)_{measured}$ data with $(S_c/D_i)_{predicted}$ data obtained from Equation 5.18 under asymmetrical approach flow conditions

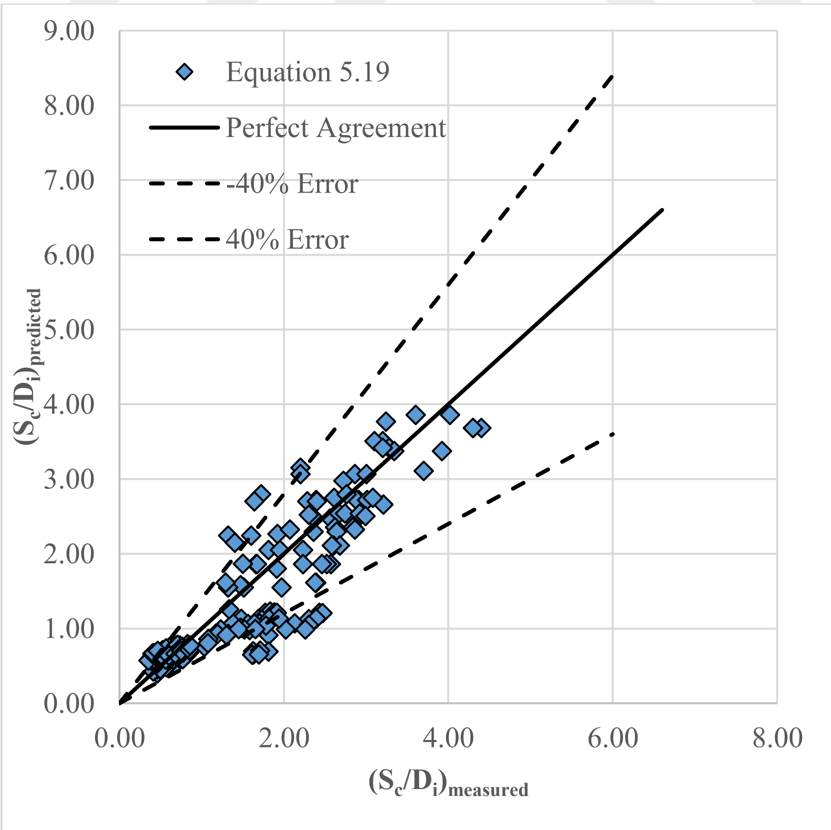

Figure 5.34: Comparison of $(S_c/D_i)_{measured}$ data with $(S_c/D_i)_{predicted}$ data obtained from Equation 5.19 under asymmetrical approach flow conditions

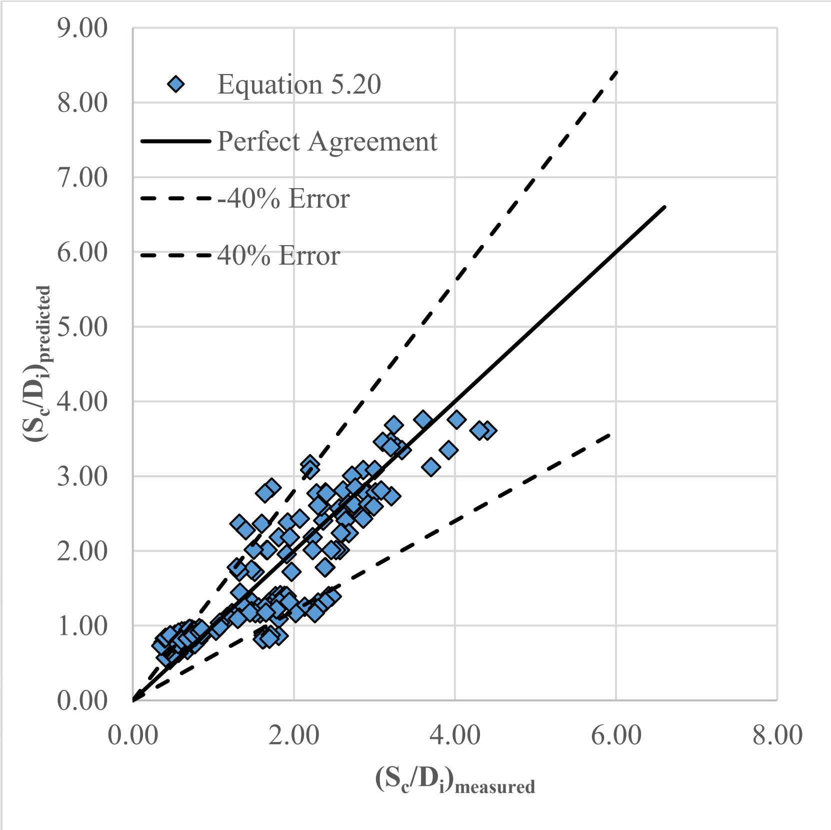

Figure 5.35: Comparison of $(S_c/D_i)_{measured}$ data with $(S_c/D_i)_{predicted}$ data obtained from Equation 5.20 under asymmetrical approach flow conditions

Figure 5.36 compares the predicted S_c/D_i values from Equation 5.6, which was developed using the combined datasets from Gökmener's, Haspolat's and Baykara's studies, with the predictions made by the empirical equations derived individually in each of these studies under symmetrical approach flow conditions [3,6,7]. Specifically, Baykara represents predictions obtained by applying his empirical equation to the combined data from all three studies [6]. Similarly, Haspolat corresponds to predictions made using his empirical equation, and Gökmener shows predictions based on his own empirical equation, all tested against the unified dataset.

The primary reason for selecting Equation 5.6 for comparison is that it does not include the approach Froude number, making it consistent with the other studies, which did not consider the approach Froude number [3,7]. Additionally, it incorporates all relevant flow and geometric parameters, providing a more comprehensive representation of the physical phenomena. The purpose of this comparison is to evaluate the generalization and predictive accuracy of Equation 5.6, which integrates the insights from all three studies, against the individual empirical models.

Most of the data points align closely with the 1:1 line, reflecting strong agreement, especially for Equation 5.6, which shows the most reliable predictive accuracy across the combined dataset. On the other hand, Baykara's equation produces a wider spread of results, particularly at higher S_c/D_i values, indicating that its applicability to broader datasets may be limited. In comparison, the equations proposed by Gökmener and Haspolat remain nearer to the 1:1 line, suggesting comparatively stronger predictive performance [3,7]. Overall, the findings highlight that Equation 5.6, by integrating the combined dataset, offers a more general and robust predictive capability than the individual empirical equations, especially under diverse flow and geometric conditions.

Figure 5.37 presents a comparative evaluation of predicted versus measured values of the dimensionless critical submergence, S_c/D_i, under asymmetrical approach flow conditions with a focus on assessing the performance of Equation 5.16, Gökmener and Haspolat's equations [3,7]. Importantly, these predictions are generated by applying each study's empirical equation to the same combined dataset used for Equation 5.16.

As seen in Figure 5.37, most of the data points associated with Equation 5.16 cluster closely around the 1:1 line and fall within the ±30% error bounds, indicating high predictive accuracy and consistency. This performance demonstrates the robustness of Equation 5.16, which was derived by integrating the datasets of both Gökmener and Haspolat, and includes key flow and geometric parameters such as the intake Froude number, Reynolds number, and the dimensionless geometric parameter ψ. As a result, Equation 16 offers a more comprehensive and physically meaningful representation of the critical submergence phenomenon [3,7]. In contrast, the predictions obtained using the original equations from both Gökmener and Haspolat display more noticeable deviations from the 1:1 line, with several points falling outside the ±30% error margins. These discrepancies suggest that while the original equations may perform well within the specific experimental conditions under which they were developed, their predictive power diminishes when applied to a broader dataset that spans varying geometries and flow regimes [3,7]. This observation highlights the limitations of single-study models in terms of generalizability. Furthermore, Gökmener's equation predicts S_c/D_i values up to more than 100 times compared to the measured S_c/D_i values while the intake Froude number $(Fr)_i$, is greater than 1.5. Since Gökmener's equation was derived by using the measured $(Fr)_i$ values within the range of 0.5 and 1.5, Gökmener's equation is not proper to predict the S_c/D_i values under flow conditions having greater $(Fr)_i$ values [3]. Consequently, the data collected from Haspolat's study, which have $(Fr)_i$ greater than 1.5, are not tabulated in Figure 5.37.

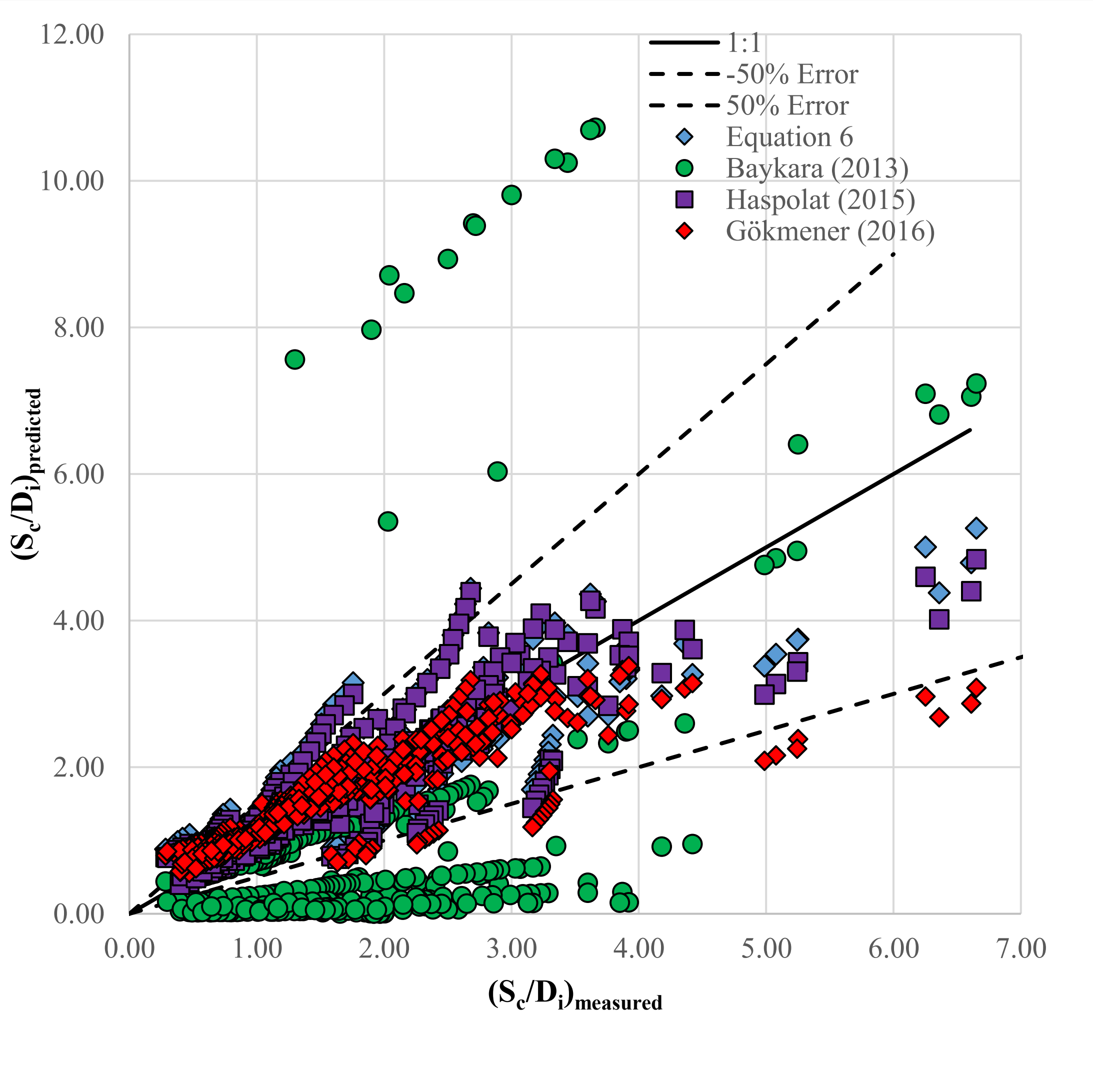

Figure 5.36: Comparison of $(S_c/D_i)_{measured}$ and $(S_c/D_i)_{predicted}$ from Equation 5.6, Baykara, Haspolat and Gökmener under symmetrical approach flow conditions

In this way, Equation 5.16 outperforms the individual empirical models in terms of accuracy and consistency across a diverse dataset. Its development from a merged data pool enhances its robustness and practical applicability. In conclusion, Equation 5.16 can be regarded as a more reliable and generalizable predictive tool for estimating critical submergence in horizontal intake structures under asymmetrical approach flow conditions, particularly when applied across a wide range of hydraulic and geometric configurations.

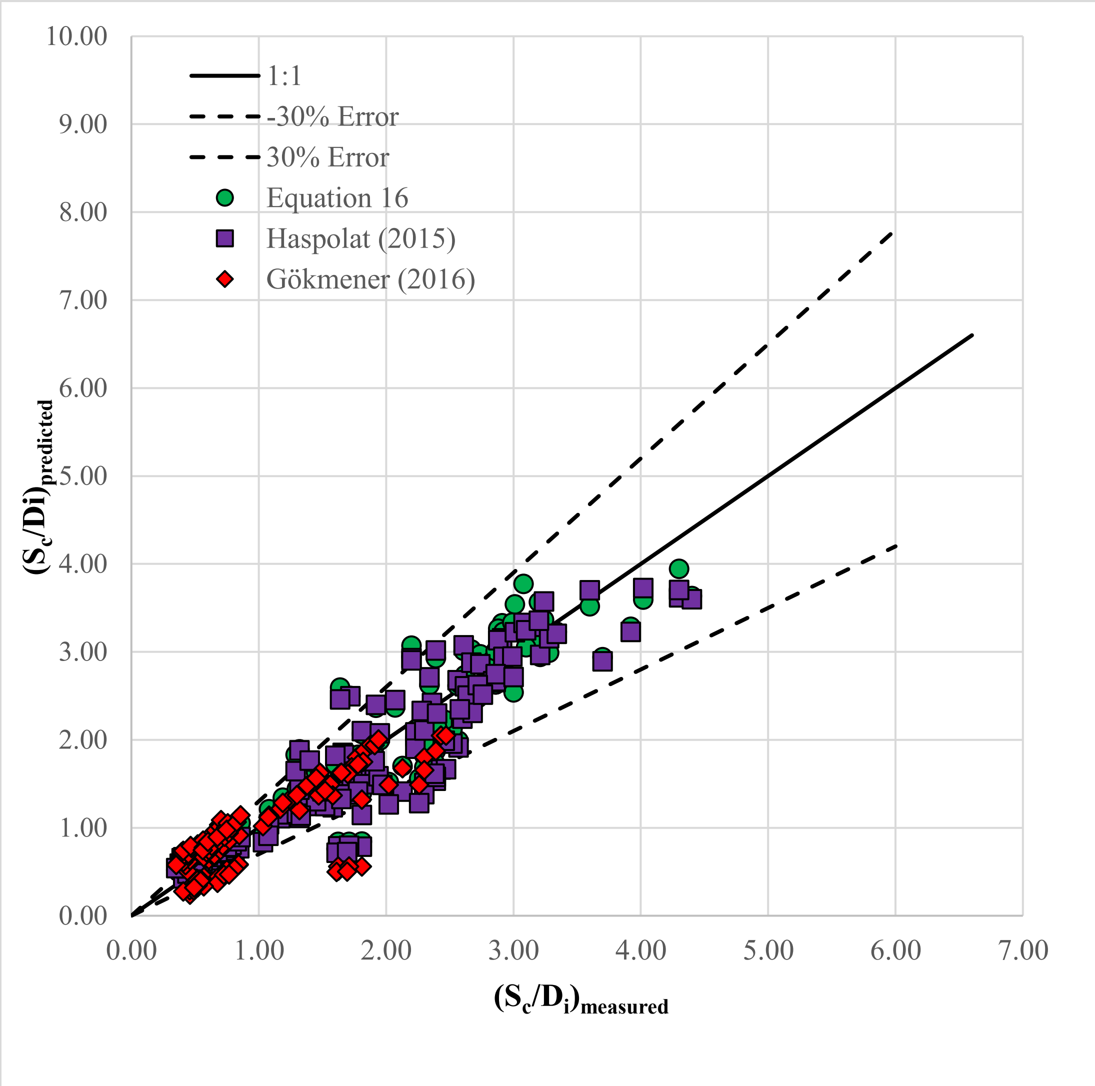

Figure 5.37: Comparison of $(S_c/D_i)_{measured}$ and $(S_c/D_i)_{predicted}$ from Equation 5.16, Haspolat and Gökmener, under asymmetrical approach flow conditions

5.3.3 Comparison of the Derived Empirical Equations from This Study with the Existing Studies in the Literature

Figure 5.38 presents a comparative evaluation of empirical equations presented in the literature and this study to predict dimensionless critical submergence, S_c/D_i, depending on only the intake Froude number $(Fr)_i$. Equations 5.10 and 5.20, developed in this research for symmetrical and asymmetrical geometries, respectively, are plotted alongside well-known empirical equations from the literature. These include those proposed by Gordon, Reddy and Pickford, Sarkardeh, Möller, Haspolat, and Gökmener [3,6,7,15,16,19,20]. In the literature, almost all of the extensive studies derived empirical equations to predict S_c/D_i depending on only $(Fr)_i$. In other words, they reduced or did not consider the effect of the Re, We and geometry parameter on the formation of air-entraining vortices. Therefore, in order to make a comparison with the existing studies in the literature, simplified equations to predict S_c/D_i, which regard only $(Fr)_i$ were considered. According to figure 5.38, a consistent increasing trend is observed across all models, indicating that higher approach flow velocities (i.e., greater $(Fr)_i$) require greater submergence to prevent air-core vortex formation at the intake.

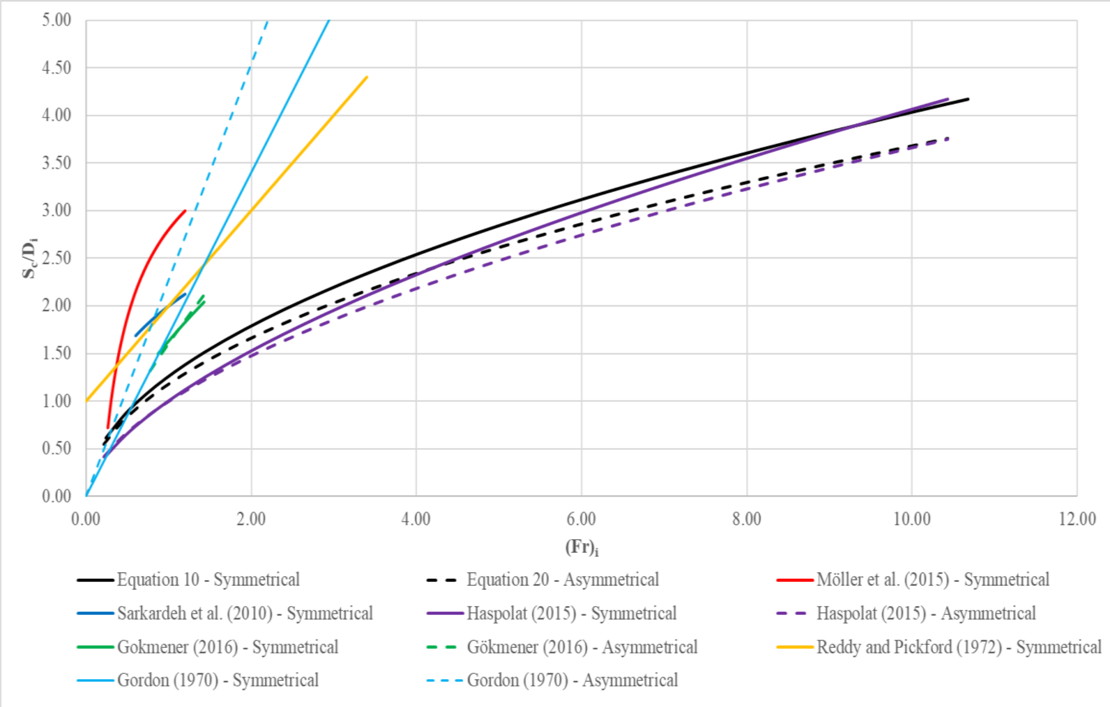

Figure 5.38: Comparison of empirical equations presented in the literature and this study to predict S_c/D_i depending on only $(Fr)_i$ for symmetrical and asymmetrical intake structures

As seen in Figure 5.38, the empirical equations proposed by Haspolat converge with the empirical equations presented in the literature, up to $(Fr)_i$ values of 0.5 [7]. However, Haspolat's equations tend to underestimate the dimensionless critical submergence S_c/D_i for a given intake Froude number $(Fr)_i$ when compared to the other empirical equations when $(Fr)_i$ is increased greater than 0.5. In contrast, the predictions obtained from the equations developed by Gordon, Reddy and Pickford, Sarkardeh, Möller, and Gökmener yield notably higher values of S_c/D_i for a given $(Fr)_i$ values and their results are found to be similar [3,15,16,19,20]. The primary reason behind this discrepancy lies in the scale of the experimental setups Haspolat conducted experiments using a relatively small-scale model, whereas Gordon, Reddy and Pickford, derived their dimensionless formulations from prototype data [7,15,16].

Similarly, both Sarkardeh, and Gökmener employed large-scale physical models, approximately at a scale of 1:30 [3,20]. On the other hand, Möller applied a different technique from the other studies to predict S_c/D_i. They establish a new relationship for critical submergence grounded in actual air entrainment data rather than solely visual observations of vortex formation [19]. As a result, the lower submergence values predicted by equation are likely influenced by scale effects, such as the dominance of viscous and surface tension forces that are more prominent in small-scale models but tend to diminish in prototype conditions due to the increased Reynolds and Weber numbers. In light of these considerations, the applicability of Haspolat's equations to real-life engineering practice may require a scale coefficient factor to account for these physical inconsistencies. Moreover, Equations 10 and 20, which are developed in the present study by integrating insights from three independent research efforts, are located between the trends of Gökmener and Haspolat's. This suggests that the proposed equations represent a balanced interpolation between small- and large-scale data and may offer improved generalizability across a wide range of hydraulic conditions.

CHAPTER VI
CONCLUSIONS AND RECOMMENDATIONS

This study has provided a detailed and data-driven investigation into the determination of dimensionless critical submergence, S_c/D_i, at single horizontal intake structures under both symmetrical and asymmetrical approach flow conditions. Utilizing a robust dataset compiled from 634 experimental measurements derived from three studies conducted by Baykara, Haspolat and Gökmener, how flow dynamics and structural geometry affect the formation of air-entraining vortices, which are critical to the safe and efficient design of water intake systems. The findings demonstrate that the intake Froude number $(Fr)_i$ is the most important hydraulic parameter influencing critical submergence. The results consistently show that as $(Fr)_i$ increases, the required submergence to suppress vortex formation also increases. However, this relationship is modulated by geometric effects, particularly the dimensionless geometrical parameter $2b/D_i$ in symmetrical cases and the ψ in asymmetrical cases. In narrower geometries (i.e., small $2b/D_i$ or ψ), more confined approach flow conditions lead to stronger rotational flow components, resulting in greater critical submergence requirements. Conversely, in wider geometries (i.e., large $2b/D_i$ or ψ), flow separation effects are diminished, and vortex intensity is reduced, allowing stable intake operation at lower submergence.

From a modeling perspective, twenty empirical equations were developed to predict S_c/D_i, each incorporating different combinations of flow and geometric parameters. Among these, equation 1 (Table 5.2) and equation 11 (Table 5.4) demonstrated the highest statistical accuracy ($R^2 = 0.988$ and $R^2 = 0.949$, respectively), suggesting that multi-variable models that integrate both hydraulic and geometric characteristics offer superior predictive capability. Notably, the intake Froude number $(Fr)_i$ and geometric parameters such as $2b/D_i$ or ψ emerged as the most influential predictors, whereas Reynolds and Weber numbers exhibited comparatively weaker effects. Furthermore, equations relying solely on the approach Froude number, $(Fr)_{app}$, proved inadequate, confirming its negligible role in capturing the physical mechanisms of vortex formation at horizontal intakes.

A comparative analysis was also conducted against well-known empirical equations from the literature, including those by Gordon, Reddy and Pickford, Sarkardeh, Möller, Haspolat, and Gökmener. This comparison revealed that equations based on small-scale experimental setups [e.g., Haspolat] tend to underestimate S_c/D_i, especially at greater $(Fr)_i$ values, likely due to the unscaled influence of viscous and surface tension effects. In contrast, equations derived from prototype data or large-scale physical models generally offer more conservative and physically consistent predictions.

The integration of datasets across multiple studies allowed for the development of generalized models specifically Equations 5.6 and 5.16 that outperform individual equations from the literature in terms of accuracy and applicability to varied conditions. These equations offer robust tools for engineering practice, particularly when assessing intake behavior under complex or site-specific configurations.

In summary, this study advances the understanding of vortex-induced air entrainment at intakes by bridging experimental evidence with empirical modeling. The results emphasize that critical submergence is a function of not only flow intensity but also intake geometry and structural configuration. The comprehensive analysis presented here provides a solid foundation for developing intake designs that minimize vortex-related risks while maintaining hydraulic efficiency.

The following recommendations are proposed to provide guidance for future research endeavors:

1. It is recommended that future intake designs consider both the intake Froude number and geometric parameters such as $2b/Di$ or ψ as primary design criteria when evaluating the risk of vortex-induced air entrainment. Simplified design approaches relying solely on the intake Froude number may underestimate critical submergence requirements, especially in narrow geometries or high-flow conditions.
2. While simplified models may be useful for preliminary evaluations, more comprehensive models should be employed during the detailed design phase to ensure higher precision and operational reliability.

3. The relationship between critical submergence and different types of intake shapes, along with varying approach channel sidewall angles, should be tested in detail.

REFERENCES

[1] GOGUS Mustafa and GOKMENER Serkan (2023), "Critical submergence for single and multiple horizontal intake structures", *Arabian Journal for Science and Engineering,* Vol. 48, No. 10, pp. 13091-13115.

[2] TASTAN Kerem (2020), "Critical submergence for a horizontal pipe intake", *AinShams Eng. J,* Vol. 11, No. 4, pp. 933–938.

[3] GOKMENER Serkan (2016), *Investigation of critical submergence at single and multiple-horizontal intake structures having air-entraining vortices* (Master's Thesis), Middle East Technical University, Ankara.

[4] KNAUSS James A. (1987), *Swirling Flow Problems at Intakes*, Hydraulic Structures Design Manual, Vol. 25, Balkema, Rotterdam.

[5] DURGIN William and HECKER George (1978), "The modeling of vorices at intake structures", *Proc. of IAHR-ASME-ASCE, Fort Colins*, Vol. 1, pp. 381-391.

[6] BAYKARA Ali (2013), *Effect of hydraulic parameters on the formation of vortices at intake structures* (Master's Thesis), Middle East Technical University, Ankara.

[7] HASPOLAT Emre (2015), *Determination of critical submergence depth at horizontal intakes* (Master's Thesis), Middle East Technical University, Ankara.

[8] YILDIRIM Nevzat and KOCABAS Fikret (1998), "Critical submergence for intakes in still water reservoir", *Journal of Hydraulic Engineering*, Vol. 124, No. 1, pp. 103-104.

[9] EROGLU Nihat and BAHADIRLI Tolga (2007), "Prediction of critical submergence for a rectangular intake", *Journal of Energy Engineering,* Vol. 133, No. 2, pp. 91-103.

[10] YILDIRIM Nevzat, TASTAN Kerem and ARSLAN Muammer Mustafa (2009) “Critical submergence for dual pipe intakes”, *Journal of hydraulic research*, Vol. 47, No. 2, pp. 242-249.

[11] YILDIRIM Nevzat, AKAY Huseyin and TASTAN Kerem (2011), “Critical submergence for multiple pipe intakes by the potential flow solution”, *Journal of Hydraulic Research*, Vol. 49, No. 1, pp. 117-121.

[12] YILDIRIM Nevzat, EYUPOGLU Abdul Samet and TASTAN Kerem (2012) “Critical submergence for dual rectangular intakes”, *Journal of Energy Engineering*, Vol. 138, No. 4, pp. 237-245.

[13] TASTAN Kerem (2016), “Critical submergence for isolated and dual rectangular intakes”, *Sadhana*, Vol. 41, No. 4, pp. 425-433.

[14] HASHID Muhammed, HUSSAIN Ajmal and AHMED Zulfequar (2021), “Critical submergence for side circular intake in an open channel flow”, *Journal of Hydraulic Research*, Vol. 59, No. 1, pp. 136-147.

[15] GORDON J L (1970), “Vortices at Intakes”, *Water Power 1970*, Vol. 4, pp. 137-138.

[16] REDDY Y R and PICKFORD J A (1972), “Vortices at Intakes in Conventional Sumps”, *Water Power 1972*, Vol. 3, pp. 108-109.

[17] RINDELS Alan J and GULLIVER John S. (1983), *An Experimental Study Of Critical Submergence To Avoid Free-Surface Vortices At Vertical Intakes*, Project Report No. 224, pp.1-89.

[18] JIMING Ma, LIANG Yuanbo and HUANG Jitang (2000), “Minimum submergence before double-entrance pressure intakes”, *Journal of Hydraulic Engineering,* Vol. 126, No. 8, pp. 628-631.

[19] MOLLER Georg, MARTIN Detert and ROBERT M. Boes (2015), “Vortex-induced air entrainment rates at intakes”, *Journal of Hydraulic Engineering*, Vol. 141, No. 11, pp. 04015026.

[20] SARKARDEH Hamed, ZARRATI Amir Reza and ROSHAN Reza (2010), “Effect of intake head wall and trash rack on vortices”, *Journal of Hydraulic Research*, Vol. 48, No. 1, pp. 108-112.

[21] KHANARMUEI Mohammadreza, HASSAN Rahimzadeh and HAMED Sarkardeh (2019), “Effect of dual intake direction on critical submergence and vortex strength”, *Journal of Hydraulic Research*, Vol. 57, No. 2, pp. 272-279.

[22] HASHID Muhammed and ELDHO (2023), “Effect of intake pipe blockage on the critical submergence for lateral dual intakes”, *Journal of Hydraulic Research*, Vol. 61, No. 4, pp. 573-582.

[23] DAS Bhagwan, AHMAD Zulfequar and SHARMA Pramod Kumar (2024), “Critical Submergence for Single Lateral Rectangular Hydraulic Intakes under Uniform Approach Flow”, *Journal of Hydraulic Engineering*, Vol. 150, No. 6, pp. 06024008.

[24] ANWAR Habib (1967), “Vortices at Low Head Intakes”, *Water Power,* Vol. 19, No. 11, pp. 455-457.

[25] ANWAR Habib (1968), “Prevention of Vortices at Intakes”, *Water Power*, Vol. 10, pp. 393-401.

[26] ANWAR Habib, WELLER James and AMPHLETT Michael (1978), “Similarity of Free Vortex at Horizontal Intake”, *Journal of Hydraulic Research*, Vol. 16, No. 2, pp. 95–105.

[27] SONMEZ Can Metin (2019), *Effect of Approach Channel Shape on The formation of Vortices at Single-Horizontal Intakes* (Master’s Thesis), Middle East Technical University, Ankara.

[28] YILDIRIM Nevzat and KOCABAS Fikret (1995), “Critical submergence for intakes in open channel flow”, *Journal of Hydraulic Engineering*, Vol. 121, No. 12, pp. 900-905.

[29] YILDIRIM Nevzat, KOCABAS Fikret and GULCAN Salih Cem (2000), “Flow-boundary effects on critical submergence of intake pipe”, *Journal of Hydraulic Engineering*, Vol. 126, No. 4, pp. 288-297.

[30] GURBUZDAL Ferhat Aral (2009), *Scale effects on the formation of vortices at intake structures* (Master’s Thesis), Middle East Technical University, Ankara.

[31] JAIN Akalank, GARDE Ramachandra, and KITTUR Ranga Raju (1978), "Vortex formation at vertical pipe intakes", *Journal of the Hydraulics Division*, Vol. 104, No. 10, pp. 1429-1445.

[32] PADMANABHAN Mahadevan and HECKER E. George (1984), "Scale effects in pump sump models", *Journal of Hydraulic Engineering*, Vol. 110, No. 11, pp. 1540-1556.

[33] ZALOGLU Cihan (2014), *Formation of air-entraining vortices at horizontal water intakes* (Master's Thesis), Middle East Technical University, Ankara.

[34] GOGUS Mustafa and GOKMENER Serkan (2023), "Critical submergence for single and multiple horizontal intake structures", *Arabian Journal for Science and Engineering*, Vol. 48, No. 10, pp. 13091-13115.

[35] WILLMOTT Cort J and MATSURA Kenji (2005), "Advantages of the mean absolute error (MAE) over the root mean square error (RMSE) in assessing average model performance", *Climate research*, Vol. 30, No. 1, pp. 79-82.

[36] MEHDI Fuladipanah, HAZI Mohammad Azamathulla and KISI Ozgur (2023), "An in-depth comparative analysis of data-driven and classic regression models for scour depth prediction around cylindrical bridge piers", *Applied Water Science*, Vol. 13, No. 12, pp. 231.

[37] VOLKART Peter and RUTSCHMANN Peter (1986), "Aerators on spillway chutes: fundamentals and applications", *Advancements in Aerodynamics, Fluid Mechanics and Hydraulics, ASCE*, pp. 162-177.

[38] ZEIGLER E R (1976), REC-ERC-76-2 *Report: Hydraulic Model Vortex Study-Grand Coulee Third Powerplant*, p. 31, Fig. 35, Ref.8

[39] TASTAN Kerem and YILDIRIM Nevzat (2010), "Effects of dimensionless parameters on air-entraining vortices", *Journal of hydraulic research*, Vol. 48, No. 1, pp. 57-64.

[40] BAYKARA Ali, GOGUS Mustafa and KOKEN Mete (2013), *Su Alma Yapılarında Girdap Oluşumu Ve Önlenmesi Için Gerekli Düzeneklerin Belirlenmesi,* (110M676), TÜBİTAK, Turkey.

[41] HASHID Muhammed, HUSSAIN Ajmal, and AHMED Zulfequar (2021), “Critical submergence for side circular intake in an open channel flow”, *Journal of Hydraulic Research*, Vol. 59, No. 1, pp. 136-147.